EPA-450/3-75-059
June 1975

EVALUATION OF SELECTED AIR POLLUTION DISPERSION MODELS APPLICABLE TO COMPLEX TERRAIN

U.S. ENVIRONMENTAL PROTECTION AGENCY
Office of Air and Waste Management
Office of Air Quality Planning and Standards
Research Triangle Park, North Carolina 27711

EPA-450/3-75-059

EVALUATION OF SELECTED AIR POLLUTION DISPERSION MODELS APPLICABLE TO COMPLEX TERRAIN

by

INTERCOMP Resources Development and Engineering, Inc.
2000 West Loop South, Suite 2200
Houston, Texas 77027

Contract No. 68-02-1085
Program Element No. 2 AC 129

EPA Project Officer: Edwin L. Meyer, Jr.

Prepared for

ENVIRONMENTAL PROTECTION AGENCY
Office of Air and Waste Management
Office of Air Quality Planning and Standards
Research Triangle Park, North Carolina 27711

June 1975

This report is issued by the Environmental Protection Agency to report technical data of interest to a limited number of readers. Copies are available free of charge to Federal employees, current contractors and grantees, and nonprofit organizations - as supplies permit - from the Air Pollution Technical Information Center, Environmental Protection Agency, Research Triangle Park, North Carolina 27711; or, for a fee, from the National Technical Information Service, 5285 Port Royal Road, Springfield, Virginia 22161.

This report was furnished to the Environmental Protection Agency by INTERCOMP Resources Development and Engineering, Inc., Houston, Texas 77027, in fulfillment of Contract No. 68-02-1085. The contents of this report are reproduced herein as received from INTERCOMP Resources Development and Engineering, Inc. The opinions, findings, and conclusions expressed are those of the author and not necessarily those of the Environmental Protection Agency. Mention of company or product names is not to be considered as an endorsement by the Environmental Protection Agency.

Publication No. EPA-450/3-75-059

PREFACE

It is regretted that the Environmental Protection Agency (EPA) and INTERCOMP Resource Development and Engineering, Inc. could not mutually agree as to the conclusions of this study. Consequently, as sponsor, EPA is obligated to caution against the uncritical acceptance of the summary statements in the report.

The EPA in 1970 and 1972 evaluated the impact of several non-ferrous smelters on air quality in mountainous regions. Similarly, in 1971 the National Oceanic and Atmospheric Administration evaluated the impact of a number of power plants located in mountainous areas. The techniques used to estimate the effects of complex terrain on the distribution of the effluents from the sources had not been used prior to these studies. The air quality estimates were much greater for nearly all facilities than would result from the use of the flat-plane formula. INTERCOMP was one of the consultants retained by industry to review EPA's analyses. Results of their model simulations were presented at formal hearings to counter the governmental estimates.

Although generalities of the INTERCOMP model were available in the literature and hearing records, the computer program (and thus the technical details) were and remain proprietary. To obtain details of the technical content of the INTERCOMP model, EPA negotiated a contract with INTERCOMP. The contract called for INTERCOMP to provide the computer program to EPA; to instruct EPA personnel in the use of the computer program; and to provide applications of the INTERCOMP and Gaussian models for comparison with observed peak short-term concentrations in complex terrain. The contract states that "...peak short-term concentrations shall be the primary consideration in the evaluation...(of the models)." This report discusses the effort of INTERCOMP to satisfy this contract.

In bringing the contractual effort to a conclusion, it became apparent that INTERCOMP and EPA project officers had some fundamental differences of a technical nature as to portions of the report. Aside from differing interpretations of the validity of various simplifying assumptions in each model, the basic differences revolve around the validity of the El Paso data used for model evaluation and around the definition of a reliable model estimate.

More specifically, EPA takes exception to statements made in the Summary and on pp. 3-28 and 3-29, and pp. 3-40 and 3-41 in the report. EPA agrees that the El Paso data are useful to demonstrate the degree of flexibility of models; that is, through successive adjustments of emission rates, etc., to obtain agreement

between the modeling results and the air quality observations. However, EPA does not agree that the El Paso emission data were sufficiently reliable to warrant judgments on the "accuracy" of models.

Also, EPA does not completely agree with INTERCOMP's interpretation of the NOAA's Huntington Canyon study. A case may be made that the results of the study indicate that the basic Gaussian model provides more reliable estimates of the peak 1-hour concentrations in this instance than either the EPA terrain or the INTERCOMP models.

Further, current short-term air quality standards (24-hour period or less) are not to be exceeded more than once per year. Hence, if modeling results are to be used directly in source-control decisions, a reliable model estimate must represent the near-upper envelope of observable concentrations. However, INTERCOMP interprets a reliable estimate as one which best fits an average of observed data. This interpretation may lead to estimates of concentrations that are incompatible with the definition of short-term standards. Thus, a degree of control based on INTERCOMP's interpretation of a reliable model estimate may not adequately protect the quality of the air.

INTERCOMP and EPA agree that both have worked in good faith to resolve these differences. They agree that further expenditures of effort and funds are unlikely to produce results that are completely acceptable to either party. Hence, the report is released with this Preface as an integral part, so that the results of the study may be available, but with the reader cautioned against the uncritical acceptance of the conclusions.

EVALUATION OF SELECTED AIR POLLUTION DISPERSION MODELS APPLICABLE TO COMPLEX TERRAIN

TABLE OF CONTENTS

TABLE OF CONTENTS (Continued)

ILLUSTRATIONS

SUMMARY

Short-term (1 hr., 3 hr., and 24 hr.) air quality criteria generally have a higher potential for being exceeded in the vicinity of large point sources than do longer term standards. In cases where terrain is unimportant, the air quality can be evaluated using the familiar Gaussian plume models. Frequently, such evaluations must involve geographical areas with important terrain relief. In such cases, regulatory and policy-making agencies have made assumptions about how the plume centerline behaves and continued to use the Gaussian models. Recently models have become available which combine wind flow calculations along with the plume dispersion assessment. Such a model has the potential to provide more accurate air quality predictions where terrain is important. As a consequence, the objective of this contract was to use air quality data collected in rough terrain to test the accuracy of several models to predict short-term concentrations.

The models tested were (1) the Gaussian calculation known as the NOAA model, (2) the EPA Gaussian model, and (3) the INTERCOMP combined wind flow and plume dispersion model. Two sets of data were used in the comparison. These data were (1) the SF_6 tracer data collected by NOAA in Huntington Canyon, Utah, and (2) SO_2 ambient data in El Paso, Texas.

The model calculations represent predictions based upon the measured or observed meteorology. That is, the calculations represent generally how the models would have been used to predict air quality around a single source. It should be noted that the comparisons included in the report were for 1 hour average concentrations, rather than the 3 or 24 hour air quality standard criteria.

The results for Huntington Canyon show the INTERCOMP combined wind flow and dispersion model predicted groundlevel concentrations with an accuracy comparable to that normally obtained with Gaussian predictions in flat terrain situations. The INTERCOMP model gave calculated results within a factor of two and one-half for all stable tests. For stable down-canyon flows, however, Gaussian predictions from a NOAA type model averaged a factor of fifteen fold higher than the measured results.

The El Paso data, though limited by emission definition data, provided comparisons over flat terrain and near, but not in, mountains. In the flat terrain cases, results with the Gaussian (NOAA) model and the INTERCOMP model were in close agreement. The EPA model gave lower predicted concentrations. In the elevated terrain cases, the INTERCOMP model predicted lower concentrations than the Gaussian type models by factors of ten to twenty.

Comparison of the various models with observations show that the addition of a wind flow calculation can improve air quality predictions. Presently available wind flow calculations are of necessity a simplification of the atmospheric flow processes. However, there are a broad range of air quality evaluations in which the accuracy of the end result can be improved by the combined approach.

1.0 INTRODUCTION

1.1 General Needs and Objective

More and more emphasis is being placed on the need to satisfy short-term (1 hr., 3 hr., and 24 hr.) air quality criteria. These needs have generally been delineated to avoid adverse effects on human health or plant and animal growth processes. Certainly no group of experts agree precisely on what concentration is sufficient to provide protection against adverse effects, but it is clear that protection is needed.

The shorter term ambient air quality standards generally are more likely to be exceeded in the vicinity of large isolated point sources than are the longer term annual standards. As a result, it is essential for regulatory and policy-making agencies to have available to them the best technology for evaluating ambient air quality concentrations which result from these point source emissions.

In cases where terrain is unimportant, the state-of-the-art method is to evaluate the short-term air quality using three-dimensional Gaussian plume models. Present Environmental Protection Agency, EPA, practice is to use such a model to provide assessments of ambient air quality and thus provide a comparison to ambient air quality standards.

Frequently such evaluations must be for geographical areas which do involve important terrain relief. Many of the coal fired power plants and non-ferrous smelters are located in areas where terrain plays an important role in the meteorology controlling plume dispersion. In such cases, EPA has made assumptions about how the plume centerline behaves in the immediate vicinity of the terrain and continued to use the cross-wind and vertical diffusivities characteristic of the Gaussian models. Basically, the modification of the wind flow by the terrain is being assumed rather than any quantitative attempt made to calculate this modification.

Within the last few years, several techniques have been described which combine a wind flow calculational model along with a plume dispersion calculational technique[1,2,3,4]. Such a model has the potential to provide more accurate plume dispersion assessments where terrain is important. As a consequence, the objectives of this contract were to:

(1) compare one of the combined flow and dispersion models, the INTERCOMP model, with the presently available EPA models, and

(2) use data from rough terrain areas to test the relative abilities of the models in predicting short-term air quality.

1.2 Description of the Models Tested

Three models have been compared with data as a result of this contract. Two of these models are Gaussian models and have been used by regulatory agencies to make air quality analyses in rough terrain areas. The third model[4] was developed by INTERCOMP and includes a wind flow calculation as well as the assessment of plume dispersion. The model is more completely described in an associated volume which documents the equations and methods of solution, but for which the distribution is restricted to EPA personnel.

Of the two Gaussian models, one has become known as the NOAA model. This nomenclature undoubtedly resulted from the use of this model by NOAA in preparing the diffusion model calculations presented in the Southwest Energy Study[5].

The second Gaussian model is that presently employed by EPA for making ambient air quality evaluations for rough terrain areas. This model (the version tested was known as C4M3D) is a modification of the plume centerline flow concept used in the NOAA model and in addition retains angular segment averaging for even short-term concentrations.

The INTERCOMP model is quite a different concept from the Gaussian models. As opposed to assuming normal concentration distributions in the cross-wind and vertical directions, the model arises from approximating turbulent fluctuations by a Fickian-type eddy diffusivity. These eddy properties are height dependent as is the windspeed. This is quite different from the average over height wind and dispersion coefficients used in a Gaussian model or even those used in a constant diffusivity model.

Even so, over flat terrain there is good agreement between the numerical model and the Gaussian results. The particular height dependence of diffusivity and wind speed which provide this agreement are discussed in a later section. Only in cases where terrain modifies the air flow do the INTERCOMP model results differ substantially from either the NOAA or EPA models. As mentioned previously, the purpose of the contract was to compare the models over rough terrain and show whether or not the increased flexibility of the INTERCOMP model actually resulted in more accurate concentration predictions.

The purpose of the contract was to compare the several models tested for their predictive ability to calculate short-term concentrations. Short-term federal air quality standards can be exceeded on a once per year basis. Ideally, the models should

define the next-highest 3 and 24 hour average concentration. However, because of the diffusion parameters used, model predictions generally represent less than 1 hour averages. The calculated 3 and 24 hour averages for comparison with standards must then be developed from these model predictions.

1.3 Approach Used in Model Comparison

Two sets of data were used in comparing the various models. These data were (1) the SF_6 tracer data collected by NOAA in Huntington Canyon, Utah[6] and (2) SO_2 ambient air quality data around the ASARCO smelter in El Paso, Texas.

Insofar as possible, the models have been compared to the data and with the other models on a point-by-point basis. That is, simultaneous comparison of predictions and measurements at all points in space where observations of significance existed. However, because the EPA model averages concentrations over an angular segment, only centerline concentrations could be compared with the data and the other models.

The meteorological input to each model in terms of atmospheric stability and wind conditions was kept as consistent as possible. Flow and diffusion coefficients over a complete range of atmospheric stability have been determined for the INTERCOMP numerical model. Use of these particular diffusivities gives good agreement with the Gaussian models for flat terrain cases. These were the coefficients used for the same atmospheric stability class as was input to the Gaussian models.

As a consequence, all model calculations actually represent predictions based upon measured or observed meteorology. That is, the best-fit set of coefficients has not been determined for use. The validation of the models in this way actually represents how they might be used in conjunction with the local climatology at a particular site to predict concentrations for applications such as:

(1) plant siting studies

(2) evaluation of design changes

(3) compliance with ambient air quality standards.

In this last category, there may be quite remote areas around a particular plant in which it is impractical to place continuous monitors. For such areas and for interpolation between monitors, diffusion model predictions can be extremely valuable.

2.0 AIR QUALITY MODELS TESTED

The following sections describe the models tested in somewhat more detail. These sections will provide the basic assumptions used in each model to cover the possibility that the above nomenclature for the models will not be totally descriptive to all readers.

2.1 The Gaussian Model

The Gaussian calculational technique utilizes the various Pasquill atmospheric stability classes. In flat terrain situations, the model is used in the classical way described in Turners' workbook[7]. Where terrain is important, however, NOAA has developed additional assumptions. For completeness, we have summarized all the important assumptions made about this model.

The assumptions can be listed as:

(1) A mean wind is used to represent the entire air layer important in atmospheric diffusion.

(2) A single mean wind direction specifies the x-axis.

(3) The plume concentrations are assumed normally distributed (Gaussian) in the cross-wind and vertical directions.

(4) The standard deviations, σ_y and σ_z, are representative of averaging times in the range of 10 minutes to one hour.

(5) The source emission rate as well as wind and atmospheric conditions must be constant over times significantly greater than the travel time to a downwind position of interest.

The above assumptions describe those necessary in the flat terrain case. For rough, mountainous terrain additional restrictions were imposed by NOAA:

(6) Under neutral or unstable atmospheric conditions, the plume centerline is assumed to flow parallel to terrain.

(7) Under stable conditions, the plume centerline flows horizontally until it encounters terrain at the plume elevation.

Some discussion of these last two points may be in order. under neutral conditions, there is little density effect inhibiting vertical flow. Thus, an obstacle in the flow path will cause substantial modification of the flow field both horizontally and vertically. The fact that the atmosphere is of neutral stability simply specifies that, if there is vertical flow and it is rapid enough that little or no heat transfer takes place to a volume of air being moved, then the density of that air volume is the same at its new elevation as other air at that level. That is, the adiabatic temperature change undergone has just compensated in its effect on density for the static pressure change.

For stable conditions, the density decreases drastically with height. In this case as air encounters an obstacle, there is more of a tendency to flow horizontally around the obstacle than up and over it.

The concept expressed by assumption (7) above is that under stable conditions vertical flow is inhibited. Carrying this to its limit, the assumption is made that the plume must flow horizontally on a straight line until it encounters the terrain. The concept in item (6) is that for neutral and unstable flows there is no retarding influence to vertical flow.

The assumption contained in item (7) cannot satisfy basic fluid flow concepts on other than an instantaneous basis and thus should be conservative in terms of overestimating groundlevel concentrations. Whereas item (6) could result in lower groundlevel concentrations than actual.

2.2 The EPA Model (C4M3D)

The EPA model is a modified version of the NOAA concepts in how it calculates terrain effects. Basically, there are two modifications which are listed below as a continuation of the set of Gaussian assumptions.

(8) The plume centerline does not intersect the terrain, but after approaching within 10 m vertical distance it remains that distance above the terrain ground surface.

(9) Angular segment averaging of the plume concentrations is done for short-term averages as well as for annual averages.

As discussed previously, a stable atmosphere restricts vertical flow. The concept of allowing the plume to remain 10 m above the terrain removes at least a portion of the conservatism contained in a centerline intersection assumption.

In item (9) the averaging is performed over a 22.5 degree angular segment. This results in concentrations which are reduced over the customary Gaussian model. This reduction depends upon downwind distance and upon atmospheric stability. The reduction in centerline concentrations is simply $\sigma y/0.157x$ where σy is the cross-wind standard deviation and x is the downwind distance from the source. For F stability, the reduction varies between 4 and 8 over the distance range of 100 m and 100 km. For C stability, the reduction varies between 1.25 and 2.6 over the same distance range.

The concept behind this angular segment averaging is that for a given wind direction, the wind direction is actually distributed uniformly throughout the entire 22.5° angular segment over a period of time of interest. For longer term averages, annual, seasonal, or monthly, the assumption is probably valid. The segment averaging concept was originally intended for annual average predictions. However, because of the need to calculate shorter term averages, the EPA model has frequently been used for these cases as well. Certainly for shorter term averages than 24 hour, the segment averaging is more questionable.

2.3 The INTERCOMP Model

This model is a numerical solution of the three-dimensional material balances for the entire air stream and the pollutant flowing with that air stream. The pollutant material balance results from the turbulent diffusion equations which approximate turbulent fluctuations by a Fickian-type eddy diffusion model. The eddy diffusivity used in the model is height dependent consistent both with turbulent fluctuation measurements and theory.

The wind flow over uneven topography is calculated by numerically solving a modified form of the three-dimensional potential flow equations. The modification allows (1) inviscid potential flow at high elevations and (2) height-dependent coefficients which account for surface friction (viscous effects) in the lower boundary layer. The empirical modification causes calculated windspeed to vary with height. This modification over flat terrain results in velocities which vary as either of two familiar forms, logarithmic or power law.

The numerical finite difference approach divides the region around the plant into a number of three-dimensional cells which can vary in size as terrain or meteorological characteristics require. The grid cell directly above a stack and at the effective stack height is used as a volume source for pollutant. The source volume can be set to represent the dilution occurring during plume rise. For a true point source, the source grid cell must be small to avoid errors due to an initial dilution effect. The numerical procedures used in the solution of both

the wind flow and pollutant flow are efficient requiring minimal computer time. The steady-state solution which is a good approximation to many practical problems can be generated in a single time step or the entire progression to steady-state can be calculated in a series of time steps.

The modified potential flow model for wind flow calculations represents a significant simplification of the combined momentum and energy equations describing air flow. However, it retains most of the important factors so necessary to a sound meteorological and engineering analysis of pollutant dispersion in rough terrain.

Of significance is the fact that over flat terrain the INTERCOMP numerical model can provide good agreement with the Gaussian models. This is true even though in the numerical model the diffusivities (and velocities) vary only with height unlike the Gaussian models where the standard deviations vary with distance downwind from the source. For constant diffusion and windspeed, the Fickian or turbulent diffusion approach gives standard deviations which vary as

$$\sigma = \sqrt{2EX/u}$$

where σ = the standard deviation
E = the eddy diffusivity
x = downwind distance
u = windspeed.

The Gaussian models indicate σ varies in almost direct proportion to downwind distance, x. The fact that the turbulent diffusion model with height dependent diffusivities and velocities gives the same result as the Gaussian models implies that the additional downwind dependence of σ could be due to the assumption of uniform winds and diffusion over the thickness of the boundary layer.

The simplification of the momentum and energy equations used in the INTERCOMP model cause some limitations in its use. These can be enumerated as

(1) the modified potential flow model prevents the formation of recirculating flow in the lee of an obstacle,

(2) the elimination of the energy balance prevents calculating the driving force for natural convective flows. However, this type of flow could be imposed by the definition of boundary conditions.

Illustrations are presented in this study which show that the modified potential flow concept calculates a good approximation to the velocity fields on the upwind side of obstacles. If the problem of interest is the recirculating flow, a more complete solution of the Navier-Stokes momentum equations is required. Such a model is described in a later section.

Natural convective flows of interest include land-sea breeze and stable valley drainage flows. Situations of this type can be studied with the model, but the flow patterns would have to be created by source-sink combinations in the wind flow grid instead of the natural density driving forces. The present model does not contain this capability although air flow source-sink can be included in a straightforward manner.

2.4 Calculation of 3 and 24 Hour Averages from Model Predictions

Each of the air quality models discussed above predict short-term concentrations generally accepted as representing 1/4 to 1 hour time averages. Values of 3 and 24 hour average concentrations must be developed for comparison with standards.

If the model prediction is accepted as a 1 hour average, longer term averages might be calculated in the following way:

(1) use measured meteorology for each hour of an entire year to calculate dispersion parameters;

(2) calculate the 1 hour average from a dispersion model; and

(3) select the second highest successive 24 hour period calculation as the predicted 24 hour average.

Recognizing that the model prediction contains uncertainty, the predicted 1 hour average should be the probable value as opposed to an extreme value. The three hour average could be developed similarly.

3.0 VALIDATION AND COMPARISON OF AIR QUALITY MODELS

3.1 General Comparisons

Extensive comparisons of the INTERCOMP model with Gaussian models have been made. As mentioned previously, it is essential that the numerical model be in rough agreement with the Gaussian models for flat terrain. Particularly important is the need to have calculated concentrations decrease roughly as the square of downwind distance. Such a decrease with distance is in marked contrast to what a Fickian-type turbulent diffusion model with constant wind velocity and eddy diffusivity would give. In the latter case, concentrations decrease in almost direct proportion to the downwind distance. Thus, we were extremely interested to see what height-dependent wind velocity and eddy diffusivities would do to calculated concentrations.

Using well-accepted power law forms for this variation of velocity and diffusivity with height gave good agreement between the Fickian-type turbulent diffusion results and the various Gaussian model results. This is illustrated in Figure 1. Note that the power law variation of velocity and diffusivity has indeed caused a much more rapid drop-off in calculated concentrations than would constant value parameters. In fact, by varying these power law forms slightly, the entire range of atmospheric stability classes can be simulated in terms of their effect on downwind concentration falloff.

The results obtained above are somewhat surprising when one considers that in the turbulent diffusion model the diffusivities are not functions of downwind distance at all as they are in the Gaussian model. As mentioned in a previous section, the deviation of the calculated concentrations for a constant diffusivity turbulent model are still dependent upon downwind distance, but upon the square root power as opposed to the more direct proportion as in the Gaussian model. The above results imply that the use of downwind distance dependence of diffusivities in the Gaussian models may indeed be compensating for the fact that these diffusivities as well as windspeed should be varying with height in the boundary layer.

Velocity and diffusivity height dependent forms have been determined with the INTERCOMP numerical model which give good agreement with the Pasquill-Gifford stability classifications used in a Gaussian model. These values are as shown in Table I.

FIGURE 1

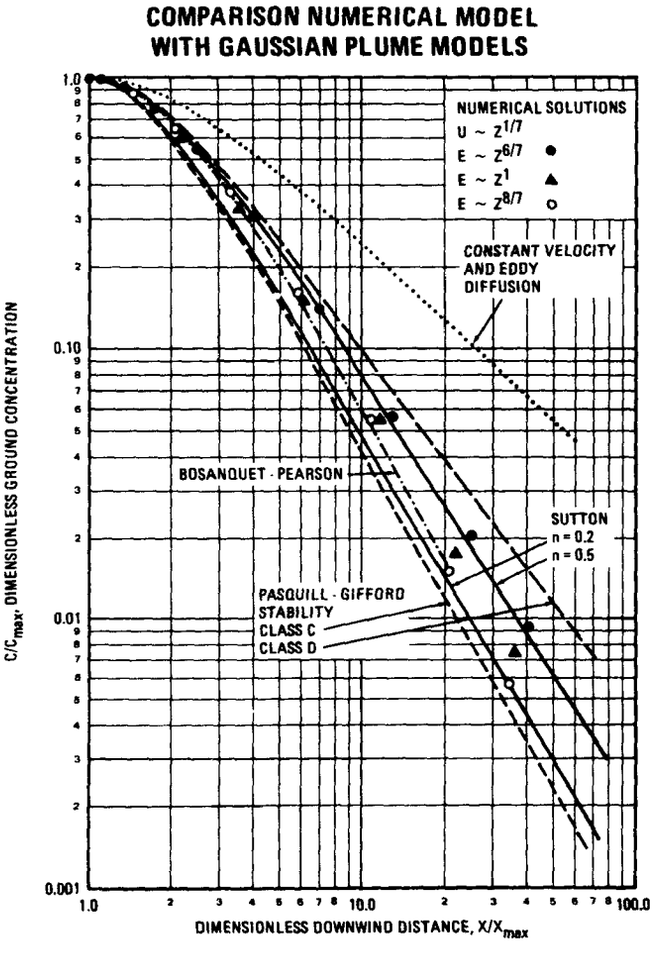
COMPARISON NUMERICAL MODEL
WITH GAUSSIAN PLUME MODELS
NUMERICAL SOLUTIONS
U ~ z^1/7
E ~ z^6/7
E ~ z^1
E ~ z^8/7
CONSTANT VELOCITY AND EDDY DIFFUSION
BOSANQUET - PEARSON
SUTTON
n = 0.2
n = 0.5
PASQUILL - GIFFORD
STABILITY
CLASS C
CLASS D
C/C_max, DIMENSIONLESS GROUND CONCENTRATION
DIMENSIONLESS DOWNWIND DISTANCE, X/X_max
1.0
0.10
0.01
0.001
10.0
100.0

TABLE I - POWER LAW FORMS WHICH

APPROXIMATE PASQUILL-GIFFORD STABILITY CLASSES

	A	B	C	D	E	F
Velocity Power	0.14	0.14	0.14	0.2	0.3	0.4
Diffusivity Power	1.76	1.38	1.14	1.0	1.0	0.67
E_{ref}, ft^2/s	2740	1140	550	440	360	310
E_z/E_y	10	2	0.7	0.2	0.05	0.008

The value listed as E_{ref} is for the horizontal cross-wind diffusivity at a reference elevation of 30 feet. As can be noted from Table I, there is roughly a factor of ten difference in the horizontal diffusivity over the range of atmospheric stabilities. Also apparent is the range in the ratio of vertical to horizontal diffusivities, E_z/E_y, necessary for the various stability classes. The ratio of E_z/E_y should approximate the square of the ratio of σ_z/σ_y and for a downwind distance of 10 km or so this appears to be the case. In addition, for the analogy to be complete, the diffusivity values should be a function of the mean windspeed. The values listed above for E_{ref} are for a windspeed of 1 MPH and should be increased or decreased in direct proportion to the mean windspeed at the reference height.

3.2 Comparison of Solution Techniques

Two solution techniques have been generally used for solving the turbulent diffusion equations. Basically, these techniques have evolved as a result of the primary interest being in two different classes of problems. In one class, advection or windspeed is the controlling influence. In such cases, the partial differential equations describing turbulent diffusion become controlled by first order space derivatives and are fundamentally hyperbolic in nature. For such applications, techniques involving (1) point tracking, (2) particle-in-a-cell, or (3) method of characteristics are advantageous. The model developed by Sklarew[8] is one of this type.

In the second class of problems, turbulent diffusion is of comparable importance to advection in spreading a trace quantity within the air flow. In such cases, the equations are parabolic in form and finite difference solution techniques are more advantageous. The INTERCOMP model[4] is of the latter type.

One of the difficulties in using finite difference approaches on advective controlled problems is that truncation error can result in an artificial diffusion term[9]. Higher order difference techniques can be used to reduce this effect, but at the expense of computing time and often stability of the difference technique[10]. There is a question, then, of when the standard finite difference techniques are adequate.

The aspect which allows the finite difference equations to be accurate for a broad range of turbulent diffusion to advection ratios is the lack of importance of the diffusivity in the primary wind direction. In Gaussian models, for example, diffusion in the downwind direction is normally neglected (unless it is an instantaneous release) because calculated answers are insensitive to the value of the downwind diffusivity. This fact leads one to suspect that a finite difference formulation would also be accurate. The effect of truncation error will be in the primary wind flow direction, but in that direction the value of total diffusivity is unimportant. Instead, it is the cross-wind and vertical diffusivities which are important in calculation of the concentration distribution. The proof of this contention is developed in the following paragraphs.

As a verification that the numerical model is not substantially influenced by truncation error, the model results for a constant diffusivity and velocity have been compared to the analytical solution for this case. This analytical solution solves the equation of one-dimensional forced convection (advection) and two-dimensional diffusion (cross-wind and vertical). This analytical solution is well-known. The effective stack height was taken as 1000 feet. The cross-wind diffusivity was 2000 $ft^2/sec.$; the vertical diffusivity was 500 ft^2/sec. The windspeed was 4 ft/sec. Block sizes in the downwind direction varied from 200 feet near the source to 6400 feet at the downwind extent of the grid. The results for concentrations along the plume centerline are shown in Figure 2. Two numerical model results are shown in Figure 2. The finite difference model is the one which represents the standard INTERCOMP air quality model. The results labeled point movement method are from a model similar to Sklarew's[8] which solves turbulent diffusion by a technique well suited to a high advection windspeed. As Figure 2 indicates, the point movement results are in slightly better agreement with the analytical solution plume centerline concentrations. The calculated results are not sufficiently different to warrant the increased computing costs, however.

Figure 3 is a similar plot of the groundlevel concentrations. The effect of space truncation error in the finite difference approach can be seen. However, the maximum concentration has been decreased only about 5% by numerical diffusion. In contrast, the point movement method was actually affected more than the finite difference method. This is probably

FIGURE 2

COMPARISON OF ANALYTICAL STACK HEIGHT CONCENTRATIONS TO MODEL CALCULATIONS VELOCITY AND EDDY DIFFUSIVITIES CONSTANT

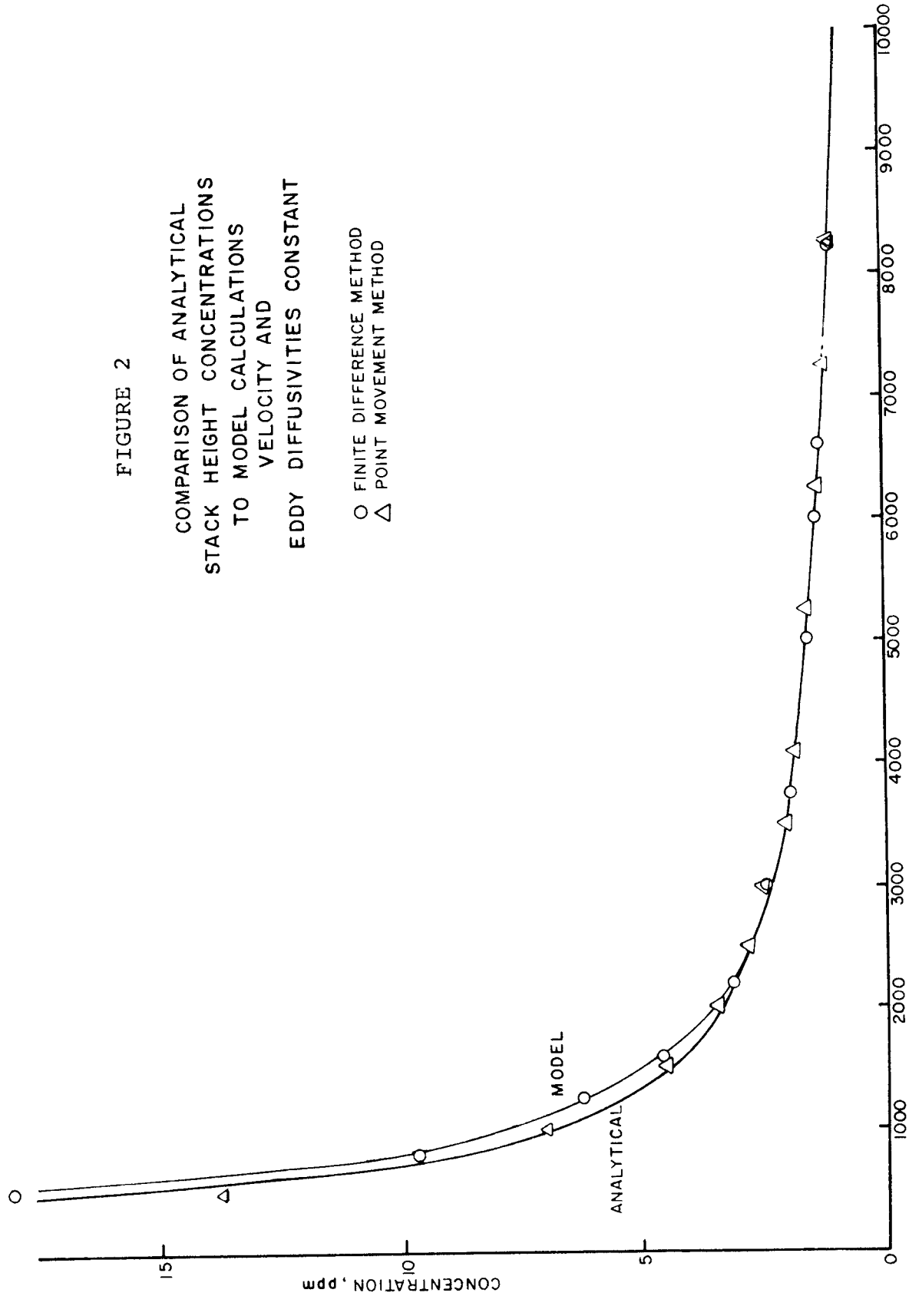

FIGURE 3

COMPARISON OF ANALYTICAL GROUNDLEVEL CONCENTRATIONS TO MODEL CALCULATIONS VELOCITY AND EDDY DIFFUSIVITIES CONSTANT

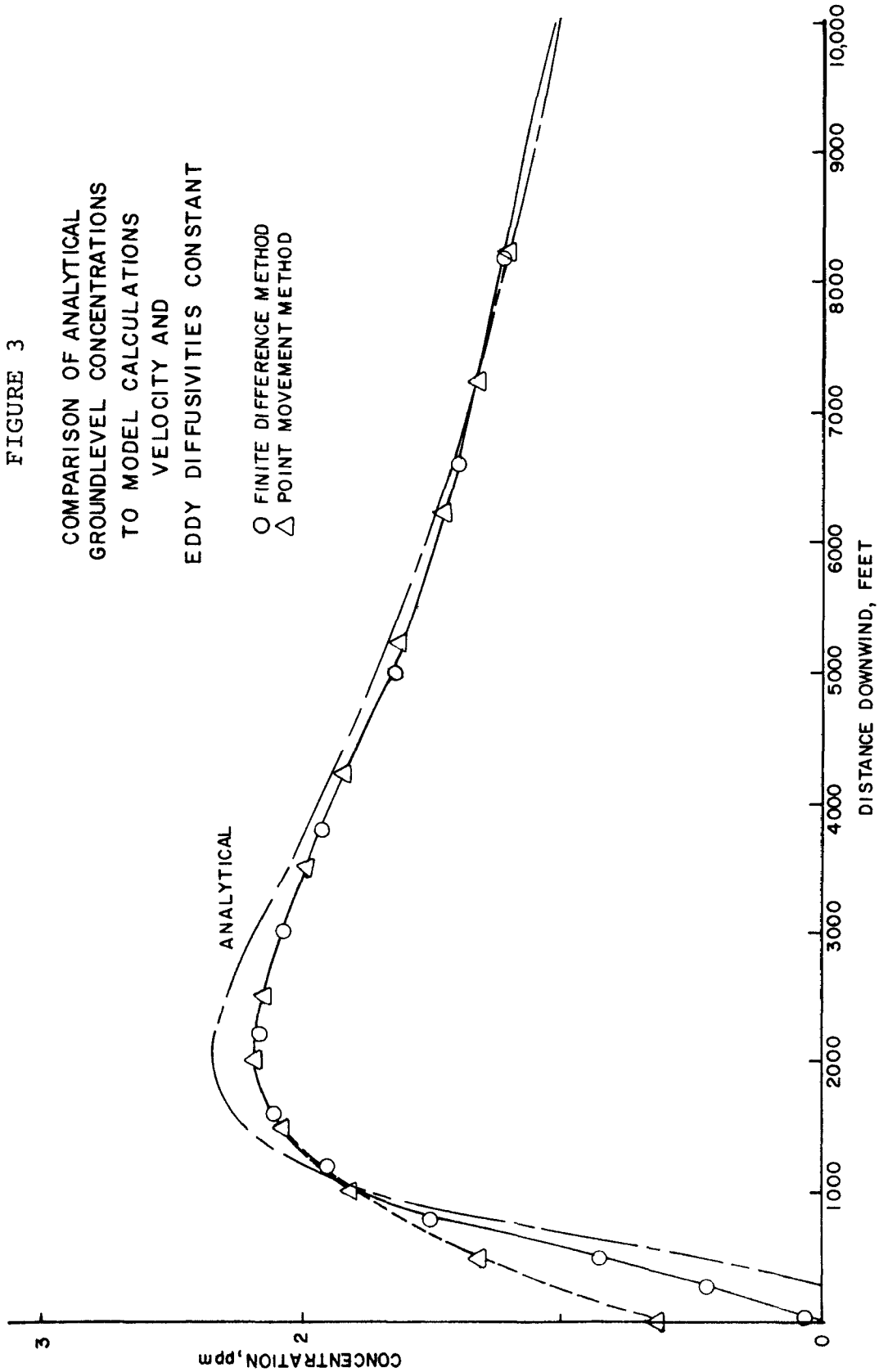

because the two ordinary differential equations solved by the point movement approach (advection then diffusion) are uncoupled. That is, the material is first advected then diffused. A part of the difference in Figure 3 is also due to the numerical calculation using a finite volume source as opposed to the analytical solution point source. It is apparent in Figure 3 that the finite difference solution can be of acceptable accuracy for air quality analyses.

It was mentioned earlier that power law variations of windspeed and diffusivity result in agreement of the turbulent diffusion approach with the Gaussian models. This is true with one important exception. On the upwind side of the maximum groundlevel concentration, the turbulent diffusion approach does give different results from the Gaussian models This is illustrated in Figure 4. Note that on the upstream side of the maximum, the groundlevel concentrations are significantly higher with the INTERCOMP model than they are with the Gaussian. To a large extent, this difference is due to the power law wind profile which gives lower windspeeds near the ground surface. The calculated concentrations in this region upwind from the maximum should better approximate the effect of surface roughness. The differences in Figure 4 are greatly exaggerated since it is plotted on log-log paper. If plotted on linear paper, the differences are not so apparent.

The resultant cross-wind concentration distributions are also different as a result of the volume source in the y-direction. Farther from the source, these differences become negligible as shown in Figure 5. The maximum deviation is for the one shown--namely the narrowest plume of class F stability.

There is strong evidence to indicate that measured results near the source are higher than Gaussian point source predictions. Plume rise or any surface roughness near the source result in much more rapid dilution than predicted by a stable Pasquill stability class. A recent summary by Bowne[11] illustrates modifications in the general shape of the dispersion coefficients to account for such effects. Such modifications are generally made to affect groundlevel concentrations for distances up to one kilometer. Such a modification which increased concentrations upwind of the one kilometer point would be in rough agreement with the results of Figure 4.

FIGURE 4

COMPARISON OF PASQUILL STABILITY CATEGORY E TO INTERCOMP MATCH OF THAT CATEGORY

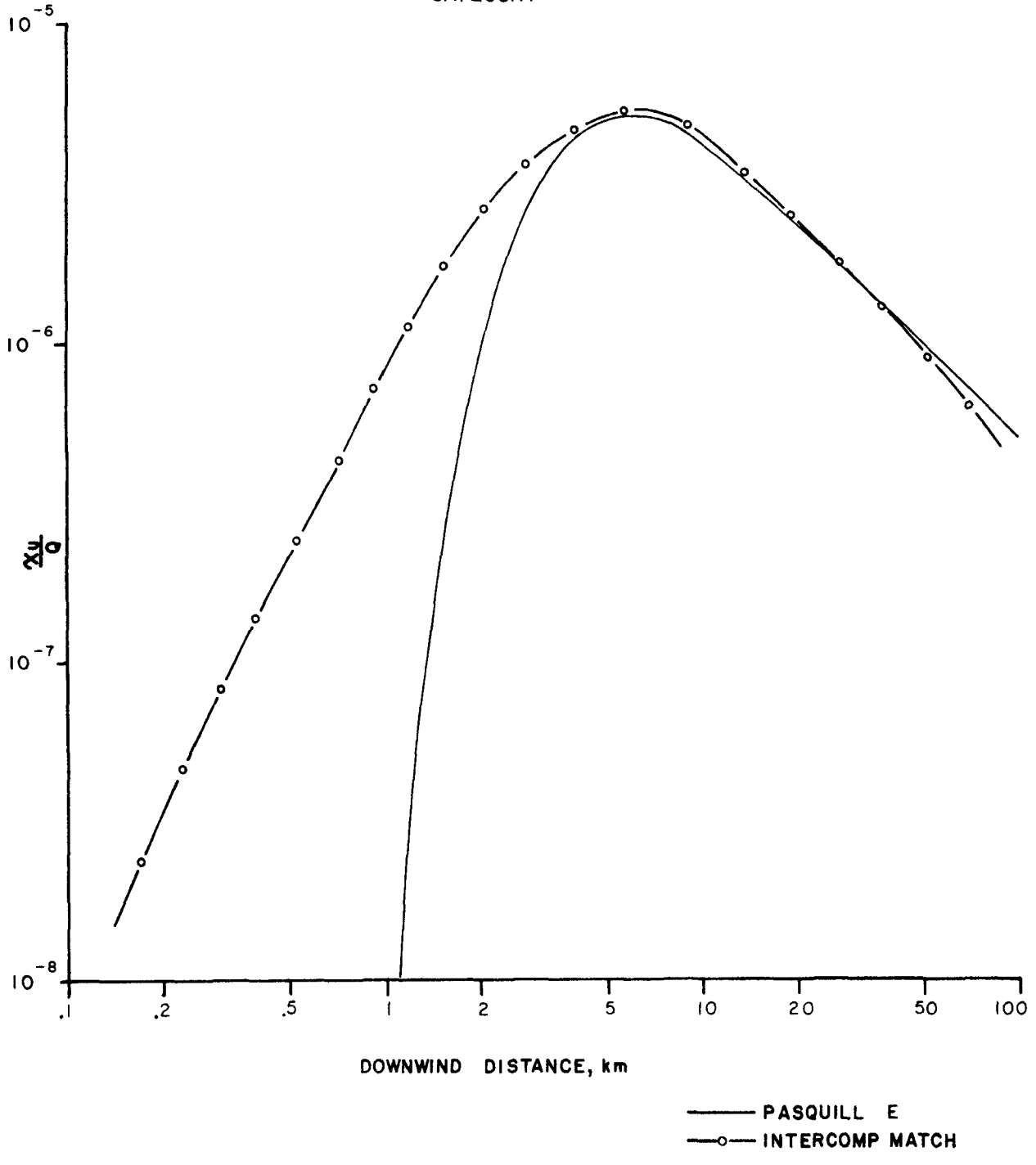

FIGURE 5

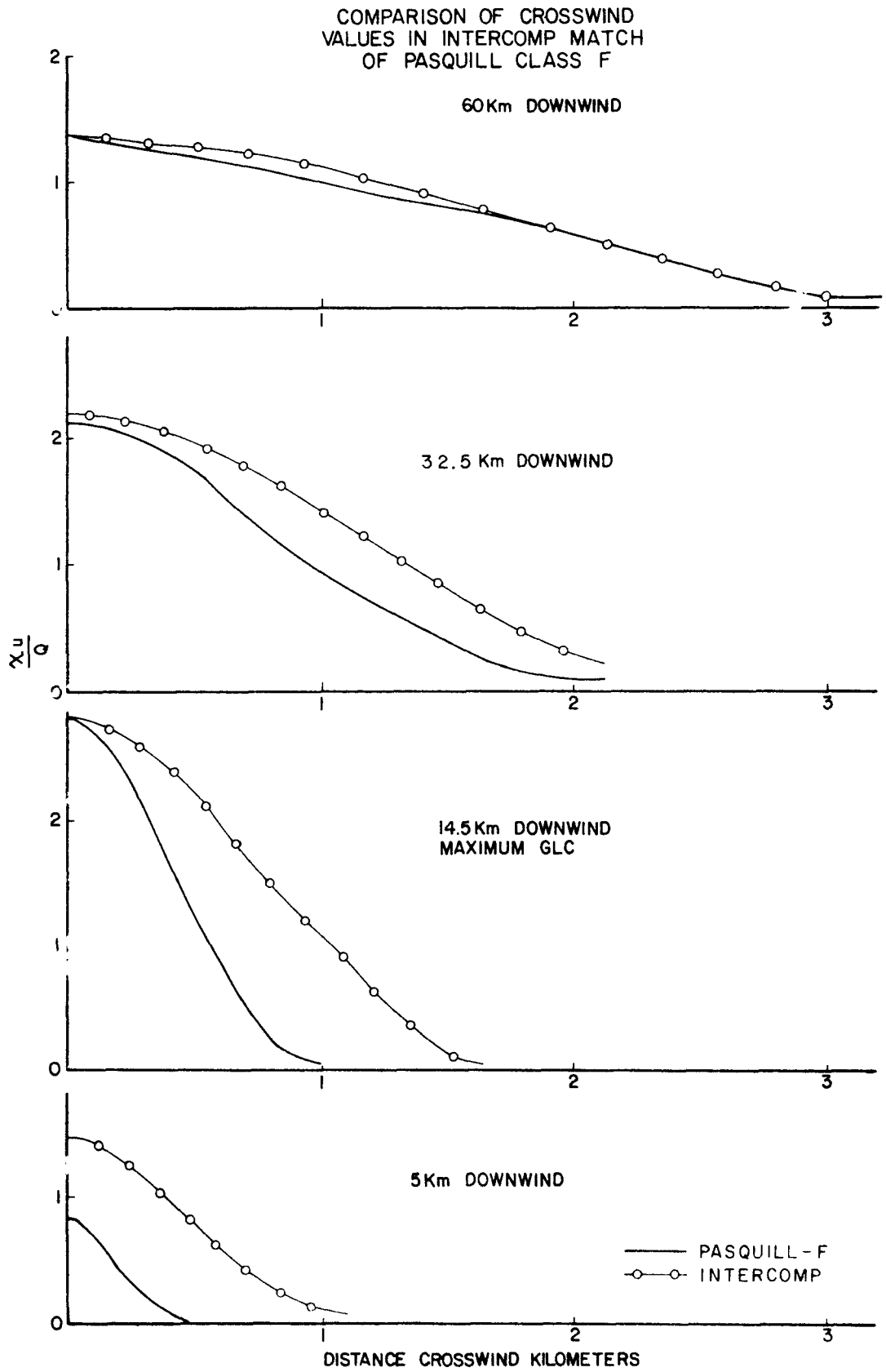
COMPARISON OF CROSSWIND
VALUES IN INTERCOMP MATCH
OF PASQUILL CLASS F
60Km DOWNWIND
32.5 Km DOWNWIND
14.5Km DOWNWIND
MAXIMUM GLC
5Km DOWNWIND
PASQUILL-F
INTERCOMP
χu/Q
DISTANCE CROSSWIND KILOMETERS

3.3 Comparison for Huntington Canyon Tracer Data

3.3.1 Data Collected

The data collected in Huntington Canyon by the Air Resources Laboratory (ARL) of the National Oceanic and Atmospheric Administration (NOAA) were intended to provide measurements of plume dispersion in rough, canyon type terrain for comparison with flat terrain results[6]. The survey was particularly oriented toward evaluating the plume centerline intersection assumption used by ARL in the meteorological report to the Department of Interior which was a part of the Southwest Energy Study[5]. A second objective was an evaluation of the dilution characteristics within a canyon.

The basic approach was to release SF_6 tracer and use mobile (helicopter) sampling for centerline dilution concentrations and fixed (canyon wall and floor) sampling for the impaction validation. No attempt was made to gather extensive meteorological data in the canyon. Wind and temperature data sufficient to describe diffusion stability classes were the meteorological data collected.

The tracer releases were made at two points. Elevated releases during lapse to neutral stability conditions were made from the top of the stack. Wind flows during such conditions were generally up-canyon. The second point of tracer release was from the canyon floor and wall at a distance of about 10 km up the canyon from the power plant stack. These releases were during strong temperature inversions and were always down-canyon flows.

The approximate tracer plume position was tracked by a cloud of white smoke emitted from a smoke generator. This enabled photographic coverage of the plume as well as plume centerline positioning for the helicopter sampling.

The helicopter samples were one-minute samples collected by an air pump which drew samples through a hose hanging 28 m below the aircraft. The ground samples were cumulative over the duration of each test run and were processed to approximate a one-hour average concentration.

3.3.2 Geographical Setting

Figure 6 is an illustration of the terrain in Huntington Canyon looking north up-canyon from behind the power plant. The various side canyons are shown and indicated by names including on the west side, Maple Gulch, Deer Creek, Meetinghouse, North Fork, Rilda, Mill Fork, and Little Bear. On the east side of Huntington Canyon, the main side canyons are Fish Creek, Bear Creek, and

FIGURE 6

HUNTINGTON CANYON TERRAIN

UP-CANYON ORIENTATION

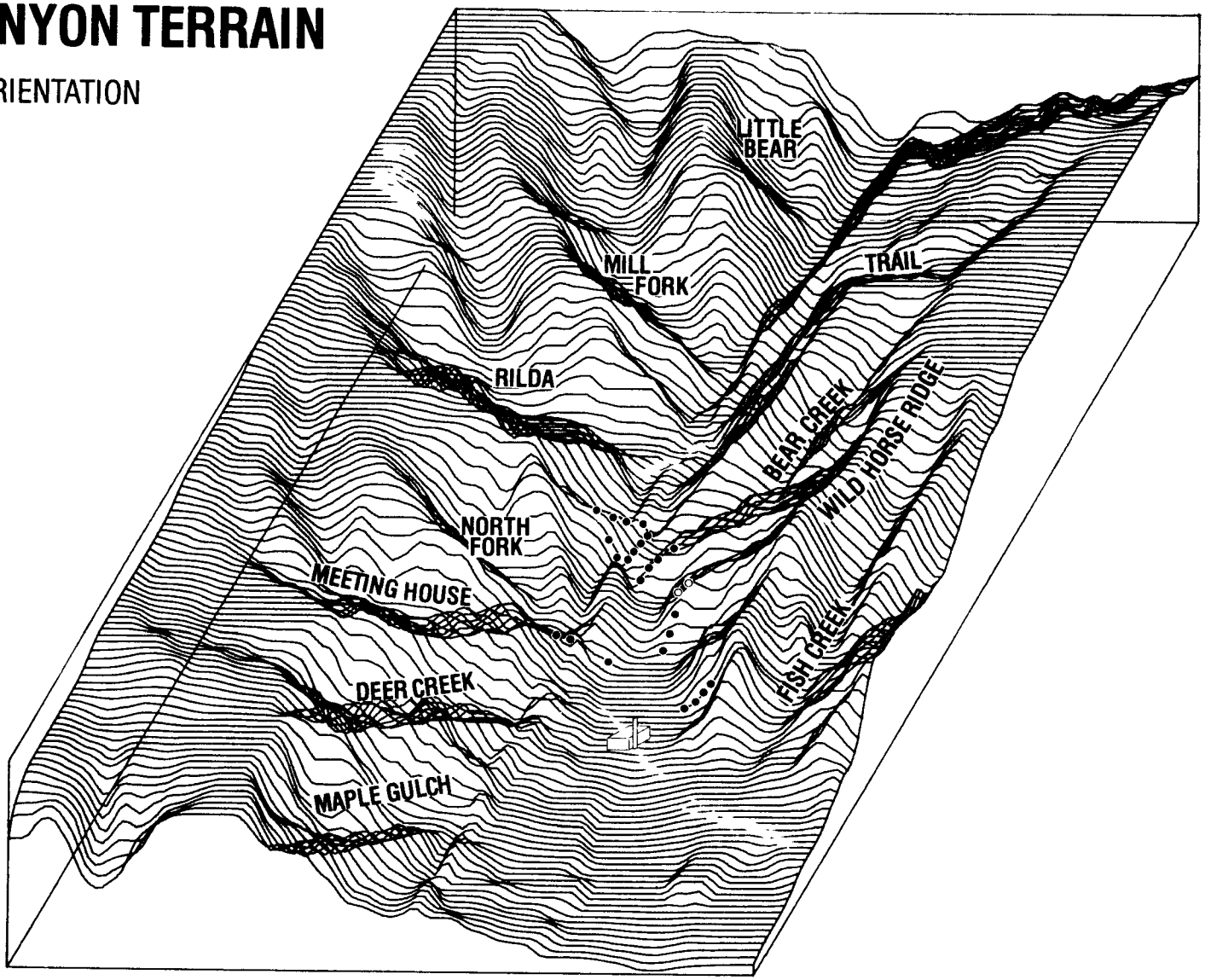

Trail. Wild Horse Ridge is also a prominent topographical feature.

The terrain illustrated in Figure 6 was prepared as a Calcomp plot from the digitized terrain file. This file can be used as input to the INTERCOMP air quality model and a plot of the type shown is normally made to verify that the digitized terrain is an adequate representation of the actual topography. There is a 2:1 vertical to horizontal exaggeration of the distance scales in Figure 6.

Also shown by solid circles in Figure 6 are the monitor locations for measuring SF_6 concentrations during the stack top releases. Moving up-canyon, the first set of four monitors just east of the plant is called Fish Ridge. Continuing up the east side of the canyon, the next set of three were known as White Ridge. The next two monitors indicated by open circles are actually in the draw behind White Ridge and were called the Wild Horse Draw monitors. The four monitors located on the south side of Bear Creek were called Wild Horse. The four on the north side were known as Bear Creek.

On the west side of Huntington Canyon, the monitor located near the flat part of the canyon was called the Meetinghouse - Dear Creek Station. The two monitors located higher up on the ridge between Meetinghouse and Deer Creek Canyons were known as the Blizzard stations. Further up the canyon between the North Fork and Rilda canyons, two monitor lines were located. On the vertical east face two monitors were located and called Red Face. The four located down the northerly slope were called Wet Man.

Figure 7 is a similar plot, but looking in a southerly direction down Huntington Canyon. Again the side canyons and ridges are shown. Two release points were used in the down-canyon orientation. These release points are indicated by the solid triangles -- one on the canyon floor and the other about 160 meters up the canyon wall. Two monitor locations were on the canyon floor downwind from the release point. These monitors were called 0.4 and 0.8 (apparently because they were about 0.4 and 0.8 miles downwind from the source). On the west side of the canyon along a rather vertical wall, four monitors termed the Trail station were located. On the opposite side along the north rim of Mill Fork Canyon there were three monitors called Mill Fork. Two sets of monitor stations farther down the canyon were used. These were the Wet Man and the Bear Creek stations described earlier.

FIGURE 7

HUNTINGTON CANYON TERRAIN

DOWN-CANYON ORIENTATION

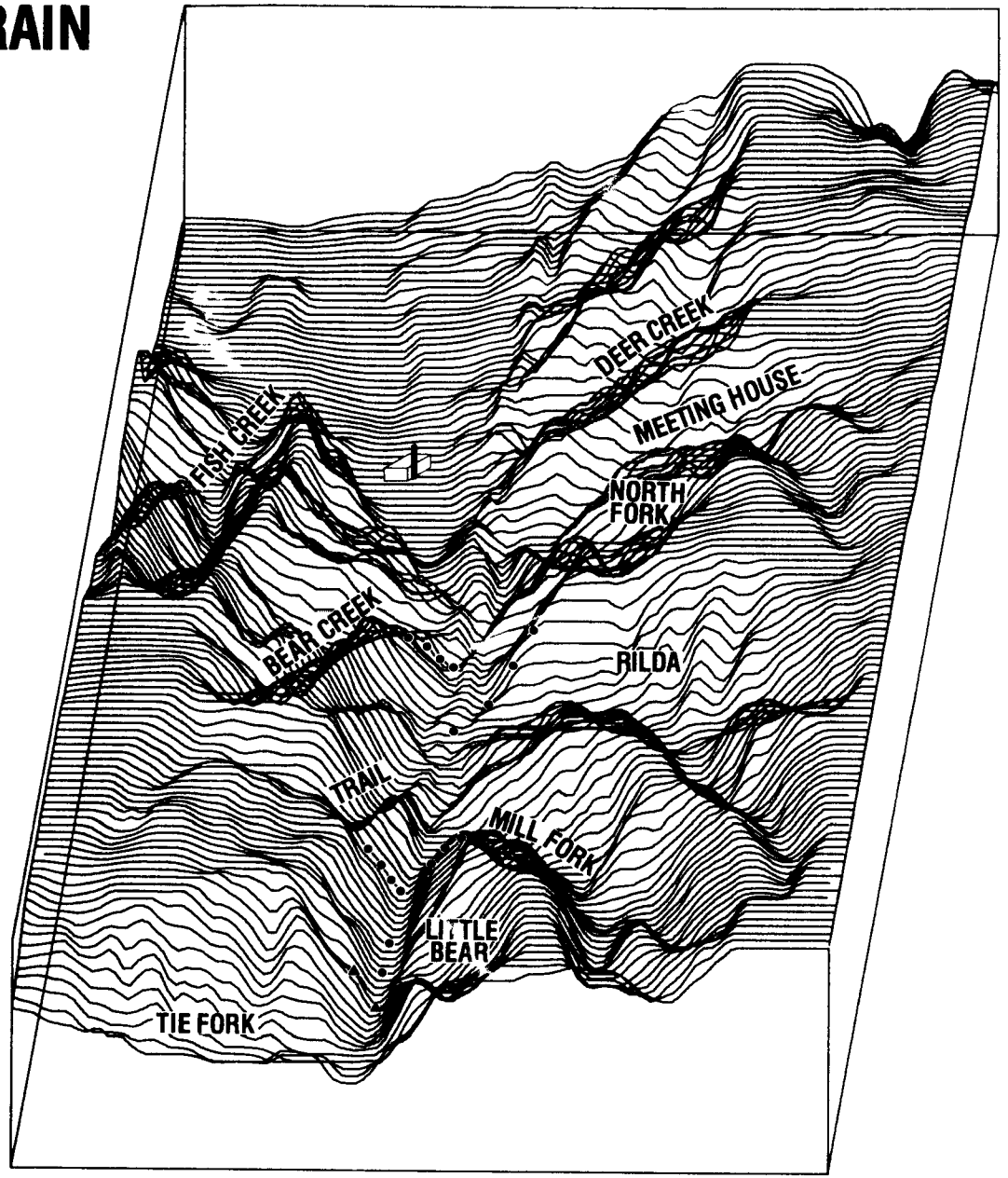

Both the up-canyon and down-canyon orientations emphasize the roughness of the terrain. Though the monitor coverage in both the vertical and crosswind directions are by no means complete, they do represent excellent data to test the centerline impaction concept. The plume dispersion in terrain such as Huntington Canyon presented a severe test of the calculational models.

3.3.3 Comparisons for a Stable Down-Valley Flow

Five down-valley tests were performed. Four were canyon floor releases and the other was an elevated canyon wall release. The various tests were classified as to stability by NOAA personnel. Surface windspeed were available at several points as well as the apparent oil fog velocities during the tracer releases. Measured temperature gradients and cloud cover were also available.

A summary of the tracer release rates, the effective windspeeds (from oil fog measurements), and the NOAA stability classifications are given in Table II. The first six tests were up-valley flows from stack top releases. The seventh test was a down-valley flow from a canyon wall release. The next four tests were down-valley flows from canyon floor releases. Also listed in Table II are the wind directions representative of each test. In general the wind direction included in Table II is a composite of the several measuring points with most weight given to the stack top anemometer. Before showing comparisons between calculated and measured values, a few comments are in order.

TABLE II - SUMMARY OF TEST CONDITIONS

HUNTINGTON CANYON

Test No.	SF_6 kg	Release Time Min.	gm/sec	Effective Wind u,m/sec	Effective Wind Direction	Stability Class
1	5.99	52	1.92	4.3	140°	B
2	5.19	44	1.97	4.5	120°	D
3	5.78	49	1.97	2.3	130°	D
4	3.54	90	0.65	10	140°	D
5	5.19	44	1.97	5.3	150°	D
6	6.60	56	1.97	3.8	110°	D
7	7.48	45	2.77	2.9	350°	F
8	6.92	48	2.40	1.8	240°	F
9	7.48	60	2.08	7.9	340°	F
10	4.65	33	2.35	3.2	300°	F
11	6.35	35	3.02	3.0	310°	F*

*NOAA personnel considered much, if not all, of the stable flows to be more stable than F.

Specific wind directions at the release point in the canyon were not included in the NOAA report. Anemometer data at the plant site indicated winds were from the NNW quadrant during the down-valley flow tests. For INTERCOMP model runs, there was little sensitivity to input wind direction. The calculated winds were for all practical purposes forced by the terrain to follow the canyon orientation.

In the case of the Gaussian (NOAA) model, wind direction is extremely important. Several assumptions could be made regarding the location of the plume centerline. Some of them can be summarized as follows:

(1) The plume could be assumed to flow horizontally at the release elevation and down the centerline of the canyon.

(2) The plume centerline could be assumed to flow along the canyon floor and down the centerline of the canyon for the canyon bottom releases.

(3) The plume could be assumed to flow horizontally and vertically without deviating until it encounters the canyon walls.

The first and last assumptions listed above probably represent how the Gaussian model would have been used if this were totally a prediction without the benefit of experimental observations. These results would not even be close to the measured concentrations. From inspection of the tracer results, assumption (2) appears to be most representative and this is the one we have used. One additional restriction was used in connection with the Gaussian models. No accounting was made for canyon sidewall reflection. This would cause calculated concentrations to be lower than they should be. As the results will indicate, however, the Gaussian model calculations were generally high and thus an unfavorable bias was not introduced.

The measured and calculated results for down-canyon flow Test 10 are shown in Table III. The results shown in Table III are all ground surface values. NOAA also attempted to make plume centerline measurements with a helicopter; however, for the canyon floor releases (such as Test 10) the aerial samples gave lower readings than the measured groundlevel results. As a consequence, these values are not summarized in Table III.

TABLE III - COMPARISON MEASURED AND CALCULATED GROUNDLEVEL VALUES

TEST NO. 10 - DOWN-CANYON - F STABILITY

Location	Elevation Ft.	Measured $\mu g/m^3$	Calculated, $\mu g/m^3$		
			INTERCOMP	EPA	GAUSSIAN
0.6 km	7170	25	186	210	(1200)
1.2 km	7120	35	80	65	(370)
Trail(1)	7120	9.5	15		40
(2)	7250	19.0	14	25.4	1 (140)
(3)	7870	-	0.5		0
(4)	8200	-	0.0		0
Mill Fork(1)	7010	3.7	5.0		50
(2)	7250	3.4	2.5	13.6	0 (80)
(3)	7700	-	0.0		0
Rilda(1)	6940	6.1	5.5		50
(2)	7240	2.1	2.0	8.5	0 (50)
(3)	7550	-	0.2		0
(4)	7950	-	0.0		0
Bear Creek(1)	6790	3.4	3.5		30
(2)	6910	2.8	2.5	6.2	9 (30)
(3)	7090	-	1.5		1
(4)	7170	-	0.2		0.3
Wet Man(1)	7170	-	1.5		30
(2)	7330	-	0.5	6.2	3 (30)
(3)	7400	-	0.0		0
(4)	7650	-	0.0		0

In Table III, only centerline concentrations have been tabulated for the EPA model. The corresponding NOAA centerline values are shown in parenthesis under the label Gaussian. There is no reason to evaluate crosswind values for the EPA model since the 22.5° angular segment averaging essentially fills the canyon to the 8000 ft. elevation point. As a consequence, the EPA model would predict uniform concentrations throughout the canyon width comparable to the calculated values listed.

The INTERCOMP model since it is a finite difference type calculation has predicted concentrations in each grid block and thus can be compared more easily on a point-by-point basis. The wind flow model has predicted correctly that peak concentration levels do follow the canyon floor (an assumption that was used in the Gaussian models). The values corresponding to individual measured points are tabulated in Table III and a contour plot is shown in Figure 8. The tabulations in Table III are actually read from the contour plot of Figure 8, with the exception of those values greater than 10 $\mu g/m^3$.

Figure 8 - **DOWN-CANYON TEST NO. 10**

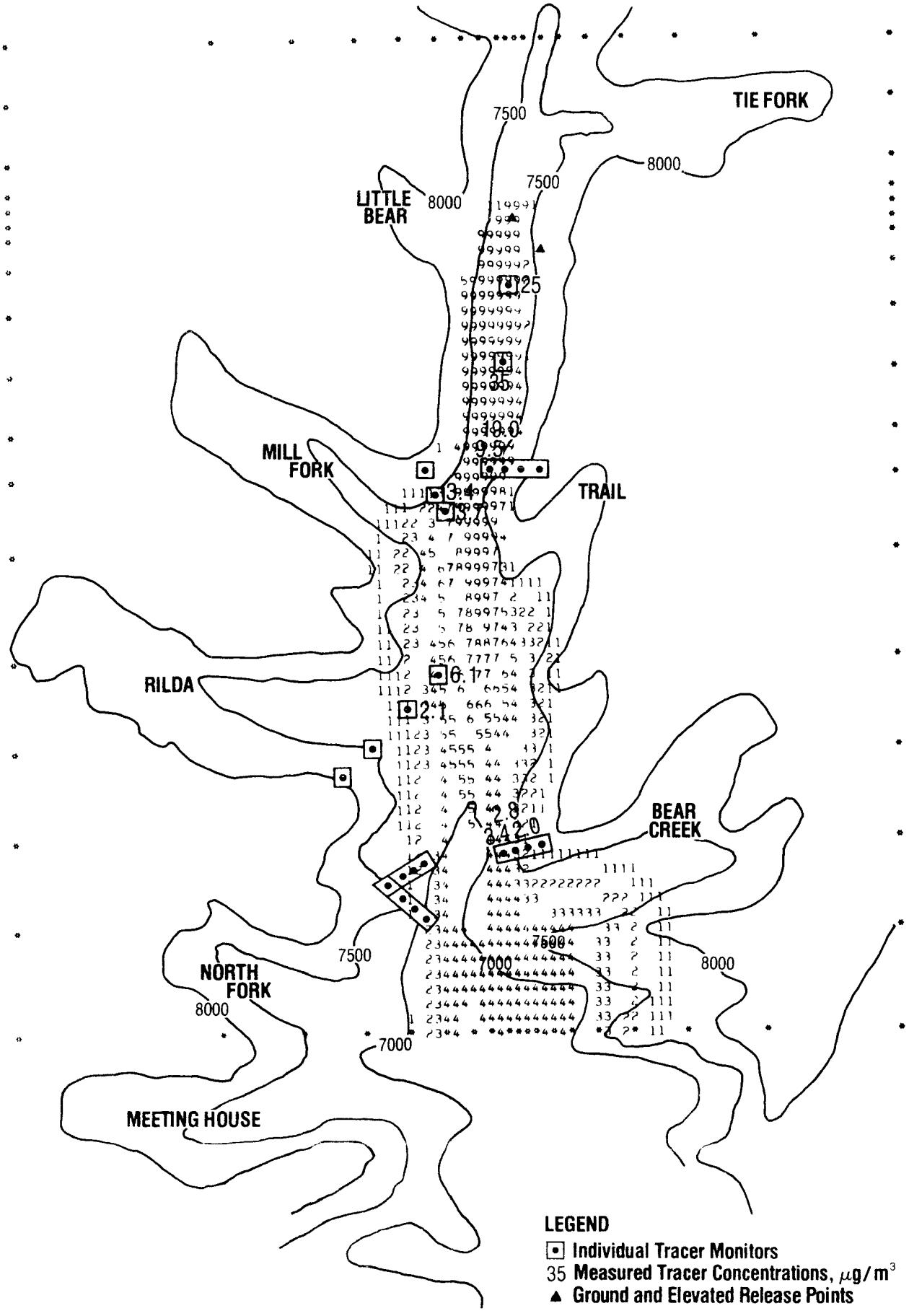

The INTERCOMP model results were calculated using the parameters of Table I for Pasquill F stability. The calculated average windspeed in the grid block nearest the canyon floor was matched to the observed effective smoke cloud speed. The relative magnitude block sizes used in both the downwind and cross-wind directions can be seen from Figure 8. The asterisks surrounding the plot correspond to the position of the grid block centers. As is evident, the grid definition of the canyon floor was much finer in detail than that describing the higher elevations. The plotted concentration contours have been normalized by dividing by 10 $\mu g/m^3$. Thus, the band of 1's represent concentrations between 0.05 and 0.1 of the 10 $\mu g/m^3$ or 0.5 to 1.0 $\mu g/m^3$, the 2's band are 1.5 to 2.0 $\mu g/m^3$ and proceeding up to the 9's band which represents any concentration greater than 8.5 $\mu g/m^3$. The blank contours separating the number contours represent the intermediate concentration levels. For example, the blanks between the 1's and 2's represent concentrations of 1.0 to 1.5 $\mu g/m^3$.

The position of the tracer monitors have been located as nearly as possible to their actual position and vertical height. The plotted concentrations are calculated groundlevel concentrations regardless of the particular grid block in which groundlevel was located. That is, a search of the complete three-dimensional grid block concentrations has been made to determine the concentration in those grid blocks which correspond to the ground surface--these are the values contoured in Figure 8.

As evident from Figure 8, the tracer plume follows the canyon alternatingly expanding and shrinking in width as it is effected by the side canyons. In Table III, measured concentrations have been tabulated only for those monitors which were listed. Monitors for which no measurement was listed were either below some minimum threshold for accurate analysis or were not analyzed. These monitor points are denoted by a dash in Table III. The calculations do agree reasonably with the concept that concentration levels at these unlisted monitor points were low. As examples, measurements at the entire Wet Man sampling network were not listed. The calculations tend to support this although concentrations on the order of 0.5 to 1.5 $\mu g/m^3$ appear at the lower two elevation monitors. Similarly, the calculation indicates a concentration slightly less than 0.5 $\mu g/m^3$ at the highest Bear station which also was unlisted. Similar results were obtained at other stations with the highest elevation monitors being located above any significant calculated concentration levels.

As a summary, we consider the comparison between INTERCOMP calculated concentrations and the measurements of Test No. 10 to be quite good. Not all of the other

comparisons were that good as will be noted later. The Gaussian type models, both EPA and NOAA, gave calculated concentrations significantly higher than observed for Test 10. Also the vertical and horizontal distribution in calculated concentrations from the INTERCOMP model is much better than that predicted by the Gaussian (NOAA) model.

3.3.4 Comparison for a Neutral Up-Valley Flow

Similar calculations have been made for the neutral up-valley stack release tests. Test 5 was selected for a detailed comparison since we had the actual tabulated data for this test. The average wind direction at stack top during this test was 150° with a measured speed of 6.3 m/sec. The observed effective smoke cloud windspeed from Table II was 5.3 m/sec. and the measured wind at about 10 m was 2.6 m/sec. The calculated windspeed in the INTERCOMP model was about 2.6 m/sec. at the 10 m elevation, but with D stability conditions, the calculated windspeed at stack top was slightly less than 5 m/sec.

The INTERCOMP calculated concentration contours are shown in Figure 9. The wind direction used in the calculation was 150° (true). Again the grid block centers are shown by the asterisks. Note the drastic effect of terrain on the concentration contours. The predominent flow calculated is directly up the main part of Huntington Canyon with apparently lesser flows moving up the Meetinghouse and Bear Creek canyons. Calculated concentrations are in quite good agreement with the measured values. The calculations indicate the plume is interacting (but not centerline intersection) substantially at the ridge on which the White Ridge monitors are located. As will be seen later, however, the calculated concentrations on the ridge are about one-half the centerline values at this downwind distance.

Tabulated comparisons between the models are illustrated in Table IV. The EPA and Gaussian results are calculated groundlevel concentrations for a plume which remains 183 m (600 ft.) above the ground surface (consistent with the NOAA model assumption for neutral stability). The Gaussian results have been calculated as this model would have been used in a predictive mode. That is, the measured stack top wind direction of 150° and the effective windspeed of 5.3 m/sec. were used. Reemphasizing the point made earlier, the plume was assumed to remain 183 m (the release height) above any receptor. That is, there is no reduction in calculated concentrations for the relative vertical positions of the monitors only a cross-wind reduction. Also shown in Table IV for the Gaussian model are the groundlevel centerline values in parentheses. The centerline values for the Gaussian model were included to provide an indication of the maximum calculated concentration levels for comparison with the measurements.

Other wind flow assumptions could have been used for the Gaussian model. The similar assumption as that used in the down-valley stable cases (horizontal flow along the minimum elevation canyon centerline) gives somewhat better agreement with the measurements. However, as the centerline values of Table IV show, the peak predicted concentrations of the Gaussian models are located too far from the stack.

The INTERCOMP model, on the other hand, predicts a maximum at about 2 km downwind consistent with the observations. The reason the INTERCOMP calculated maximum is closer to the source occurs because of the terrain rise in the downwind direction.

No attempt has been made to calculate the cross-wind decrease in concentrations for a point-by-point comparison of the EPA model with the measurements. This model because of the angular sector averaging still gives relatively uniform predictions throughout the width of the canyon.

TABLE IV - COMPARISON MEASURED AND CALCULATED GROUNDLEVEL VALUES

TEST NO. 5 - UP-CANYON

Location	Elevation Ft.	Measured $\mu g/m^3$	Calculated, $\mu g/m^3$		
			INTERCOMP	EPA	GAUSSIAN
Deer Cr-Mtnghouse	6650	0.2	0.5	0.01	0.0 (0.02)
White Ridge (1)	6740	1.2	1.0		0.01
(2)	6870	1.0	1.0	0.03	0.03 (0.04)
(3)	7080	-	0.5		0.04
Wild Draw (1)	6750	1.6	1.2	0.07	0.09 (0.11)
(2)	6960	0.8	1.5		0.11
Wild Horse (1)	6650	1.0	1.0		0.0
(2)	6740	1.3	1.2	0.08	0.0 (0.15)
(3)	6900	1.2	1.2		0.0
(4)	7360	1.0	1.0		0.0
Bear Creek (1)	6790	0.6	1.0		0.0
(2)	6910	0.7	1.0	0.17	0.0 (0.33)
(3)	7090	0.6	1.0		0.0
(4)	7170	0.4	1.0		0.0
Red Face (1)	6950	0.3	0.5	0.17	0.0 (0.33)
(2)	7380	0.4	0.5		0.0
Wet Man (1)	7170	0.1	0.7		0.0
(2)	7330	0.1	0.6	0.18	0.0 (0.37)
(3)	7400	0.2	0.5		0.0
(4)	7650	-	0.1		0.0

FIGURE 9

UP-CANYON TEST NO. 5

150° S. WIND

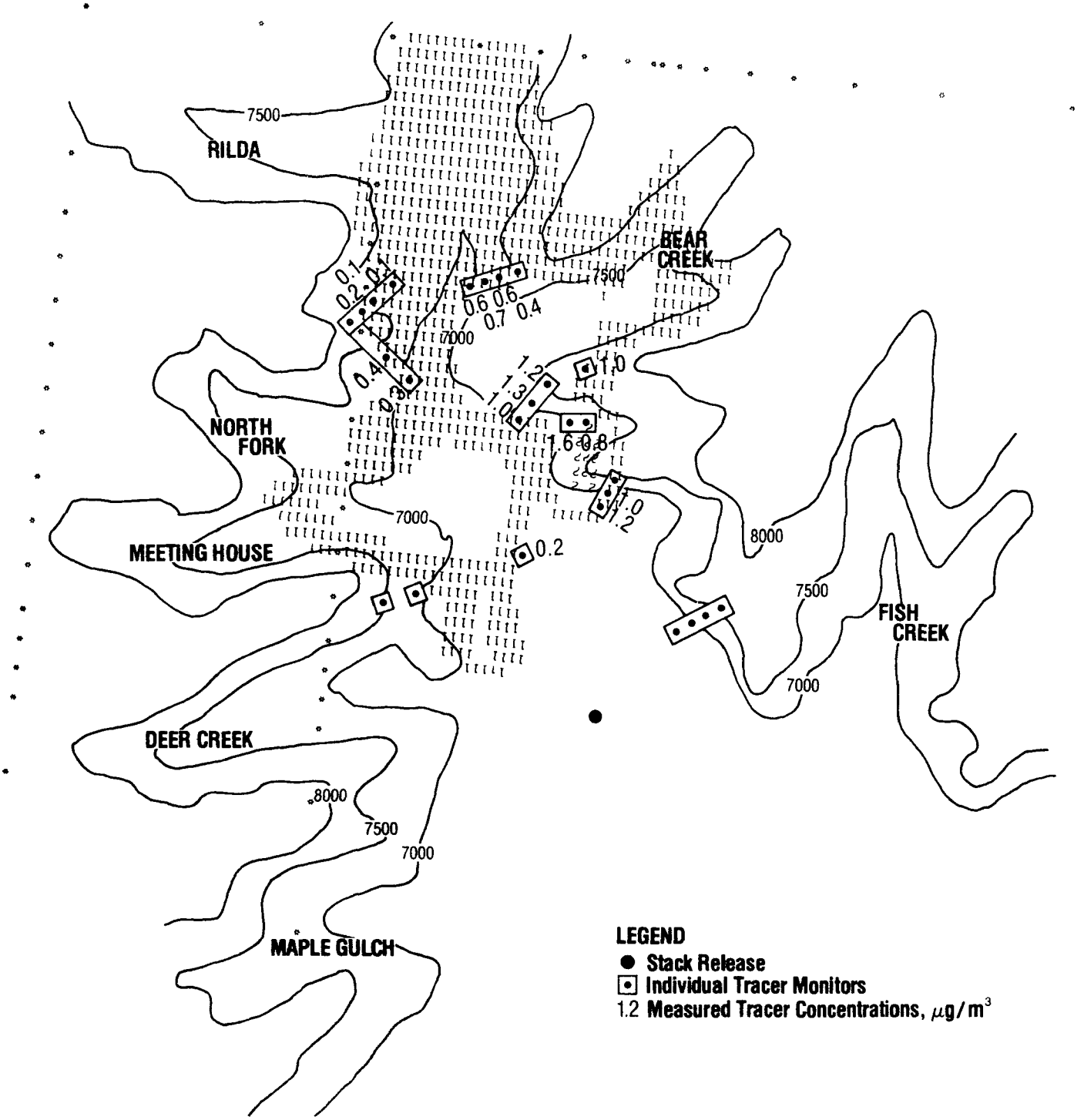

TABLE V - COMPARISON MEASURED AND CALCULATED CENTERLINE VALUES

TEST NO. 5 - UP-CANYON

Location	Measured $\mu g/m^3$	Calculated, $\mu g/m^3$		
		INTERCOMP	EPA	GAUSSIAN
H-1 (0.8 km)	32	10		38
H-2 (1.7 km)	5.7	2.5		13
H-3 (3.9 km)	1.4	1.0		4
H-5 (1.3 km)	3.2	3.7		15
H-6 (1.8 km)	7.6	2.4		12
H-7 (2.8 km)	1.1	1.3		6

A comparison of helicopter measurements and calculated centerline concentrations for Test 5 is presented in Table V. For the range of distances included in Table V, the concentrations for Gaussian centerline values are for all practical purposes one-half those for a ground release. Beyond 10 km, ground reflection begins to affect the centerline values and the reduction over that of a ground release is less than one-half.

Figure 10 presents the sensitivity of the INTERCOMP results to input wind direction. In this calculation, the specified wind direction was 135° which is more in line with the canyon axis. For this case the calculated plume is more narrow and results in slightly lower concentrations at the monitors. Calculated plume centerline values were, however, higher. A wind direction of 135° does not give as good a match as the results of Figure 9 for a 150° wind direction.

A summary plot in the usual Gaussian form of $\chi u/Q$ is shown in Figure 11 for both Tests 5 and 10. In Test 5, Gaussian results are shown for the groundlevel centerline concentrations. The upper dashed curve for Test 5 are the Gaussian results for a ground release. As mentioned previously, a reduction by a factor of two in this curve at a downwind distance of 10 km or less would approximate the plume centerline predictions. Note that this represents a conservative upper envelope for the aerial samples. The INTERCOMP plume centerline predictions are shown as the solid curve extending diagonally toward the upper left-hand corner. These results appear to represent more of an average value of the helicopter results. This is undoubtedly a reflection of the extremely short-term (one minute) samples whereas the diffusivities used in the INTERCOMP model more nearly represent 15-minute to one-hour time averages.

FIGURE 10

UP-CANYON TEST NO. 5

135° S. WIND

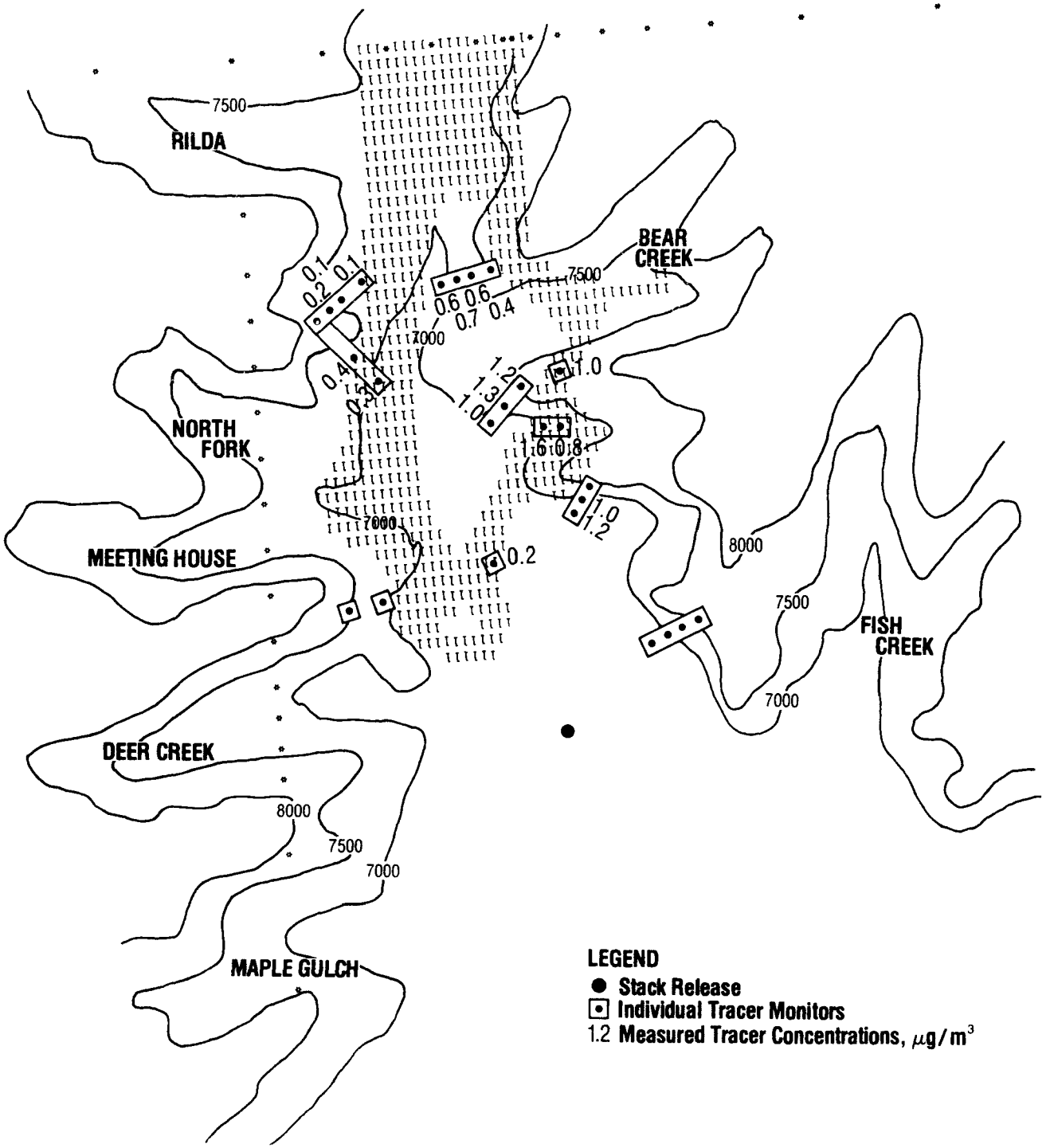

FIGURE 11

COMPARISON OF MEASUREMENTS WITH CALCULATIONS

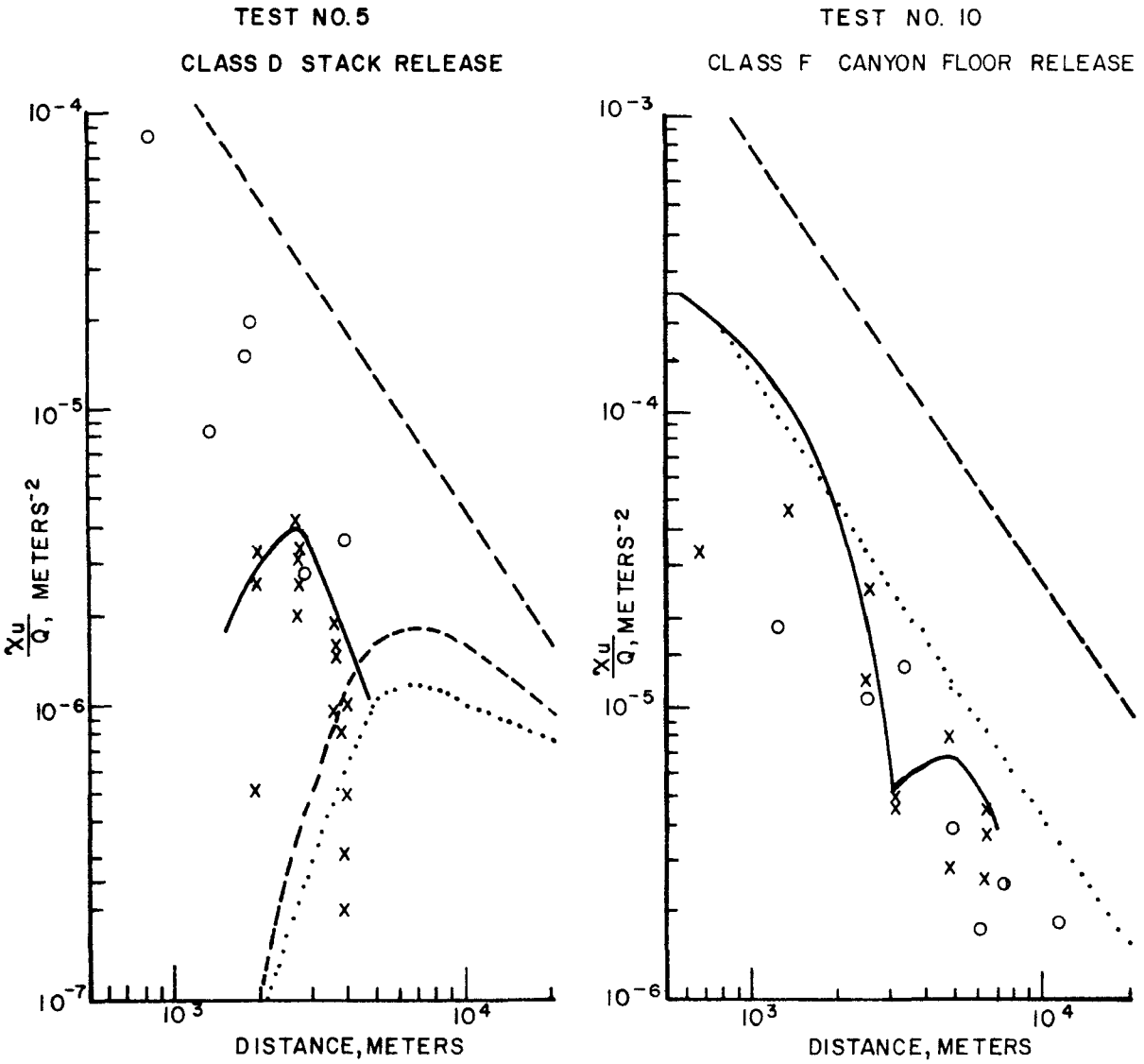

The Test 10 Gaussian results represent the plume centerline for a ground release. The INTERCOMP model results plotted are the peak concentration predicted at any of the monitoring sites downwind. The break in the curve occurs primarily because the plume is narrow at the Mill Fork monitor site and does not affect significantly the monitor positions. The plume has widened out by the time it reaches the Rilda site and now envelops the lower elevation monitor points.

3.3.5 Other Test Comparisons

Figure 12 illustrates a plot of $\chi u/Q$ values for Tests 1 and 7. Test 1 was the only up-valley flow, stack top release which had other than neutral class D stability. Test 7 was the only down-valley flow which was an elevated release along the canyon wall instead of from the canyon floor. During Test 7, the plume moved upward along the shaded wall due to natural convection. Thus, none of the models performed well in simulating this behavior.

We have chosen to show the Gaussian curves which were presented in the NOAA Huntington Canyon report. In addition, since both Test 1 and Test 7 were elevated releases, we have added the calculated Gaussian curves for an elevated release. Calculations for both the EPA and NOAA models have been included on an elevated release for Test 1. Note that for Test 1 with class B stability, there is only a small difference between the EPA and NOAA models.

The comparison between each of the models for Test 1 is reasonably close. Again the INTERCOMP calculations have a maximum nearer the stack than the Gaussian models and then it decreases more abruptly with downwind distance. This is undoubtedly the effect of rising terrain in that directions.

Calculated ground concentrations for Test 7 are interesting from the standpoint that the Gaussian models predict no increase of groundlevel values with distance over the range in which the monitors were located. This is because the release was at a 163 m height. The INTERCOMP model, however, does predict significant concentrations at ground surface. The tendency is to predict too low concentrations near the source and too high concentrations farther from the source. The INTERCOMP model also underestimated centerline concentrations near the release. This was probably due to the finite volume source represented by a grid block instead of the more nearly point release of the tracer. The high predictions farther from the release were undoubtedly due to the model neglecting the natural convective flow along the shaded wall.

FIGURE 12

COMPARISON OF MEASUREMENTS
WITH CALCULATIONS

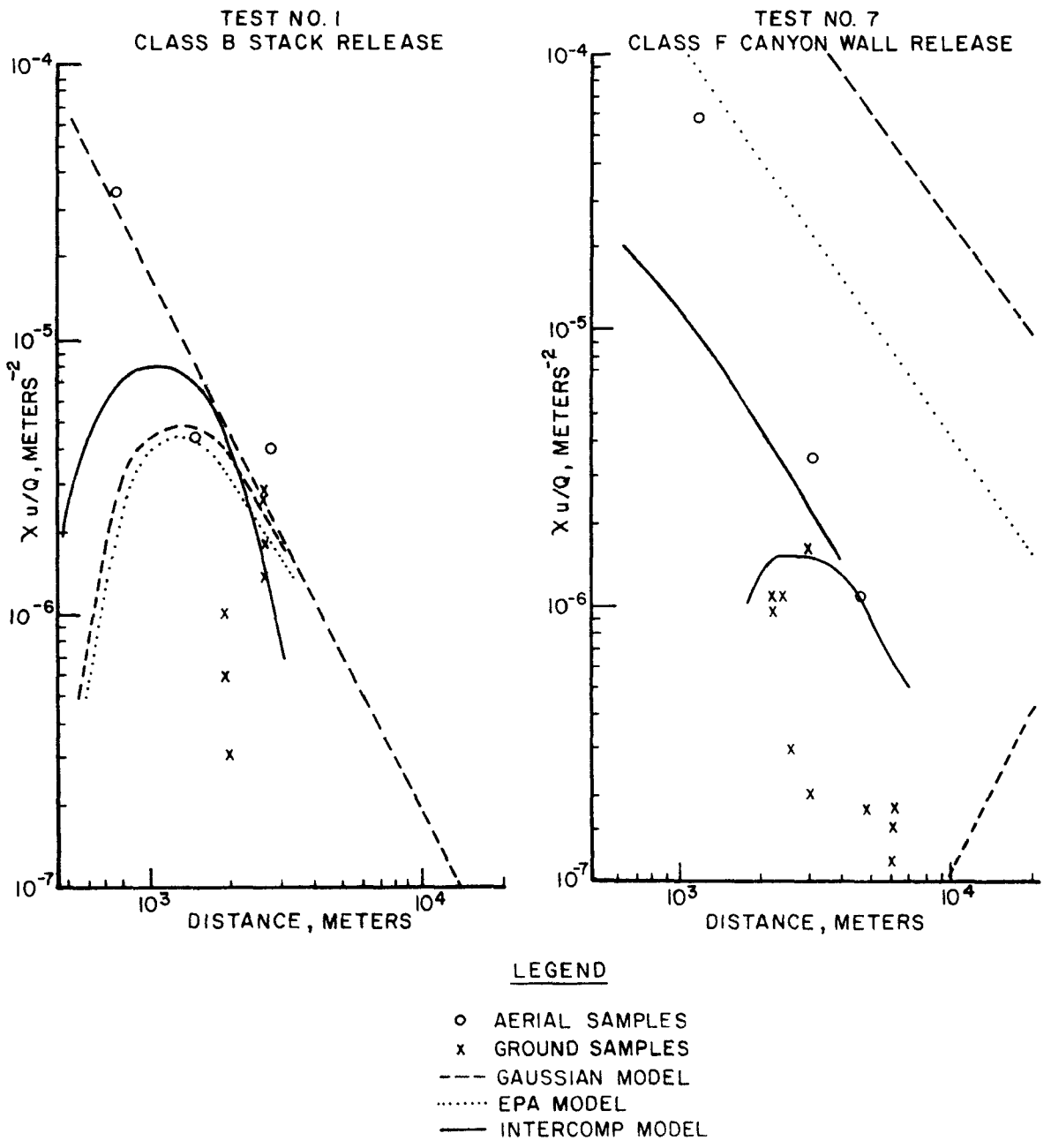

Tabulated values of the point-by-point INTERCOMP calculations as well as the centerline Gaussian and EPA model results are compared with the measurements for the remaining tests in Appendix B. These calculations utilized the tabulated stability class windspeed, and wind direction of Table II, with the exception that the down-canyon flows always used a wind oriented along the canyon (approximately 320°). In the down-valley comparisons, wind direction was not important. For the up-valley flows, wind direction has a significant effect on calculated concentrations. Two of the up-valley flow tests have not been included in Appendix B. These tests are 2 and 6. The wind direction for these two cases was 120° or even more easterly and measured groundlevel concentrations were quite sparse. Test 2, for example, contained only two groundlevel measurements. As a consequence, we have not made calculations for these two tests with the easterly wind direction.

Statistical comparisons of the measured and calculated results have been made. Of the many statistical comparisons which could have been used, we have chosen a statistic representing the ratio of calculated to observed concentrations. Such a statistic has also been used in the Huntington Canyon report[6] where Table IV summarizes a comparison of the Gaussian results with centerline measured concentrations.

The ratio statistic for the INTERCOMP model comparison with data was computed as follows:

(1) the ratio of calculated to observed concentrations for each individual monitor point and each test was computed;

(2) the logarithmic mean value (the arithmetic mean of the logarithm of the above ratio) was calculated; and

(3) the antilogarithm of the logarithmic mean value became the mean value ratio statistic.

This ratio statistic can be compared directly to the Table IV values from the Huntington report. The above procedure produces an almost identical result with their procedure which was to plot the best logarithmic mean line of the data which had the same slope with downwind distance as did the Gaussian calculation. The comparisons in the Huntington report were of helicopter (centerline) samples with calculated ground release centerline values. Our ratio statistic was somewhat more meaningful because all ground concentration points were included. Table VI illustrates the ratio comparison along with a simple arithmetic mean value comparison between calculated and measured values.

TABLE VI - STATISTICAL COMPARISONS

Test No.	Mean Values, $\mu g/m^3$		Mean Value, CALC/OBS	
	MEASURED	CALCULATED	INTERCOMP	GAUSSIAN
1	0.74	0.64	0.43	1.4
3	2.12	2.00	1.10	3.7
4	0.21	0.16	0.59	-
5	0.71	0.91	1.62	5.6
7	0.45	0.73	2.30	14.7
8	9.8	42.7	1.83	14.8
9	9.2	15.2	0.42	-
10	10.2	28.9	1.27	18.9
11	84.6	37.4	0.41	11.8

The last column labeled Gaussian of Table VI comes from the Huntington report[6]. The value listed for Test 7 has been modified from that contained in the report. Their tabulated value was 29.3. Their value was divided by two since the elevated centerline predictions should have been decreased by a factor of two to account for the lack of ground reflection. In the report they had compared centerline ground release concentrations with the helicopter measurements, but out to distances of nearly 10 km the ground reflection is not important.

The results of Table VI clearly show the improvement of the INTERCOMP predictions over those of the Gaussian (NOAA) model. The mean value, calculated to observed, ratio from the INTERCOMP model makes results for terrain as rough for flat terrain--roughly within a factor of two.

The EPA model because of the angular segment averaging in general gave improved results over the NOAA model for the down-canyon flows. However, the Gaussian model was a better approximation for the neutral to unstable up-valley tests. Both of the Gaussian type models are difficult to use in terrain as complex as Huntington Canyon if the multiple reflections from canyon walls are included. The INTERCOMP model automatically accounts for these factors.

3.3.6 Summary

The results from the Huntington tests clearly show the INTERCOMP model gave better predicted results than the Gaussian models in terms of comparison with averages of point-by-point observed data. The data corresponded to time averages ranging from one-half to 1 hour.

Our comparisons of the models have been aimed, in general, at calculations as the models would have been used in a predictive study. That is, no attempt was made to adjust diffusion coefficients to give a best match and for the Gaussian models no attempt was made to move the plume centerline location so that it best matches the measured concentrations. As pointed out previously, the INTERCOMP predictive results for Huntington Canyon provide accuracy comparable to Gaussian model results for flat terrain. That is, the addition of a simplified flow model to a calculation based upon Pasquill stability classes has given results for Huntington Canyon comparable to the Gaussian model accuracy with flat terrain. Whereas the Gaussian model accuracy was significantly decreased by the presence of elevated terrain.

The INTERCOMP model with the simplified flow model did provide adequate predictions at a number of different space points. That is, the comparison of calculated and observed results was simultaneously good at many space points both in the cross-wind, downwind, and vertical directions instead of simply good for an isolated space point.

3.4 Model Comparisons at El Paso

3.4.1 General Site and Data Description

El Paso, Texas, is the site of a large smelting complex for American Smelting and Refining Company (ASARCO). The plant area emits significant quantities of sulfur oxides from two tall stacks, one for the copper process and one for the lead. The present stack heights are 252 meters (826 feet) for the copper stack and 186 meters (610 feet) for the lead stack. Even these heights are not sufficient to prevent significant groundlevel concentrations and an intermittent process curtailment system has been in operation for the last few years. A large system of as many as twenty-two sulfur dioxide monitoring sites was established in the vicinity of the smelter and a feedback system of control has been utilized.

The data available to EPA for analysis at El Paso was the monitored sulfur dioxide concentrations for the period July, 1970, through December, 1971. Although less complete, the meteorological data for periods from February through December, 1971, was also included. The meteorological data sheets also provided volumetric flow rates and percent sulfur dioxide from both tall stacks. These were converted to source emission rates by the EPA suggested method. There is some question about the accuracy of the SO_2 stack measurements; however, the reported percentages were taken at face value. Also included in the data

were temperature measurements at four levels up to 800 feet, as well as the rawinsonde and hourly surface observations at the El Paso International Airport.

Figure 13 provides an overall view of the topography and monitor site locations around the ASARCO plant. The plant site (lower center of the figure) lies in the Rio Grande Valley on the Texas side of the southward flowing river. The most prominent topographic feature is the relatively long ridgeline of the Franklin Mountains. These mountains are northeast of the plant and extend from a position due east of the plant to 15 miles or more northward. The city of El Paso lies mostly off the figure to the southeast. The Missouri monitor site is located in the downtown area. Residential areas extend east of downtown along the Rio Grande Valley and northward along both sides of the Franklin Mountains. A fairly evenly spaced line of monitors runs due north-south through the residential area on the west side of the mountain ridge. These monitors were expected to include concentrations for stable plumes directed at a mountain line-ridge. Other monitors were placed on the Texas side of the Rio Grande some four miles west of the plant. These instruments should monitor fumigation or unstable maximum groundlevel concentrations.

The meteorological measurements at the plant site reflect for the most part local terrain effects. The measured wind directions tend to be mostly parallel to the river valley. This is not too surprising considering that even the ZINC station, 165 feet above ground, is below the 4000 foot contour which defines a one-mile wide valley. The stack emissions generally respond because of their greater height to much less localized meteorology. The Franklin Mountains are offset on the Mexican side of the river as the equally high Sierra Muleros. These mountains start about 10 miles south of the plant site. The two mountain chains channel the flow from the stacks in a northwest or southeast direction. Inversions, both radiative and synoptic occur with relatively high frequency and intensity. In general, stable flows tend to take the plume northwest or southeast of the plant site. In this case, the plume is not interacting with the mountain ridge. On some occasions, however, the synoptic flow will be from the southwest directing the plume at the Franklin Mountains even during nocturnal inversions. During the day when local effects predominate and winds are flowing along the valley, the plume can be trapped below synoptic subsidence inversions or the breakup of nocturnal inversions can lead to fumigation.

FIGURE 13

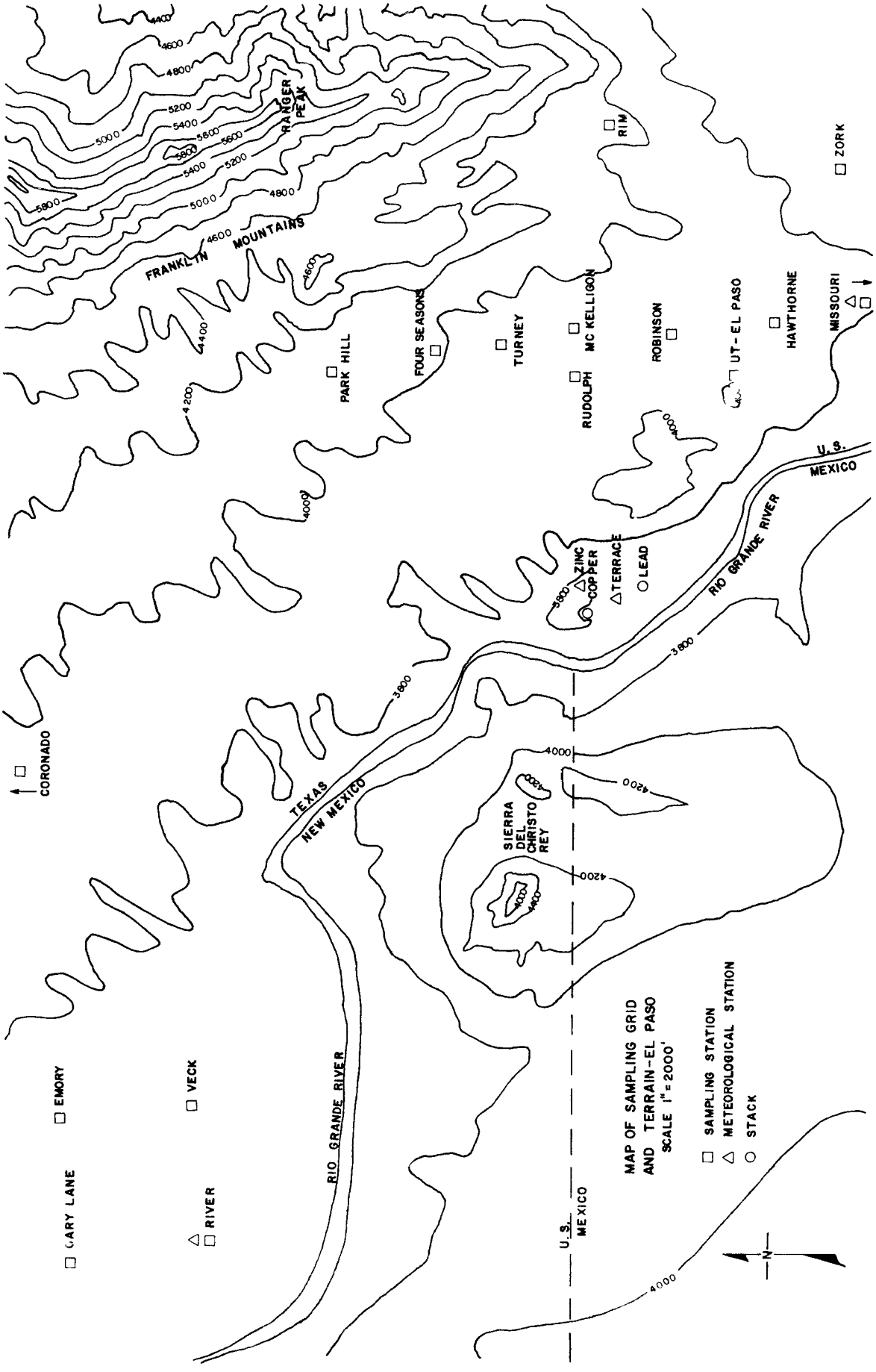
CORONADO
EMORY
VECK
GARY LANE
RIVER
RIO GRANDE RIVER
TEXAS
NEW MEXICO
U.S.
MEXICO
FRANKLIN MOUNTAINS
RANGER PEAK
PARK HILL
FOUR SEASONS
TURNEY
RUDOLPH
MC KELLIGON
ROBINSON
RIM
UT-EL PASO
HAWTHORNE
MISSOURI
ZORK
ZINC COPPER
TERRACE
LEAD
SIERRA DEL CHRISTO REY
MAP OF SAMPLING GRID
AND TERRAIN-EL PASO
SCALE 1" = 2000'
SAMPLING STATION
METEOROLOGICAL STATION
STACK
N

The available groundlevel sulfur dioxide concentrations showed 62 half-hour readings exceeding one part per million. These were associated with 39 different "events" of one or more sites above 1 ppm. A review of these "events" resulted in a list of five occasions which in terms of data availability were suitable to test against model calculations. One case for each of the two types of flow was selected for model comparison.

3.4.2 Flow to the Northwest

The case selected from among the available data at the cluster of monitors to the northwest of the plant was for October 21, 1971. The actual concentrations at the five monitor stations are shown in the boxes in Figure 14. It can be readily seen that the plume centerline appears to lie somewhere among the monitor stations. The time period for which the concentrations are shown is the half-hour ending at 10:30 a.m. Temperature measurements over the 800 feet on the copper stack indicated a +6°F temperature difference at 6:00 a.m. which was altered to isothermal by 9:00 a.m. and at 10:00 a.m. reached the dry adiabatic lapse rate. This strongly indicates that inversion breakup was occurring and probably passed through plume height between 10:00 and 10:30 fumigating the plume to the ground.

The early morning rawinsonde at the airport indicated that the surface based inversion extended beyond 600 meters. The inversion is, therefore, deep enough to include the entire plume.

The maximum groundlevel concentrations would result with an inversion base slightly above the plume height that was present while the plume was in the stable inversion layer. The model calculations were, therefore, performed for such a situation with an inversion base of 500 m above the plant elevation.

In the INTERCOMP model the diffusion coefficients in the inversion layer were set to approximate Pasquill F stability and those below the inversion base were set to approximate Pasquill C. In the EPA model (C4M3D) and Gaussian calculations, Pasquill C stability and a mixing depth of 500 meters were utilized. That constitutes a perfectly reflecting surface at the 500 m height.

The windspeed of 10 miles per hour as recorded at the plant site was utilized in the models and a wind

FIGURE 14

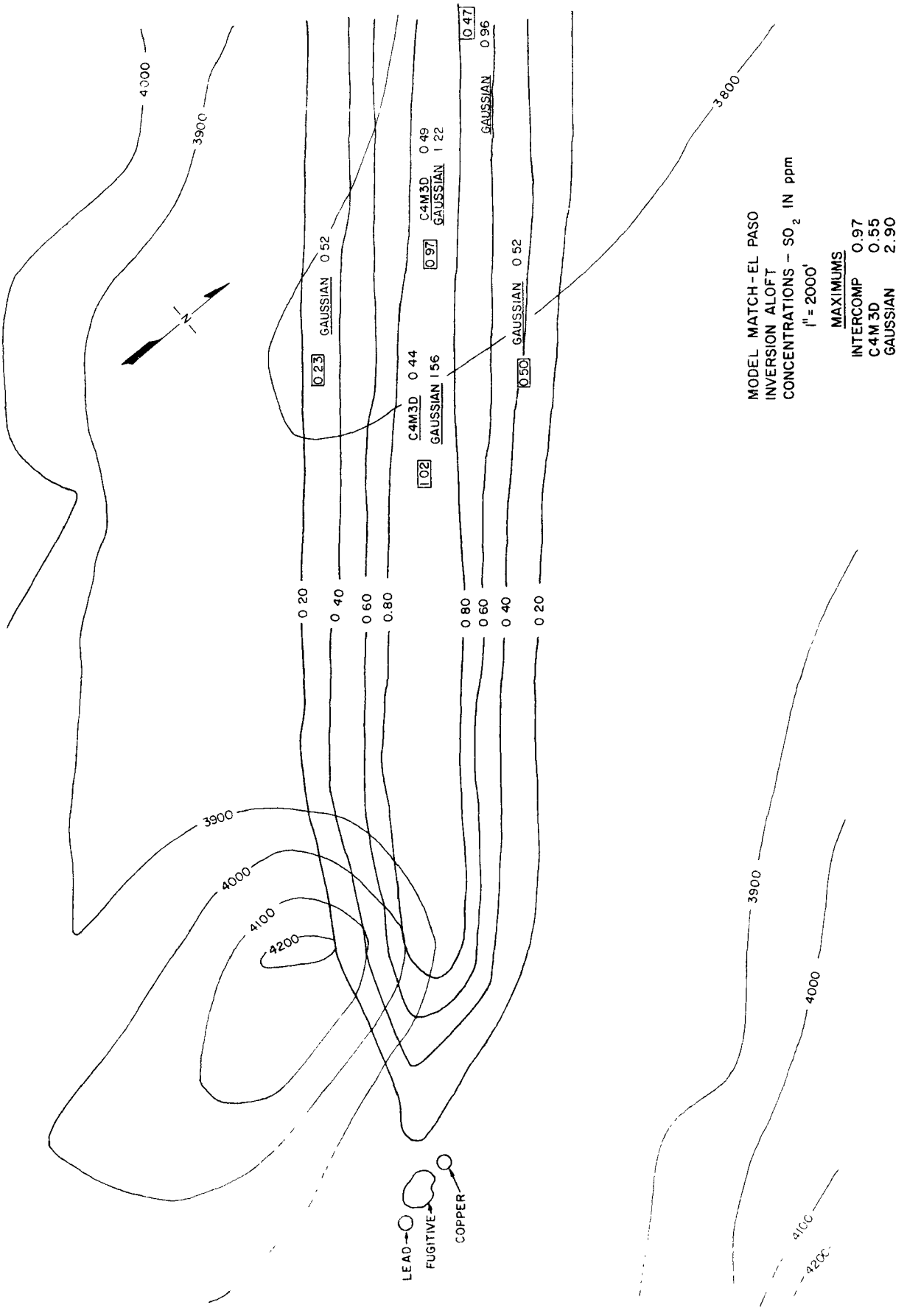
MODEL MATCH-EL PASO
INVERSION ALOFT
CONCENTRATIONS - SO_2 IN ppm
1" = 2000'
MAXIMUMS
INTERCOMP 0.97
C4M3D 0.55
GAUSSIAN 2.90
0 23 GAUSSIAN 0 52
C4M3D 0 44
GAUSSIAN 1 56
1 02
C4M3D 0 49
GAUSSIAN 1 22
0 97
0 47
GAUSSIAN 0 96
0 50 GAUSSIAN 0 52
0 20
0 40
0 60
0.80
0 80
0 60
0 40
0 20
3900
4000
4100
4200
3800
LEAD
FUGITIVE
COPPER
N

direction of 125° true was used to line up the copper stack and the two central monitor stations. The plant site anemometer was actually recording a direction 20° more southerly. The INTERCOMP model wind flow calculation simulated a more southerly direction near groundlevel because of the influence of the Sierra Del Christo Rey. This effect can be seen in the groundlevel concentration isopleths of Figure 2 close to the plant site.

The model calculations for each monitor station are presented in Figure 14. All values are in SO_2 concentrations in ppm (1 ppm is equivalent to 2370 $\mu g/m^3$). The INTERCOMP model calculations are shown by isopleths. Turner's workbook Gaussian plume model calculations (the multiple reflection equation) with a 500 m mixing depth provide the calculations labeled Gaussian. Both the INTERCOMP and Gaussian results are in good agreement with the measured concentration levels at the five stations. The width of the plume is reasonably approximated by either of the two models. The INTERCOMP model did predict peak concentrations closer to the stack than did the Gaussian model. The cross-section of Figure 15 illustrates the topography which leads to downward flow and causes this effect. The EPA model because of 22.5° sector averaging predicted concentrations of roughly one-half the peak values of the other two models.

A vertical cross-section along the plume centerline from the INTERCOMP model calculations is presented in Figure 15. Added to the plumes from the two tall stacks is a fugitive emission equal to 3% of the total sulfur dioxides from the two stacks. The reason for inclusion of these values is described more fully in the next section. As evident from Figure 15, the INTERCOMP model allows pollutant to diffuse into the inversion layer because there is only a change of coefficient and not a totally reflecting surface. Partial reflection does occur at that boundary and the isopleths of concentration approach uniformity in the vertical at a distance beyond 3-4 miles to some extent confirming the uniform vertical mixing assumption often utilized with the Gaussian model.

In this fumigation case there is comparatively flat terrain. The results, however, indicate that the EPA model gave values about one-half those of the INTERCOMP centerline calculations. The Gaussian calculations were in the same range as the INTERCOMP calculations. The INTERCOMP model gives reasonable values at all monitors while accounting for the terrain effects which are present.

FIGURE 15

MODEL MATCH-EL PASO
INVERSION ALOFT
VERTICAL CROSS-SECTION
SULPHUR DIOXIDE CONCENTRATIONS IN ppm

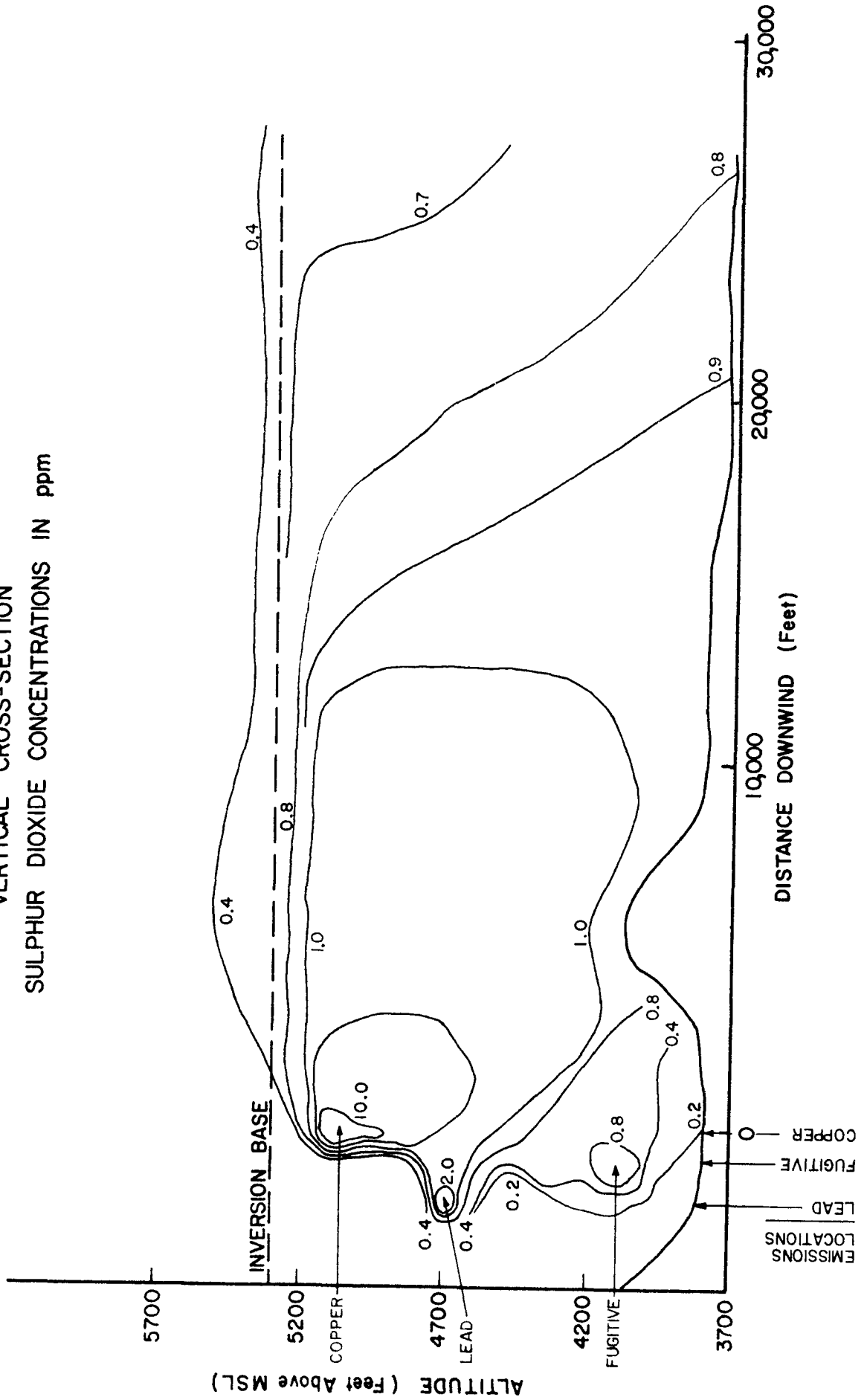

3.4.3 Stable Flow

In general, stable flows are directed along the river valley and the plume moves southeast or northwest of the plant. On occasion stable plumes are directed at the Franklin Mountains because of the influence of synoptic wind patterns. Several cases of high groundlevel concentrations of sulfur dioxide at the monitor sites east of the plant were found under these conditions. The data from December 8, 1971, were chosen as representative. Winds recorded at the plant site on this day were directed at the monitor receiving the highest concentration.

The initial attempts to simulate this case were completely unsuccessful because essentially no concentration reached groundlevel at the monitor sites. The vertical cross-section provided in Figure 16 is for the centerline of the December 8 stable plume. It graphically shows the reason for the model's inability to simulate measured stable ground concentrations. The emissions from the copper and lead stacks are so high above the monitor sites that no material diffuses down to them with the restriction to vertical diffusion imposed by a stable atmosphere. During the half-hour ending at 1:30 a.m. on December 8, there was a temperature differential of +13°F over the 800 feet of the copper stack. This certainly indicates a stable atmosphere with little vertical transfer.

It is possible, however, to explain high groundlevel concentrations at the monitor sites in terms of drainage. Several cases in the data appear to exhibit this drainage effect. The Rim monitor (see Figure 13) on several occasions responded to high sulfur dioxide concentrations during stable conditions and then in the following half-hour McKelligon, Robinson and Zork, all at lower elevations, would have peak values. This indicates that pollutant was draining down along the terrain to produce relatively high concentrations at lower elevations. Diffusion does occur during this drainage process so that the monitored values would not reflect maximum groundlevel concentrations. Another mechanism exists for getting groundlevel concentrations at the Park Hill site (most northerly of the line of monitors). When the stable plume travels due north from the plant site and the wind direction then shifts to the north, the stable plume is swept back along the mountainside draining as it returns and effecting the low level monitor sites. In both mechanisms, however, significant dilution will occur and concentrations in the 1-2 ppm range are not probable. No attempt was made to model this type of situation.

FIGURE 16

TERRAIN
VERTICAL CROSS-SECTION
STABLE CASE - EL PASO

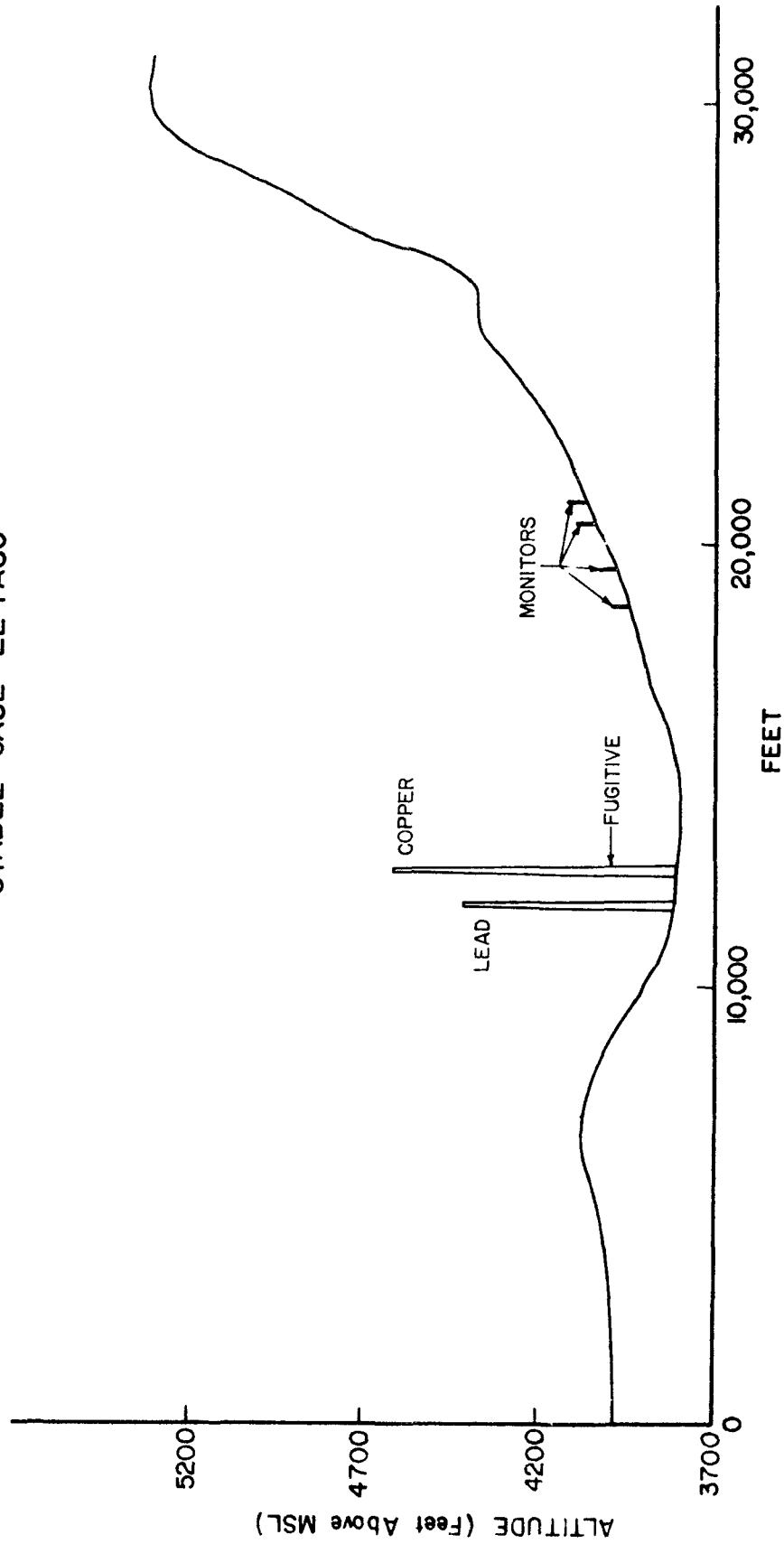

The monitor sites do not have individual anemometers so that in the case of December 8 it is difficult to tell whether drainage is an important influence. The temperature measurements up the stacks show that the temperature profile was isothermal above 500 feet and that the total +13°F differential was in the lowest 500 feet. This creates a situation where the steepest slopes on the Franklin Mountains may well be isothermal and drainage flows would then not be as important. This factor along with the wind direction at the plant being toward the monitors virtually necessitated stable winds directed at the terrain. To get significant measured concentration levels, we required a source of sulfur dioxide lower than 500 feet above ground. There is a 350 foot zinc process stack which could be the source, but no measurements of sulfur dioxide emission were available. Fugitive emissions from the plant process buildings are another potential source of sulfur dioxide. The major monitor of interest (Park Hill) is situated almost 300 feet above the plant site. A few runs with the INTERCOMP model showed relatively little difference in predicted concentrations for a range of plume heights between 100 and 300 feet. A source emission strength of 3% of the combined emissions for the two stacks gave best agreement with the concentrations found at the monitors. The results for 3% fugitive emissions with a 200 foot plume height are shown in Figure 17. The fugitive emissions were considered to be emitted between the two stacks as an approximation. As in earlier figures, the INTERCOMP model values are shown in isopleth form. The INTERCOMP model prediction at the Park Hill monitor was 1.51 ppm. The maximum value of 2.14 ppm was located a little north of the monitor. The Park Hill monitor is actually located on a small plateau not evident in Figure 17 which drops off in elevation both to the south and north. As a consequence, changes in the wind direction result in highest ground concentrations on either side of the monitor rather than at the measurement site. Other wind directions and source strengths also do not agree as well with the values at the other three monitors.

In the cases of the EPA and Gaussian calculations, the height of the source emission has more effect on the results. The values shown in Figure 17 are for a 200 foot effective fugitive emission height. These calculations indicate much higher values at the Park Hill monitor. In the case of the EPA model, a value more than twice the measured value at the monitor and a maximum of 4.76 ppm downhill from the monitor were calculated. This is similar in location to the INTERCOMP model simulation. The Gaussian calculations, without benefit of sector averaging and the EPA model restriction for the centerline

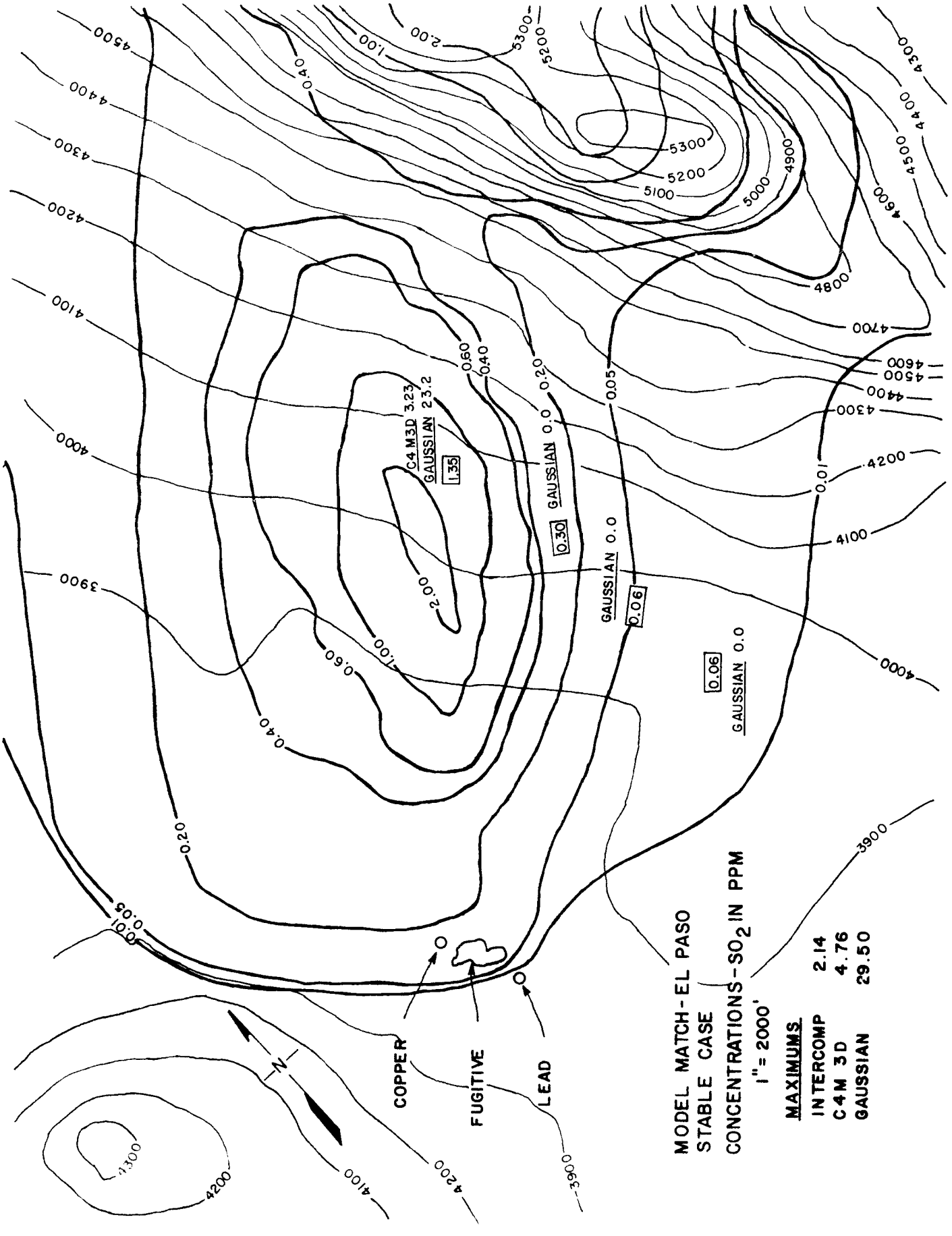
MODEL MATCH-EL PASO
STABLE CASE
CONCENTRATIONS-SO_2 IN PPM
1"= 2000'
MAXIMUMS
INTERCOMP 2.14
C4M 3D 4.76
GAUSSIAN 29.50
C4 M3D 3.23
GAUSSIAN 2.3.2
1.35
GAUSSIAN 0.0
0.30
GAUSSIAN 0.0
0.06
GAUSSIAN 0.0
0.06
COPPER
FUGITIVE
LEAD
N

FIGURE 17

remaining 10 m above groundlevel, yield values an order of magnitude higher than the EPA model. This calculation assumes plume centerline values are along the ground from the point of intersection of the terrain on up the side of side of the mountain. The position of the maximum is the same. If the source height were increased to 300 feet, the predicted maximums for the EPA model and the Gaussian would be to shift the monitor location and are about the same magnitude as those predicted for the lower source height.

Smelting personnel generally agree that a fugitive emission level of 3% is not out of line with normal operations and, in fact, may be low. To obtain a best fit of the monitored data, fugitive emissions of less than 1.5% would be required for the EPA model and less than 0.3% for the Gaussian calculations.

Almost certainly the plumes from the two tall stacks interacted with the Franklin Mountains at elevations above the monitor sites. The initial runs with the INTERCOMP model indicated maximum concentrations on the order of 10 ppm. Gaussian intersecting calculations show values of 400 ppm. Both of these calculations are for F stability. Neither set of calculations can be compared to monitored data.

The stable case plume simulation shows the flexibility of the INTERCOMP model as an evaluation tool for determining what unknown source rates might be. Simulating the results at a series of monitors gives some confidence in the approximate 3% level for fugitive emissions. The comparison between the models is not extremely definitive since the source rate and its resultant plume height are not known.

3.4.4 Summary

In summary, the ASARCO smelter data provide data useful in comparing the three models. Two types of atmospheric conditions were examined. In the limited mixing cases, the same mixing depth and atmospheric stability were used in the mixing layer for each model. Results indicated good agreement between the INTERCOMP model and the Gaussian (NOAA) model. Both models were in good agreement with measured data for such an atmospheric condition. The EPA model, because of the angular sector averaging even for short-term peak concentrations, was lower by a factor of roughly two.

In the stable flows with winds directed at high terrain, our study showed little effect of the stack emissions on concentrations measured at the monitors. Instead a fugitive emission was hypothesized to be responsible for these measured concentration levels. At a fugitive level of 3% of the combined stack emissions, good agreement was obtained between calculated concentrations with the INTERCOMP model and the measured values. Both the EPA model and the Gaussian (NOAA) model calculated concentration levels much higher than measured values for the 3% emission levels. Of course, a reduction in emission level could have been used; however, this caused the Gaussian type models to give poor agreement with measured values in terms of crosswind spread.

The finding that stack emissions are, in all probability, not affecting monitored concentration levels is interesting from the standpoint of intermittent process curtailment effectiveness. It would appear that the fugitive emissions would have to be quantified to provide realistic control. It is probable that plant curtailment affects fugitive levels in exactly the same way as it affects the stack emissions although this point would need investigation.

3.5 Validation of the INTERCOMP Flow Model

3.5.1 General

Every mathematical model of physical phenomena is subject to the assumptions used in its formulation. Therefore, most mathematical models are restricted to a certain class of problems. Such a model is considered to be valid, if it simulates correctly the physical phenomena that were intended to be included in its formulation. Specifically, the INTERCOMP flow model is designed to simulate air flow over terrain on a large scale necessary for ambient air quality studies. Because this model is based on a "modified potential" flow concept[12], there is certainly a question of the adequacy of such a model for a complete range of problems which are of interest. Ultimately, this can best be answered by extensive comparison to field data. However, it is possible to obtain a reliable answer also by comparison of the model with more sophisticated calculation techniques--in this case with a model based solving Navier-Stokes equations for viscous, slightly compressible flow. Although at the present time, the use of a Navier-Stokes formulation for large-scale air quality models appears to be impractical because of cost (see reference 13, 14, 15, and 16), such models can serve as a standard for comparison of simpler models. Two such

models have been reported for solving air quality problems[2,3]. In making comparisons between the "modified potential" model results and the Navier-Stokes model results, one has to bear in mind that the potential formulation cannot simulate phenomena that are unique to viscous flow, i.e. wakes and vortices. However, in many cases wakes will not form due to atmospheric stability or will only exist on a small scale below the resolution limit of simulation (e.g. for flow over gently sloped terrain). Even in the case when a wake develops on the downstream side of an obstacle, the simplified solution may be adequate for cases where it can be shown that the presence of the wake does not affect the flow in the regions of real interest--e.g. on the upwind side or above the obstacle. Thus, the Navier-Stokes model can also serve to determine a range of adequacy for the "modified potential" flow model.

In the comparisons included in this report no attempt has been made to verify the modified potential model for all flow conditions. Rather two basic conditions of neutral and stable conditions were investigated.

3.5.2 Navier-Stokes Flow Model

3.5.2-1 Mathematical Development

The numerical model is based on the "primitive variable" formulation used by the Los Alamos group[17,18,19] as well as the Colorado group[20] and others[21,22]. This formulation has been chosen in preference to the vector potential formulation[23], because it can be easily extended to turbulent flow and variable density. For a current survey of computational approaches to the Navier-Stokes equations, see reference 24 and 20. The details and equations used in our calculational model are developed in Appendix A.

The particular form of the momentum and continuity equations used are subject to the following assumptions:

(1) Pressure changes do not affect density.

(2) Density changes have a negligible effect on viscous terms. This assumption is quite justified in view of the uncertainties associated with turbulent viscosities.

(3) Turbulent effects are included as Reynolds stresses expressed through a turbulent eddy viscosity (this will be discussed in more detail later).

(4) Density can be described as a function of position. Although the model includes the capability for solving simultaneously an energy equation, buoyancy effects were simulated by a stable temperature field. This would be the case at steady-state which was of primary interest and it greatly simplifies the calculations.

The numerical solution method discretizes the momentum and continuity equations. The finite difference discretization of the momentum equations also satisfies the discretized continuity equation (see Appendix A).

The momentum equations use a forward difference for the time derivatives. The procedure consists of implicitly solving for the pressure field with the righthand side evaluated at the old time level, then an explicit updating of the velocity field using the new pressures. Central time differencing, preferred by some authors[16,25,26], gives smaller time truncation errors, but introduces weak instability and increases core requirements.

The program has the capability of solving both two-dimensional and three-dimensional problems. The solution method for the pressure equation is LSOR, with direct elimination as an option for two-dimensional problems. Handling of boundary conditions permits arbitrary specification of terrain as in the standard INTERCOMP air quality simulator. The program has a restart capability and an automatic time step control, based on the convective stability condition.

3.5.2-2 Comparison with Results for Laminar Flow

The problem chosen for testing of the laminar flow model is the flow in an entrance region of a straight channel. Steady-state solutions of incompressible Navier-Stokes equations for this problem are given by Morihara and Cheng[27], who also compare many of the earlier results reported in boundary layer literature. Because the INTERCOMP Navier-Stokes model does not have the capability to solve directly for the steady-state velocities, unsteady solutions were computed until reasonably close to steady-state. Comparison of results of

Re = 200 are shown in Figure 18 where the continuous lines show literature results[27] and the circles result from the INTERCOMP model. The agreement with literature values[27] is satisfactory. The main difference is that our solution has almost no bulges in the velocity profile (although they have been observed in runs other than those shown). The reason for this difference is the relatively course grid used and the fact that the referenced work[27] used higher order approximations for convective terms. The differences closer to the inlet are due to the fact that our solution is not quite at steady-state.

Similar results were obtained from other Reynolds numbers.

3.5.2-3 Eddy Viscosity Model for Turbulent Flow

Presently, the most practical way of treating turbulent flow is via the eddy viscosity concept[28, 29, 30]. The turbulent (eddy) viscosity is a complex tensor function of the flow field. Many turbulent models have been proposed for calculation of eddy viscosity coefficients, some of them very complex (see reference 20 and especially 31). While it is necessary to construct complex turbulence models as tools for better understanding of the turbulence phenomenon, their present accuracy does not justify their use for practical calculations. Our aim has been to use the simplest approach that would be adequate for the class of problems of interest. In air pollution applications, there is generally one direction of the prevailing wind. Over flat terrain, the velocity distribution often follows an approximate power law dependence on height.

Our turbulent viscosity model then is based on the assumption that over a flat surface, the velocity variation in the vertical will approximately follow a power law dependence. If the thickness of the boundary layer, z_∞, is sufficient so that turbulence essentially disappears at z_∞ (see e.g., Sutton[29], Chapter 7), then the viscosity at the top of the boundary layer, μ_∞, can be taken as the molecular viscosity. Molecular viscosity is generally negligible compared to the maximum turbulent viscosity, μ_m. An example of the variation of this viscosity model and the resultant velocity versus height are shown in Figure 19 for a power law exponent of $\alpha = 1/7$. As shown in Appendix A, the above development of turbulent viscosity can be interpreted in terms of Prandtl's mixing length hypothesis and agrees well with experimental results for one-dimensional flow.

FIGURE 18

COMPARISON OF CALCULATED
LAMINAR ENTRANCE FLOW

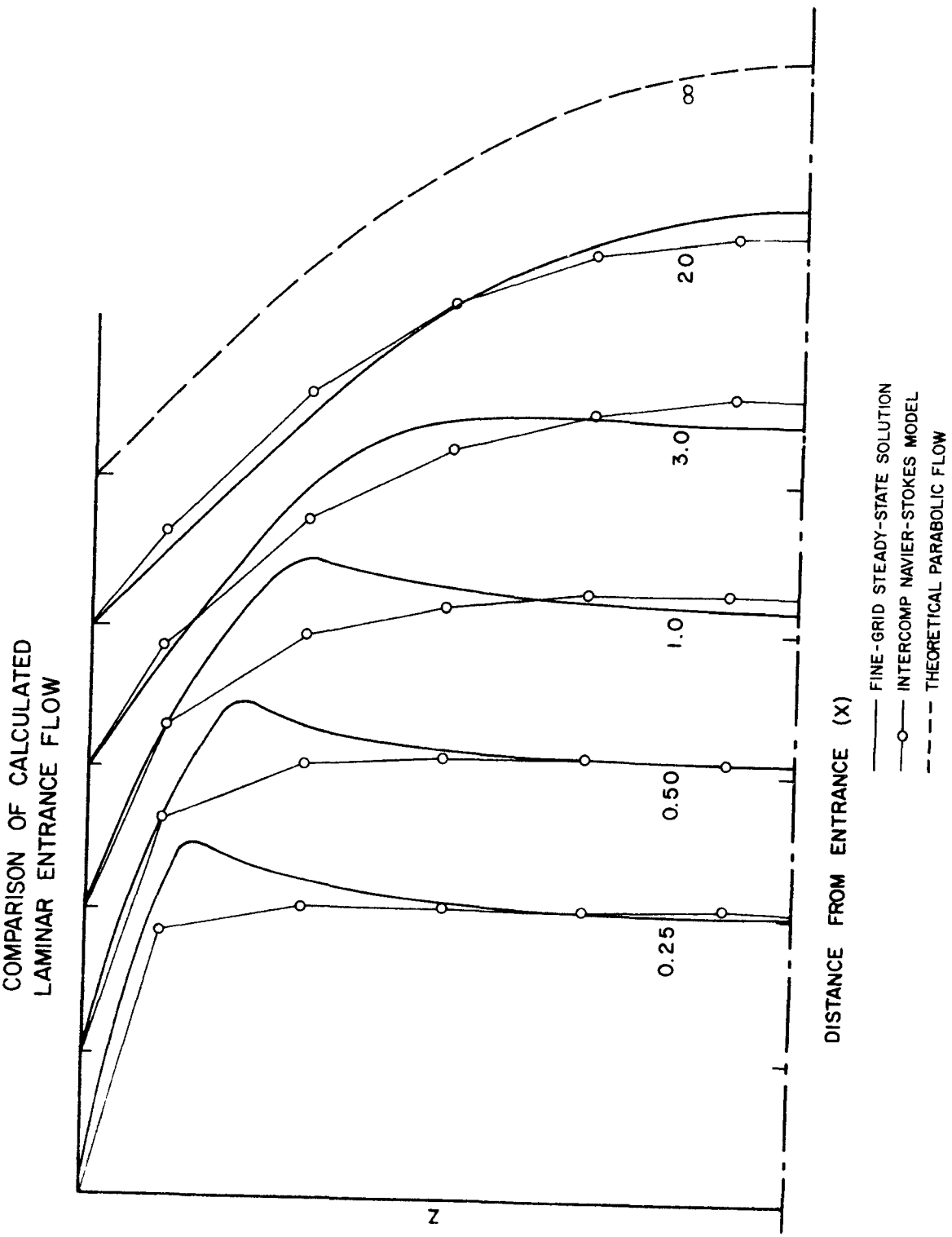

FIGURE 19

VERTICAL VARIATION OF
EDDY VISCOSITY

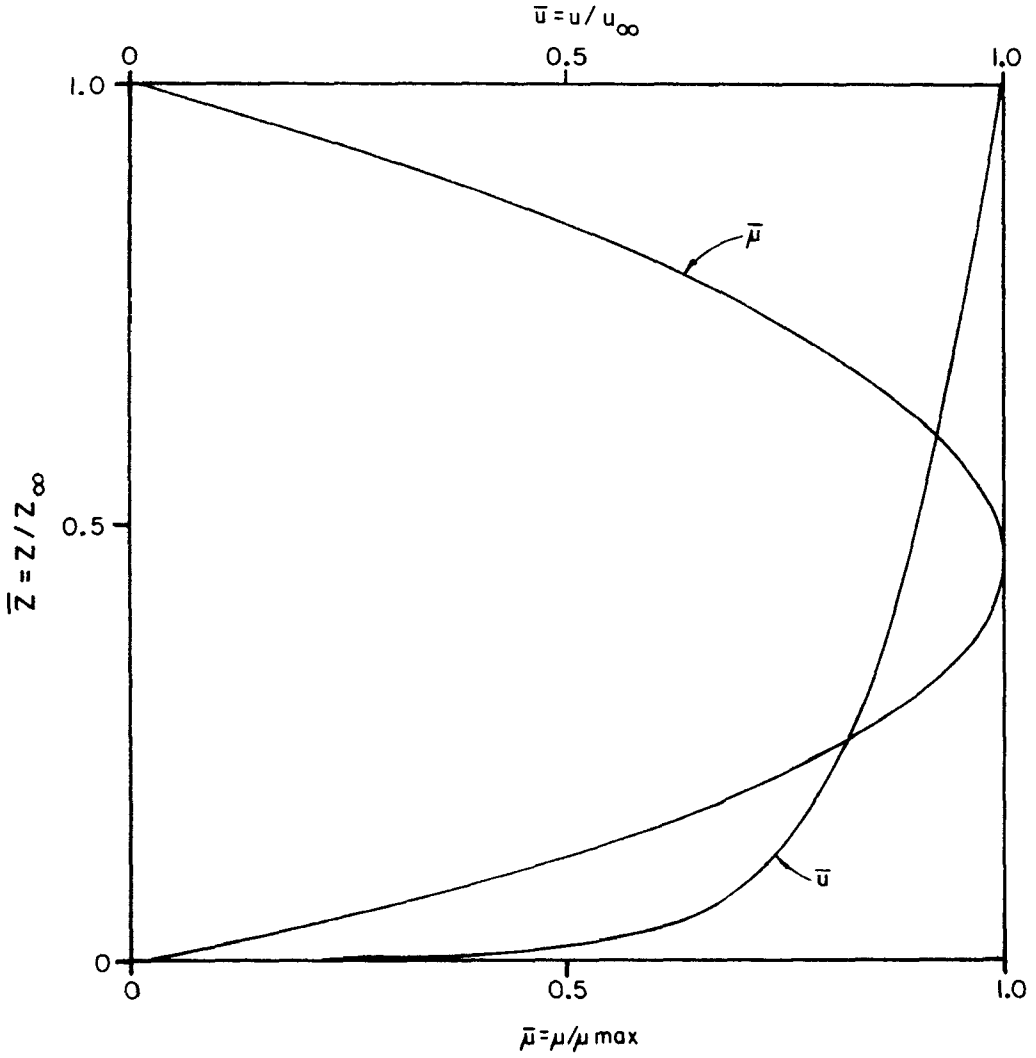

The above procedure defines only one component (namely μ_{xz}) of the viscosity tensor. The remaining components are obtained by scaling of μ_{xz} using ratios of turbulent fluctuations (dependent upon stability) and derivatives of velocities based on the "order of magnitude" argument common in boundary layer theory. Our experience has shown that a change of some components of viscosity by an order of magnitude did not have a noticeable effect on the results; therefore, this approximation seems justifiable. However, the simulator is not restricted to the above described treatment of turbulence, and could use a more elaborate model of turbulence if desired.

To test if this turbulence model gives numerical solutions that approximate a power law, the "entrance region" was solved again in turbulent flow. Because of the symmetry condition at z_∞, the result also represents a solution of turbulent flow over flat terrain, with uniform inlet velocity. Figure 20 shows an example of the velocity profile at a large distance from the entrance, where the velocities are fully developed. In this case, the Reynolds number, corresponding to the maximum eddy viscosity is 10^3 (Re was calculated from a molecular viscosity of about 10^5).

This can be compared with a one-dimensional exact solution for the same eddy viscosity model which results in a power law velocity profile. As evident in the log-log plot, the numerical solution follows a power law variation near the ground, but deviates at the top of the boundary layer. This is due to the fact that the boundary condition at the top ($\bar{z} = 1$) is $\partial u/\partial z = 0$, which is not satisfied by a power law velocity profile. Thus, the numerical model gives a more realistic approximation than the exact power law profile for atmospheric flow which should approach a condition of nearly zero vertical gradient at the top of the turbulent boundary layer.

An additional test of the numerical model was performed in three-dimensional flow by numerical simulation of wind tunnel measurements obtained by Halitsky[32]. Figure 21 shows the caluclated and measured u-velocities at a distance 12 m behind the building (the wind tunnel results were scaled to the original size). Although this comparison is only qualitatively significant, because of difficulties in scaling and generating the turbulence in wind tunnel tests, the agreement confirms the validity of the numerical results.

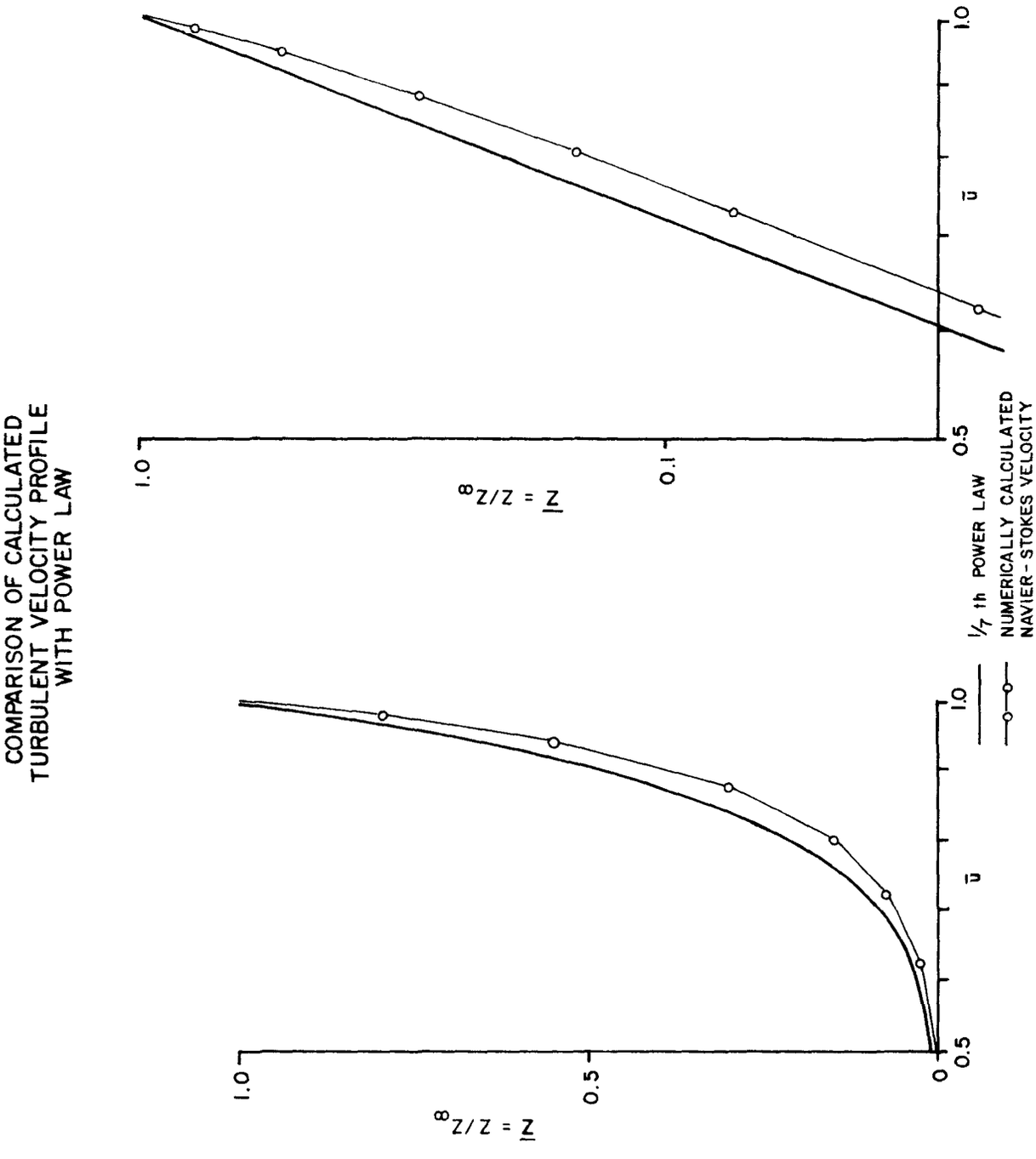
COMPARISON OF CALCULATED
TURBULENT VELOCITY PROFILE
WITH POWER LAW
$\bar{Z} = Z/Z_\delta$
1.0
0.5
0
$\bar{u}$
0.5
1.0
0.1
1.0
$\bar{Z} = Z/Z_\delta$
$\bar{u}$
0.5
1.0
1/7 th POWER LAW
NUMERICALLY CALCULATED
NAVIER-STOKES VELOCITY

FIGURE 21

COMPARISON – CALCULATED WIND PROFILES
AND TUNNEL EXPERIMENTS

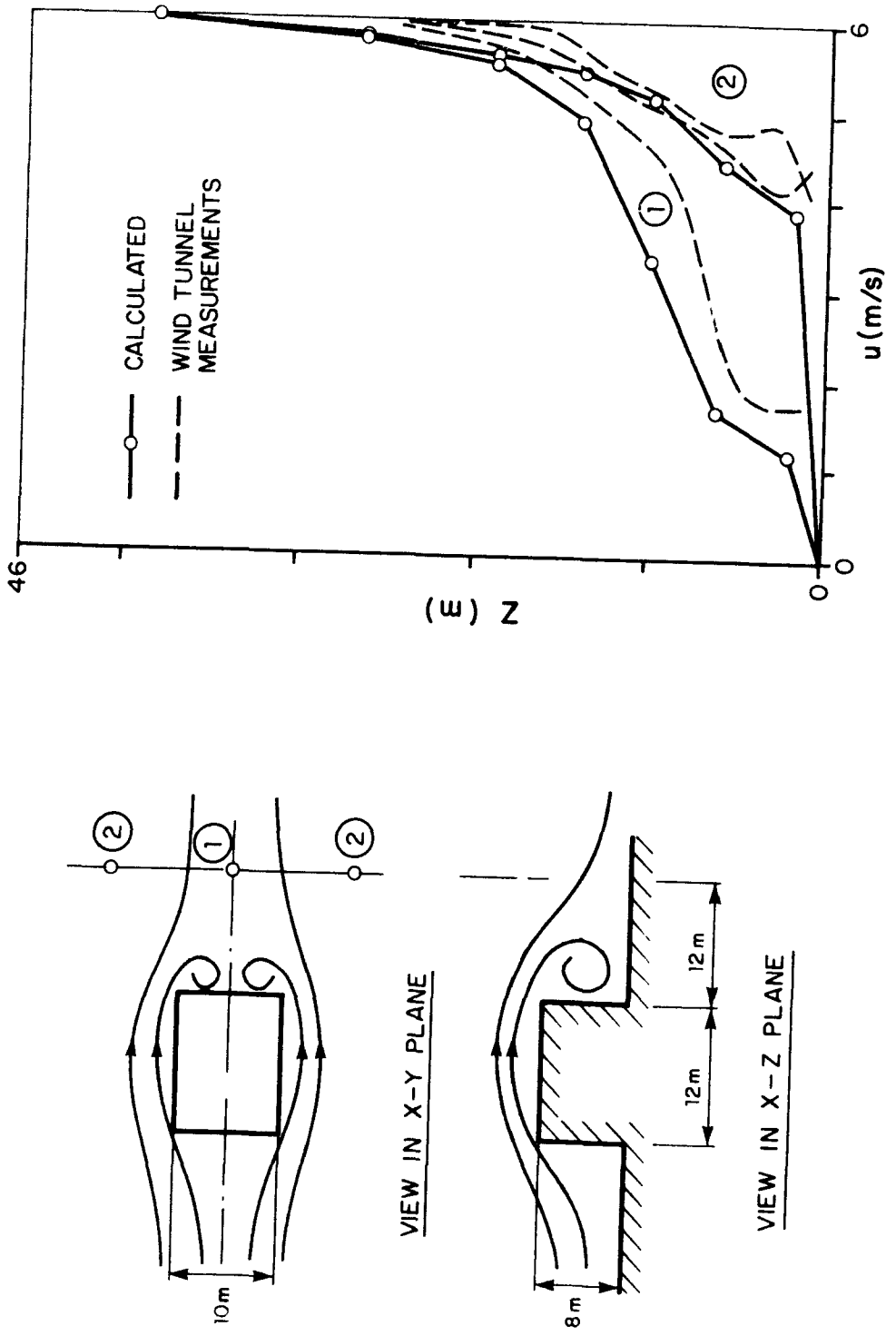

3.5.3 Comparison with the Modified Potential Model

3.5.3-1 Influence of Wake Regions on Flow Field Around an Obstacle

As mentioned before, the modified-potential model cannot simulate wake regions behind buildings or other obstacles. It is, therefore, important to establish the effect of such a wake on the flow field upstream and above the obstacle.

This question was investigated by solving flow fields around obstacles of the same height, but of different lengths in the direction of flow. The flow fields at a time close to steady-state were then compared. Figures 22 and 23 show the two respective flow fields in the two-dimensional case, first for a short obstacle, and second for an obstacle of "infinite" length. Recirculation develops in the first case in the wake region behind the obstacle. In both cases it was assumed that a fully developed flat terrain velocity profile exists at the entrance to the simulated region, i.e., the entrance velocity satisfies a power law profile. The comparison of the horizontal velocities, u, are shown in Figure 24. It is evident that the presence of a wake on the downstream side does not affect the velocity profile in front of the obstacle and only slightly affects it above the wake (in cross-section B-B). Similar results were obtained in the three-dimensional cases. It may, therefore, be concluded that the simulation of a wake is not important for the flow field except directly behind the obstacle. Consequently, the comparisons with the modified potential model were carried out for obstacles extending to infinity, for which recirculation regions are not present.

3.5.3-2 Comparison for Two-Dimensional Flow

All two-dimensional runs were made with a 16x7 grid. Irregular grid spacing was used in order to obtain adequate definition around the upstream side of the obstacle. The influx velocity was assumed to satisfy a power law profile according to a prescribed exponent α. The first series of runs were made without the effect of density,

FIGURE 22

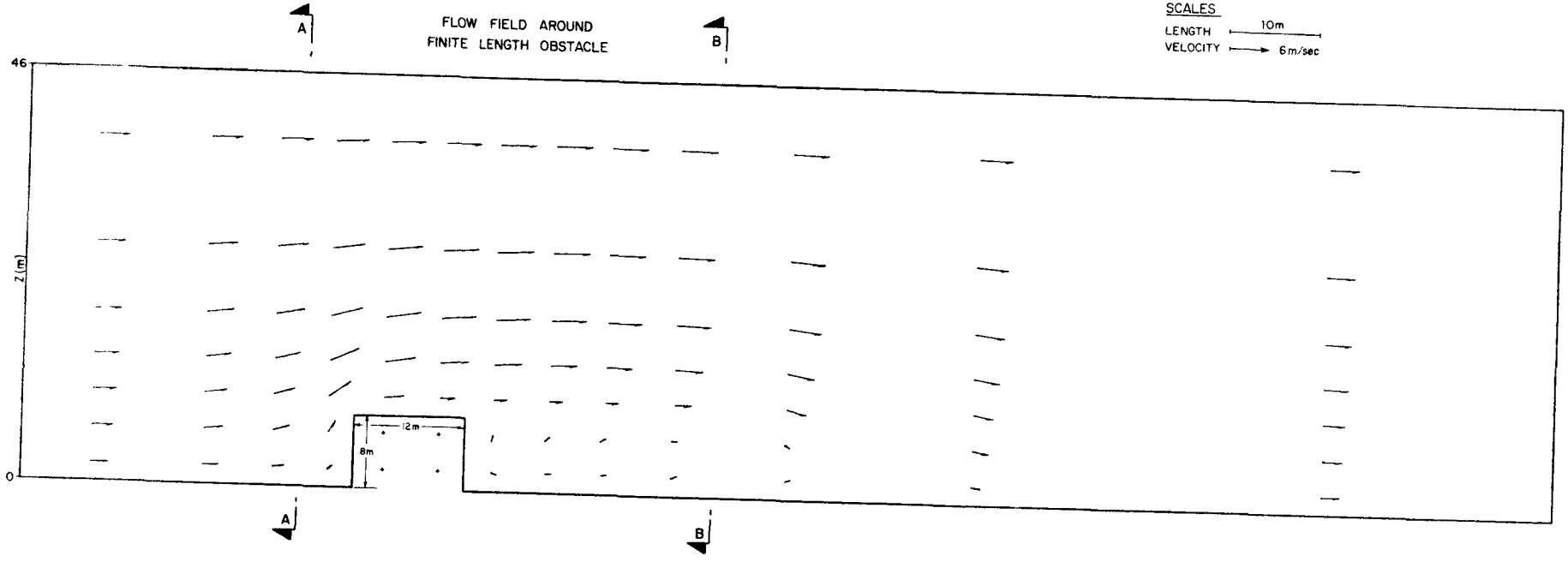
FLOW FIELD AROUND
FINITE LENGTH OBSTACLE
A
B
SCALES
LENGTH 10m
VELOCITY 6 m/sec
46
Z (m)
0
12m
8m
A
B

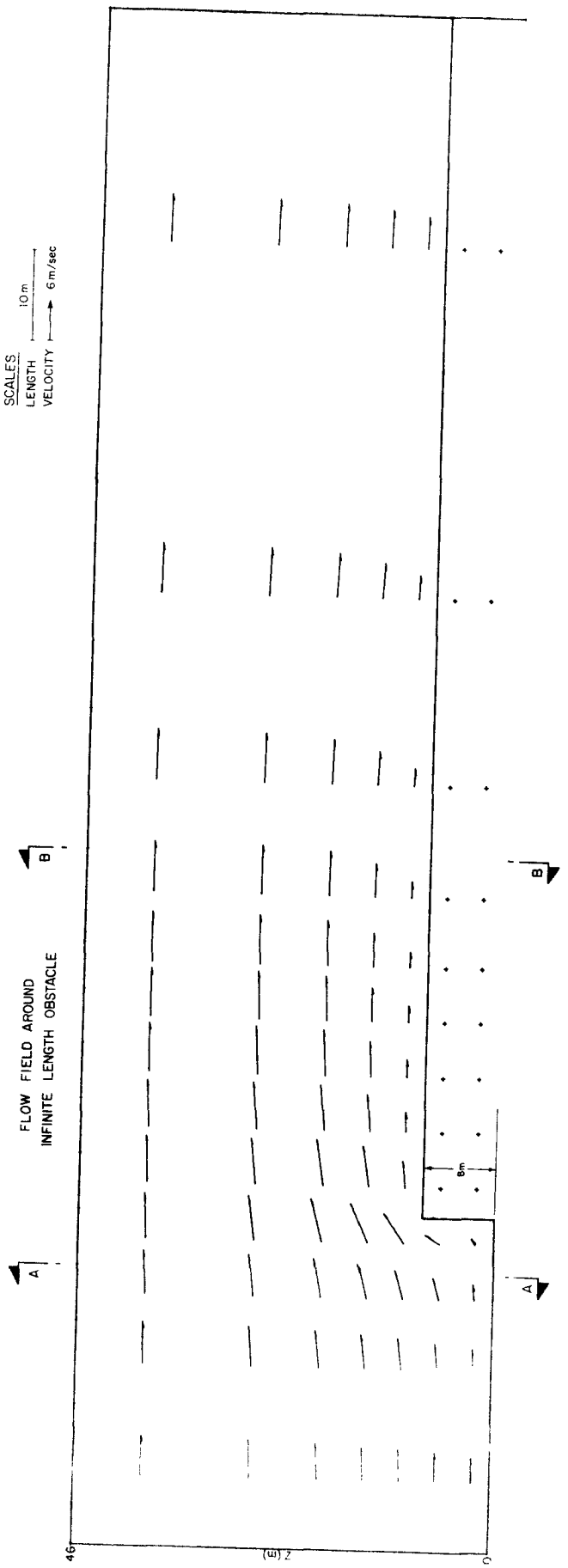
SCALES
LENGTH 10 m
VELOCITY 6 m/sec
FLOW FIELD AROUND
INFINITE LENGTH OBSTACLE
A
A
B
B
8m
46
z (m)
0

FIGURE 23

FIGURE 24

COMPARISON OF NAVIER-STOKES SOLUTIONS
WITH DIFFERENT OBSTACLES
VELOCITY CROSS-SECTIONS

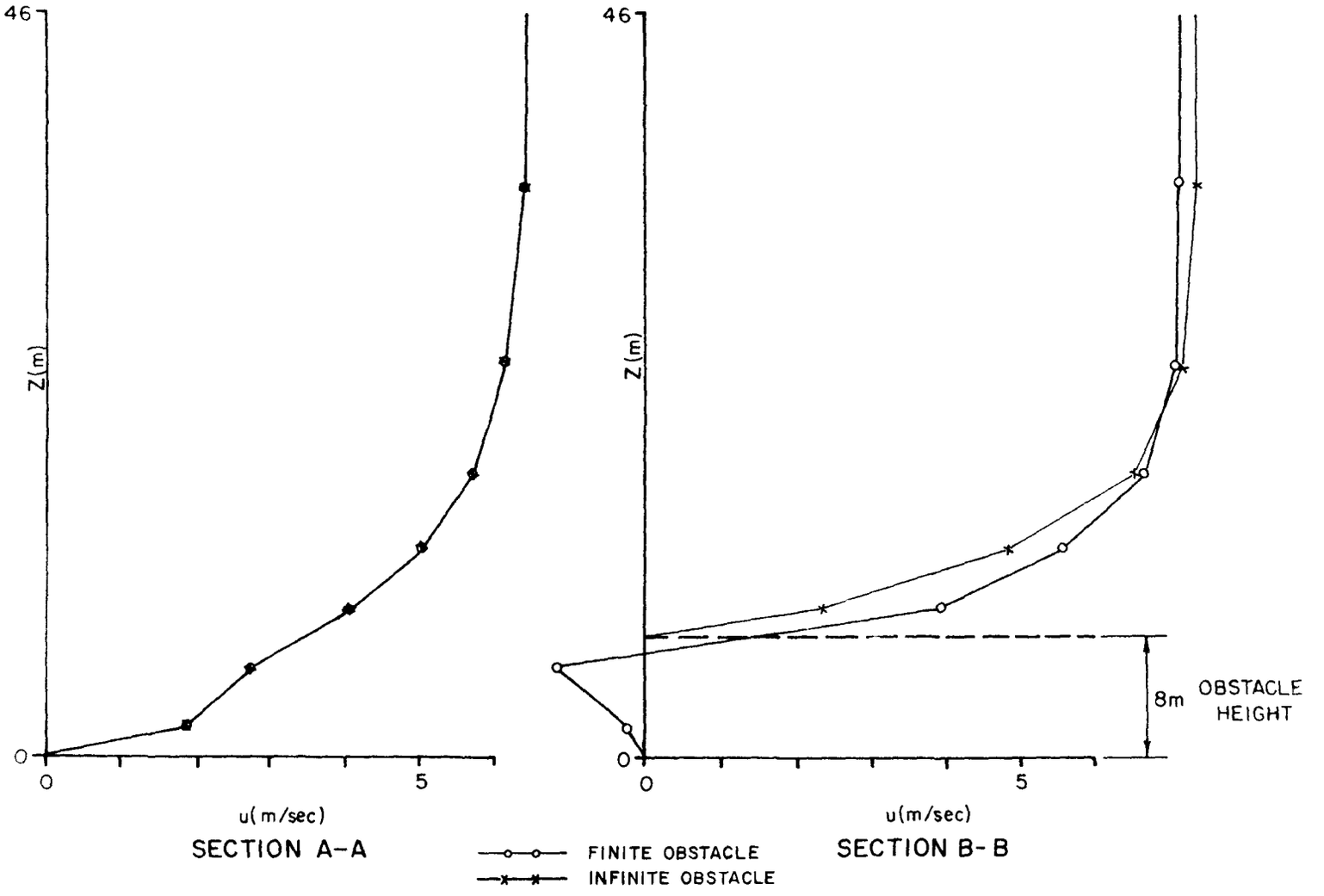

and $\alpha = 1/7$ which corresponds to a neutral atmosphere. It was found that the modified potential solution gives good agreement with the Navier-Stokes solution (presented in Figure 23) when $K_z/K_x = 1$ for the flow coefficients in the potential model. Figure 25 shows the comparison of these two results at four vertical cross-sections. The agreement is good except on the top of the obstacle, where the potential solution does not reflect the amount of viscous friction that it should.

A second series of runs simulated stable atmospheric conditions. For the Navier-Stokes solution it was assumed that the ground is an isothermal surface and a constant density gradient of $-0.001 g/cm^3/m$ was assumed. The effect of density variations is best seen by plotting the velocity difference between the stable and neutral cases as shown on Figure 26. In stable flow velocities at the ground decrease and at the top of the boundary layer increase causing the circulation pattern of Figure 26. In the modified potential model, a best match was obtained for this case with $K_z/K_x = 0.7$. Comparison of these two results is in Figure 27 and has the same character as the results of Figure 25.

3.5.3-3 Comparison for Three-Dimensional Flow

The example for three-dimensional testing has the same grid in the x-z plane as the two-dimensional problem. The dimension of the obstacle in the y direction is 10 m. Because x-z is a symmetry plane, only one-half of the problem need be solved as shown in Figure 28. Illustration of the three-dimensional results is more complicated, mainly because it is difficult to display the data in three dimensions[19,2].

In the neutral case, the velocity field in the symmetry plane (x-z) is very similar to the field obtained in the two-dimensional case, and y-velocities are small except around the upstream side of the obstacle. The modified potential model gave good results when $K_z/K_x = 1$. Figures 29 and 30 show a comparison of u-velocities in the two planes perpendicular to the x-axis. Figure 29 gives a two-dimensional velocity profile

FIGURE 25

NEUTRAL ATMOSPHERE
COMPARISON OF NAVIER-STOKES
AND POTENTIAL VELOCITY SOLUTIONS

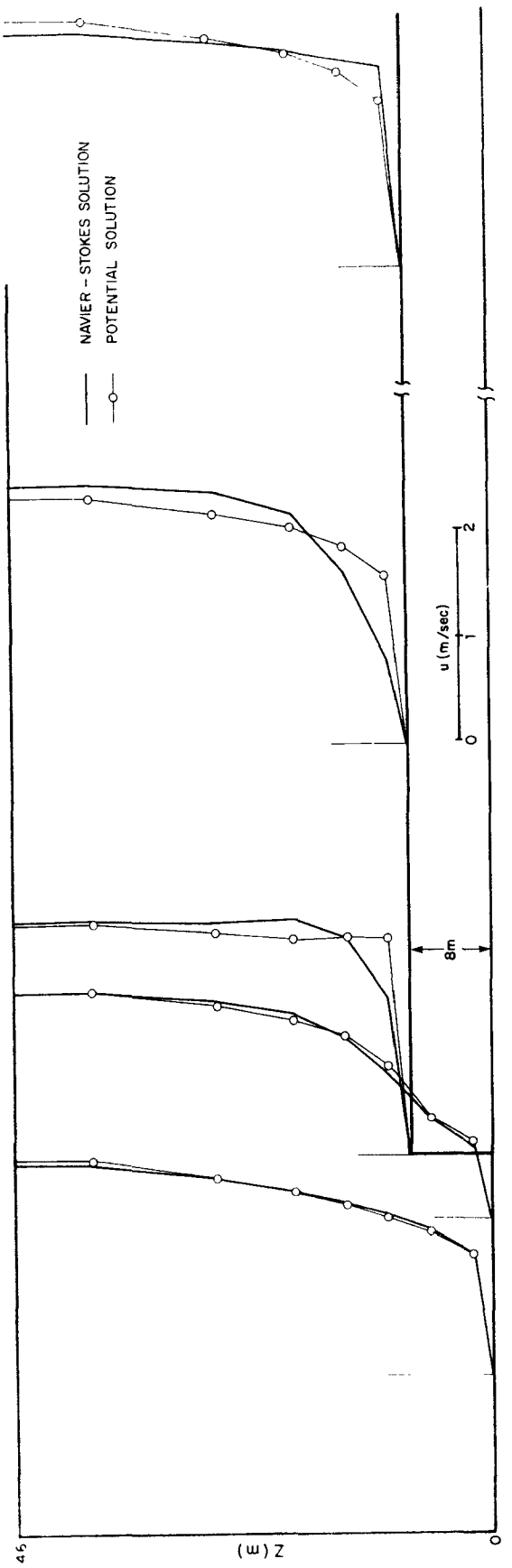

FIGURE 26

DIFFERENTIAL VELOCITIES
FOR STABLE TO NEUTRAL ATMOSPHERE

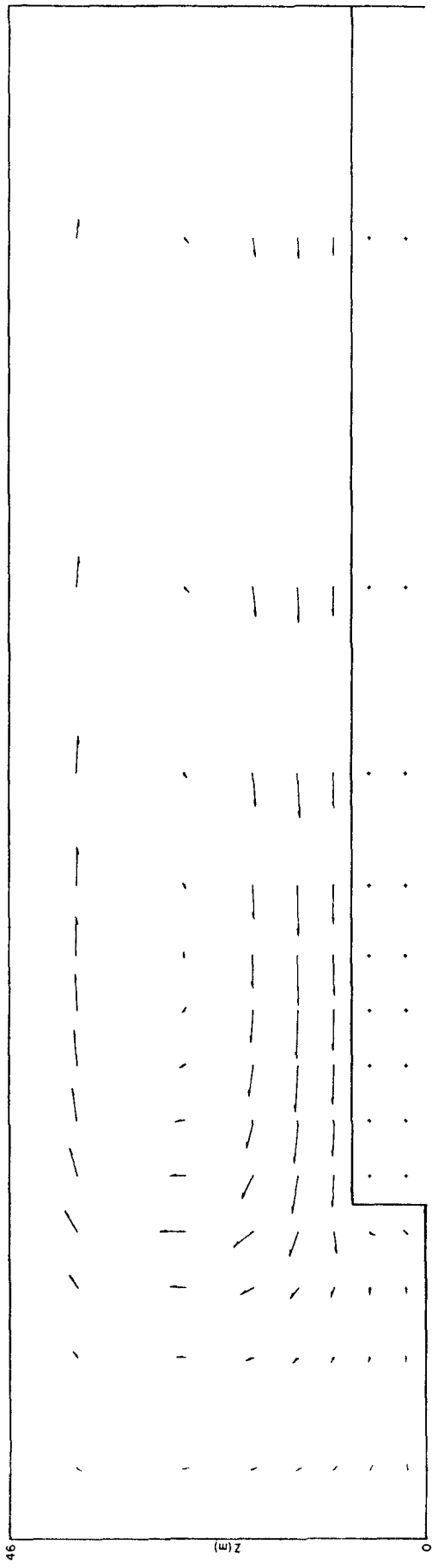

FIGURE 27

STABLE ATMOSPHERE
COMPARISON OF NAVIER-STOKES
AND POTENTIAL VELOCITY SOLUTIONS

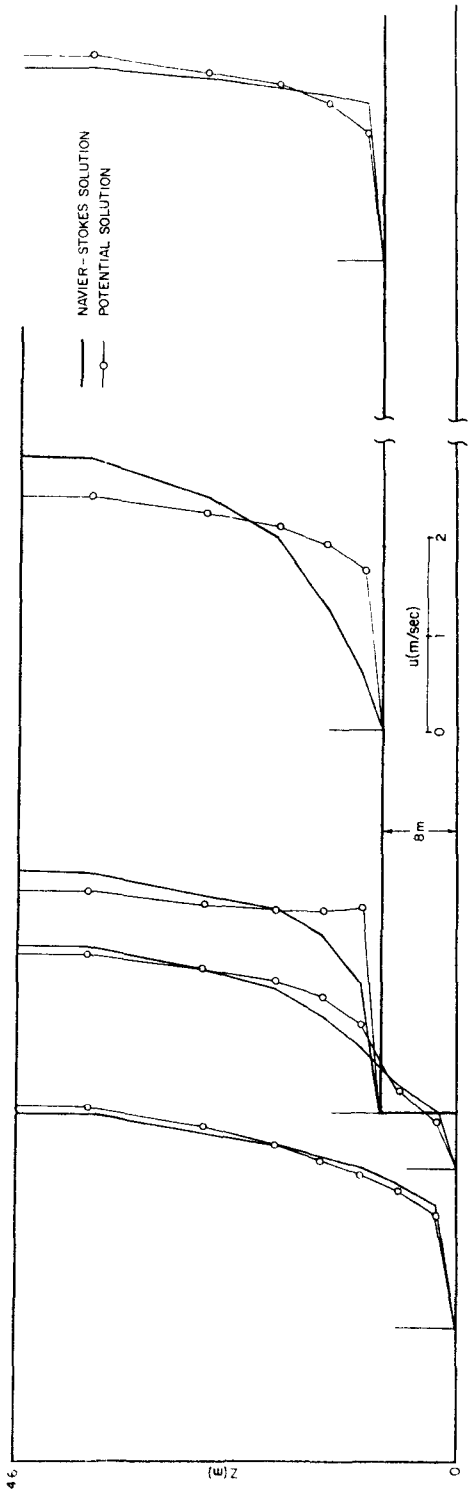

FIGURE 28

THREE-DIMENSIONAL TEST PROBLEM

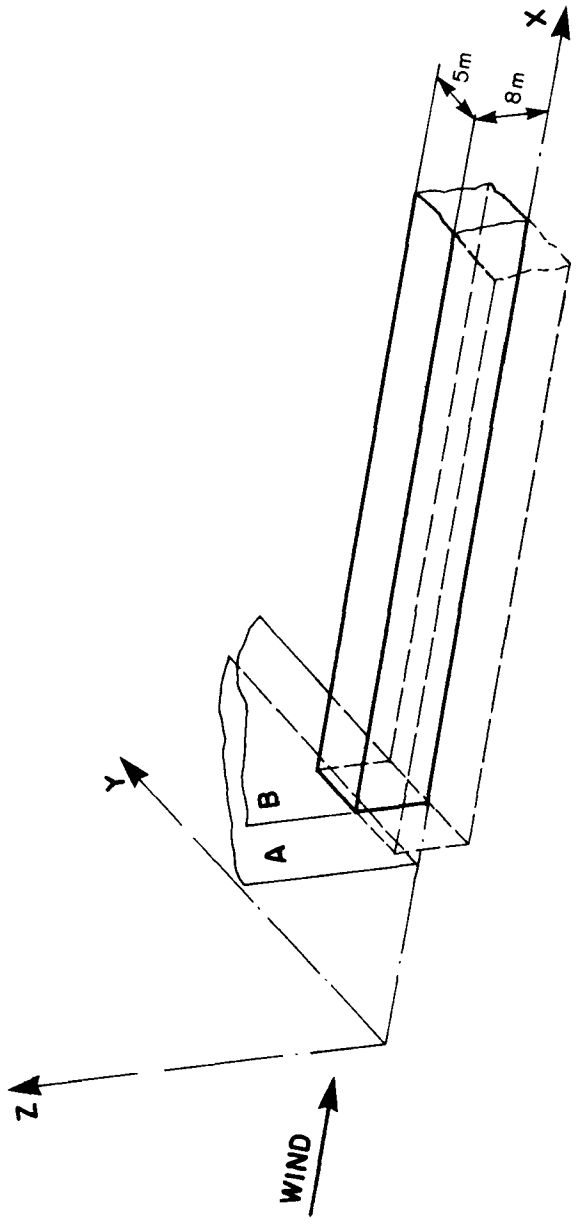

FIGURE 29

COMPARISON OF NAVIER-STOKES AND POTENTIAL SOLUTION

IN FRONT OF OBSTACLE-NEUTRAL

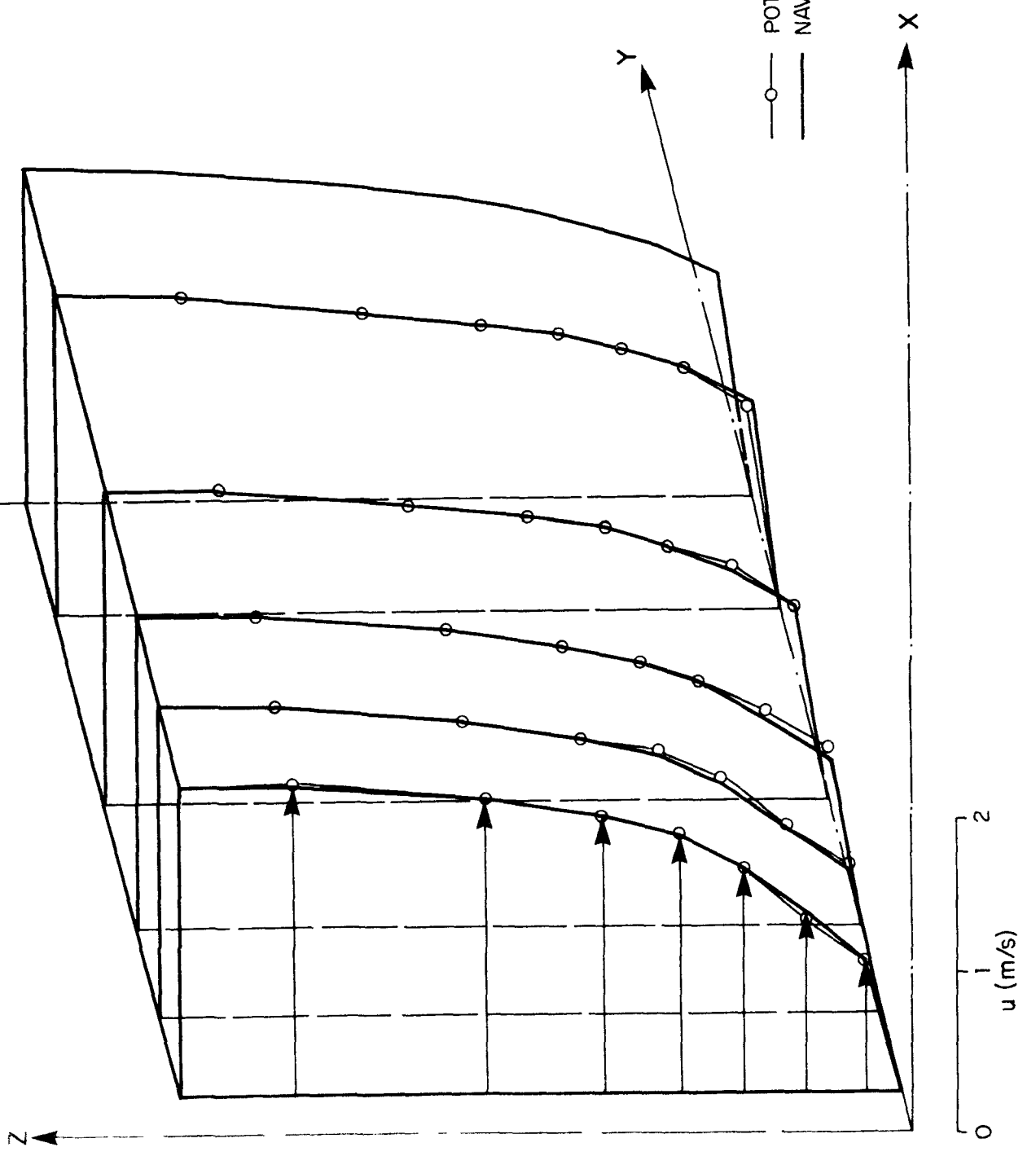

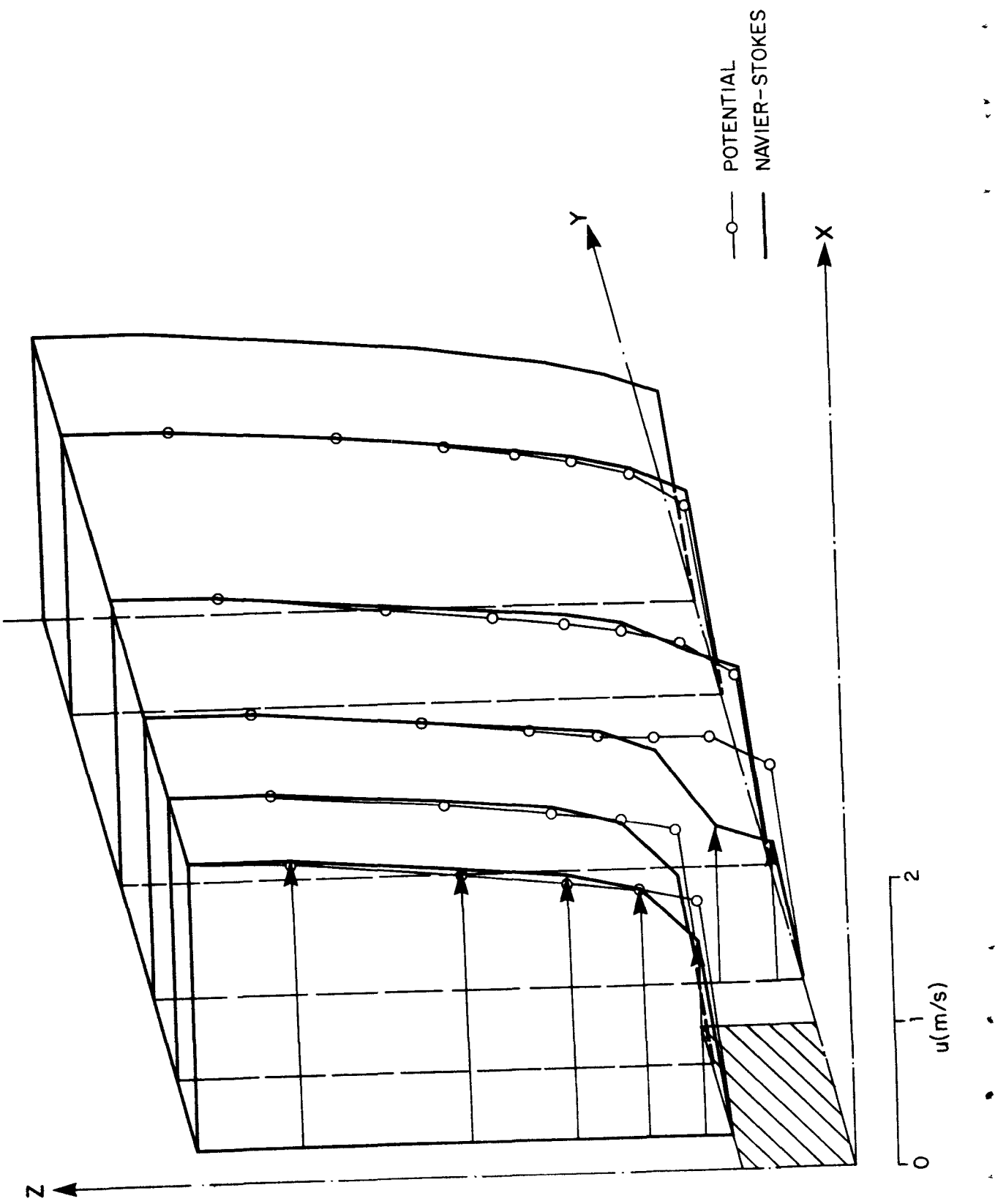

FIGURE 30
COMPARISON OF NAVIER-STOKES AND POTENTIAL SOLUTION
AT THE FACE OF OBSTACLE-NEUTRAL

in the plane A (Figure 28) in front of the obstacle and Figure 30 in plane B through the face of the obstacle. The agreement is generally good with the exception of velocities close to surface, especially on the side of the obstacle. Good agreement was also found in the z and y components of the velocity field.

In the stable case, the imposed density gradient causes superimposed circulation at the front side of the obstacle similar to Figure 26. Also, the density gradient in the y direction (on the side of the obstacle) has an effect of superimposing transversal circulation patterns. The three-dimensional equivalent of Figure 26 showing the difference between stable and neutral velocity fields is schematically shown in Figure 31. In this case, u-velocities on top of the obstacle are decreased and v-velocities, which were small in the neutral case, increase in the downstream direction. A true circulation pattern is formed on the side of the obstacle if it is long enough. Comparison runs with the modified potential model showed that it is possible to obtain a good match of velocities on the upstream side of the upstream side of the obstacle by reducing K_z/K_x.

3.5.4 Summary of Comparisons and Conclusions

3.5.4-1 Range of Adequacy for the Modified Potential Flow Model

Numerical comparisons described in the preceeding paragraphs show convincingly that the modified potential model will be adequate for many situations typical in air pollution modeling, particularly:

(a) for flow over terrain where no wakes and recirculation regions are expected to develop because of stability, and

(b) for flow around buildings or over rough terrain, if the areas directly behind obstacles are not of primary interest.

FIGURE 31

DIFFERENTIAL VELOCITIES FOR STABLE TO NEUTRAL ATMOSPHERE COMPARISON IN 3-D

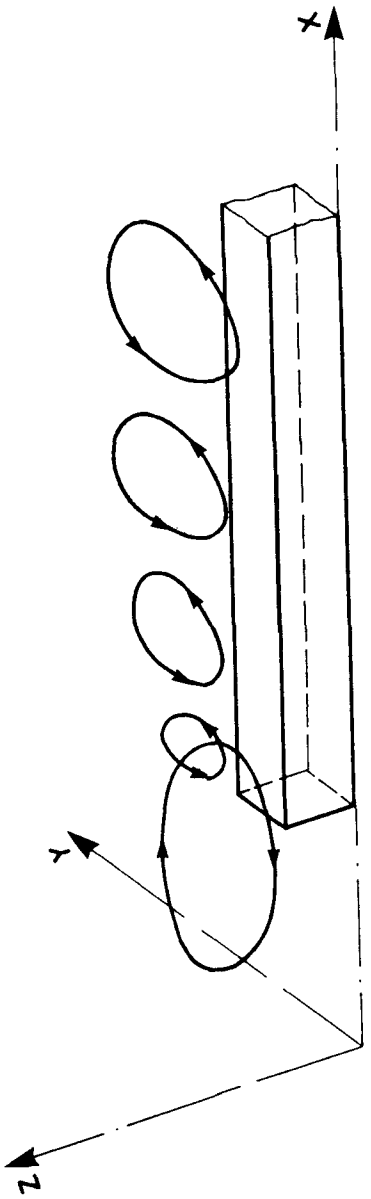

3.5.4-2 Limitations

The basic limitation of the modified potential model is given by the fact that it cannot simulate properly viscous effects. Therefore, the model will not be adequate, for example, for investigation of downwash of pollutants in a wake behind a building, for investigation of pollutant sources located in building cavities, and other similar applications. These cases represent mostly simulations on a much smaller scale than is usual in typical air quality studies. Similar limitations are found when temperature effects are considered. The model will be adequate if thermal effects are relatively uniform and are mainly reflected in a change in the stability of the atmosphere.

3.5.4-3 Accuracy and Expected Errors

The results of this study show that the INTERCOMP modified potential model is generally an adequate flow model for environmental engineering studies. A different simplified model was also proposed by Hino[30]. Such simplifications of the problem at present, still seem to be the only way for solving practical size problems efficiently.

The problem is the large computer requirements for numerical integration of the full Navier-Stokes equations. For the examples given here, computer time for the Navier-Stokes solutions was 10-100 times more than for the modified potential model. For a large three-dimensional problem this ratio would probably be closer to the upper end of this range.

It is important, for this reason, to continue development and improvement of simplified flow models. Navier-Stokes models can then be used for validation of these models and in situations where the simple models are known not to be adequate.

4.0 REFERENCES

1. Hino, M., Computer Experiment on Smoke Diffusion Over Complicated Topography, Atmos. Env. 2, 1968.

2. Hotchkiss, R. S., Numerical Calculation of Three-Dimensional Flows of Air and Particulates About Structures, Proceedings Air Pollution, Turbulence, and Diffusion Symposium, Dec., 1971.

3. Djuric, D. and Thomas, V., A Numerical Study of Convective Transport of a Gaseous Air Pollutant in the Vicinity of Tall Buildings, Proceedings Air Pollution, Turbulence, and Diffusion Symposium, Dec., 1971.

4. Lantz, R. B., Coats, K. H. and Kloepfer, C. V., A Three-Dimensional Numerical Model for Calculating the Spread and Dilution of Air Pollutants, Proceedings Air Pollution, Turbulence, and Diffusion Symposium, Dec., 1971.

5. Van der Hoven, I., et. al., Report of Meteorology Work Group, Southwest Energy Study, Appendix E, 1972.

6. Start, G. E., Dickson, G. R., and Wendell L. L., Diffusion in a Canyon within Rough Mountainous Terrain, NOAA Tech. Memo ERL, ARL-38, August, 1973.

7. Turner, D. B., Workbook of Atmospheric Dispersion Estimates, US DHEN 999-AP-26, 1969.

8. Sklarew, R. C., Fabrick, A. J. and Prager, J. E., Mathematical Modeling of Photochemical Smog Using the PICK Method, APCA Journal, 22, 1972.

9. Lantz, R. B., Quantitative Evaluation of Numerical Diffusion (Truncation Error), SPE Journal, 1971.

10. Price, H. S., Varga, R. S. and Warren, V. E., Application of Oscillation Matrices to Diffusion-Convection Equations, Journal Math. and Physics, 45, 1966.

11. Bowne, N. E., Diffusion Rates, Presented at 66th Annual Meeting of APCA, Chicago, Illinois, Time, 1973.

12. Lantz, R. B., McCulloch, R. C., and Agrawal, R. K., The Use of Three-Dimensional Numerical Air Pollution Models in Planning Plant Location, Design and Operation, J. Canada Pet. Tech., July-Sept., 1972.

13. Hirt, C. W., Heuristic Stability Theory for Finite-Difference Equations, J. of Comput. Physics, 2, 1968.

14. Deardorff, J. W., A Numerical Study of Three-Dimensional Turbulent Flow at Large Reynolds Numbers, J. Fluid Mech., 1970, Vol. 41 (2).

15. Deardorff, J. W., Numerical Study of that Transport by Internal Gravity Waves Above a Growing Unstable Layer, Phys. of Fluids Supplement II, 1969.

16. Fox, D. G., Numerical Simulation of Three-Dimensional Shape - Preserving Convective Elements, J. of Atm. Sci., Vol. 29, March, 1972.

17. Welch, J. E., Marlow, F. H., Shannon, J. P., and Daly, B. J., The MAC Method, Report LA-3425, Los Alamos Scientific Laboratory of the University of California, 1965.

18. Harlow, F. H. and Welch, J. E., Numerical Calculation of Time-Dependent Viscous Incompressible Flow of Fluid with a Free Surface, Phys. Fluids, 8, 1965.

19. Hirt, C. W. and Cook, J. L., Calculating Three-Dimensional Flows Around Structures and Over Rough Terrain, J. Comp. Physics, 10, 1972.

20. Fox, D. G. and Deardorff, J. W., Computer Methods for Simulation of Multidimensional, Nonlinear, Subsonic, Incompressible Flow, J. Heat Transfer, Trans. ASME, Nov., 1972.

21. Williams, G. P., Numerical Integration of the Three-Dimensional Navier-Stokes Equations for Incompressible Flow, J. Fluid Mech., 1969, Vol. 37, Part 4.

22. Lilly, D. K., Numerical Solutions for the Shape-Preserving Two-Dimensional Thermal Convection Element, J. Atm. Sci., 21, 1964.

23. Aziz, K. and Hellums, J. D., Numerical Solution of the Three-Dimensional Equations of Motion for Laminar Natural Convection, Phys. Fluids, 10, 1967.

24. Ames, W. F., Some Computation in Fluid Mechanics, SIAM Review, 15 (2), 1973.

25. Deardorff, J. W., Numerical Study of Heat Transport by Internal Gravity Waves Above a Growing Unstable Layer, Phys. of Fluids, Supplement II, 1969.

26. Deardorff, J. W., A Three-Dimensional Numerical Investigation of the Idealized Planetary Boundary Layer, Geoph. Fluid Dynamics, Vol. 1, 1970.

27. Morihara, H. and Cheng, R. Ta-Shun, Numerical Solution of the Viscous Flow in the Entrance Region of Parallel Plates, J. Comput. Physics, 11, 1973.

28. Hinze, J. O., Turbulence, McGraw-Hill, New York, 1959.

29. Sutton, O. G., Micrometeorology, McGraw-Hill, New York, 1953.

30. Schlichtling, H., Boundary-Layer Theory, 6th Edition, McGraw-Hill, 1968.

31. Launder, B. E. and Spalding, D. B., Mathematical Models of Turbulence, Academic Press, London and New York, 1972.

32. Halitsky, J., Validation of Scaling Procedures for Wind Tunnel Model Testing of Diffusion Near Buildings, Report No. TR-69-8, Geophysical Sci. Laboratory, New York Univ., 1969.

APPENDIX A

NAVIER-STOKES FLOW MODEL

Mathematical Development

The numerical model is based on the "primitive variable" formulation used by the Los Alamos group[17,18,19] as well as the Colorado group[20] and others[21,22]. This formulation has been chosen in preference to the vector-potential formulation[23] because it can be easily extended to turbulent flow and variable density. For current survey of computational approaches to Navier-Stokes equations, see reference 24 and 20.

The equations solved are

$$\left.\begin{aligned} \rho\frac{Du}{Dt} &= \frac{\partial p}{\partial x} + \nabla\mu\nabla u \\ \rho\frac{Dv}{Dt} &= \frac{\partial p}{\partial y} + \nabla\mu\nabla v \\ \rho\frac{Dw}{Dt} &= \frac{\partial p}{\partial z} + \nabla\mu\nabla w - \rho g \end{aligned}\right\} \qquad \text{(A-1)}$$

$$\text{where } \rho\frac{Du}{Dt} = \frac{\partial \rho u}{\partial t} + \frac{\partial \rho u^2}{\partial t} + \frac{\partial \rho uv}{\partial y} + \frac{\partial \rho uw}{\partial z}$$

$$\text{and } \mu = \mu_L + \mu^T_{k,l}$$

$$\frac{\partial \rho}{\partial t} + \frac{\partial \rho u}{\partial x} + \frac{\partial \rho v}{\partial y} + \frac{\partial \rho w}{\partial z} = 0 \qquad \text{(A-2)}$$

$$\rho = f(x,y,z) \qquad \text{(A-3)}$$

These equations can be derived from the full Navier-Stokes equation if it is assumed that:

(1) Pressure changes do not affect density.

(2) Density changes have a negligible effect on viscous terms. This assumption is quite justified in view of the uncertainties associated with turbulent viscosities.

(3) Turbulent effects are included as Reynolds stresses expressed through a turbulent eddy viscosity (this will be discussed in more detail later).

(4) Density can be prescribed as a function of position. Thus, although the model does not solve simultaneously the energy equation, it can approximate the buoyancy effects in cases when the temperature field is relatively stable. Such cases are often of practical interest.

This model is more comprehensive than the incompressible, laminar viscosity model, used e.g. in reference 19.

The pressure equation can be obtained from (A-1) by differentiating each equation with respect to its direction coordinate and summing

$$\nabla^2 p = -\left[\frac{\partial}{\partial x}\left(\rho\frac{Du}{Dt}\right) + \frac{\partial}{\partial y}\left(\rho\frac{Dv}{\partial t}\right) + \frac{\partial}{\partial z}\left(\rho\frac{Dw}{\partial t}\right)\right] -$$

$$- \left[\frac{\partial}{\partial x}\nabla\mu\nabla u + \frac{\partial}{\partial y}\nabla\mu\nabla v + \frac{\partial}{\partial z}\nabla\mu\nabla w\right] =$$

or $$\nabla^2 p = -RI - RV \qquad \text{(A-4)}$$

Therefore, both inertia terms, RI, and viscous terms, RV, act as sources in the pressure equation. It is worth noting that the right-hand side of (A-4) is much more complicated than for the case of laminar incompressible flow, where it can be shown that RV $\equiv$ 0 by continuity and

$$RI = \frac{\partial^2(u^2)}{\partial x^2} + \frac{\partial^2(v^2)}{\partial y^2} + \frac{\partial^2(w^2)}{\partial z^2} + 2\frac{\partial uv}{\partial x\partial y} + 2\frac{\partial uw}{\partial x\partial z} + 2\frac{\partial vw}{\partial y\partial z} .$$

In the original MAC method and its later applications, the entire right-hand side was also carried in the computation in order to help the approximate solution satisfy continuity when iterative methods were used. In the present turbulent model, the viscous terms must be retained because they do not cancel out in (A-4), regardless of the solution method used.

The numerical solution method employs equations (A-1) and (A-4), discretized by finite differences. With suitable discretization, the finite-difference equations will also satisfy the discretized continuity equation (A-2).

The momentum equations (A-1) use a forward difference for the time derivative. The procedure consists of implicitly solving for the pressure field with the right-hand side evaluated at the old time level, then an explicit updating of the velocity field using the new pressures. Central time differencing, preferred by some authors[16,25,26], gives smaller time truncation errors, but introduces weak instability and increases core requirements.

Boundary Conditions

The region in which the equations are solved is rectangular in the x and y direction as shown on Figure A-1. In the z direction,

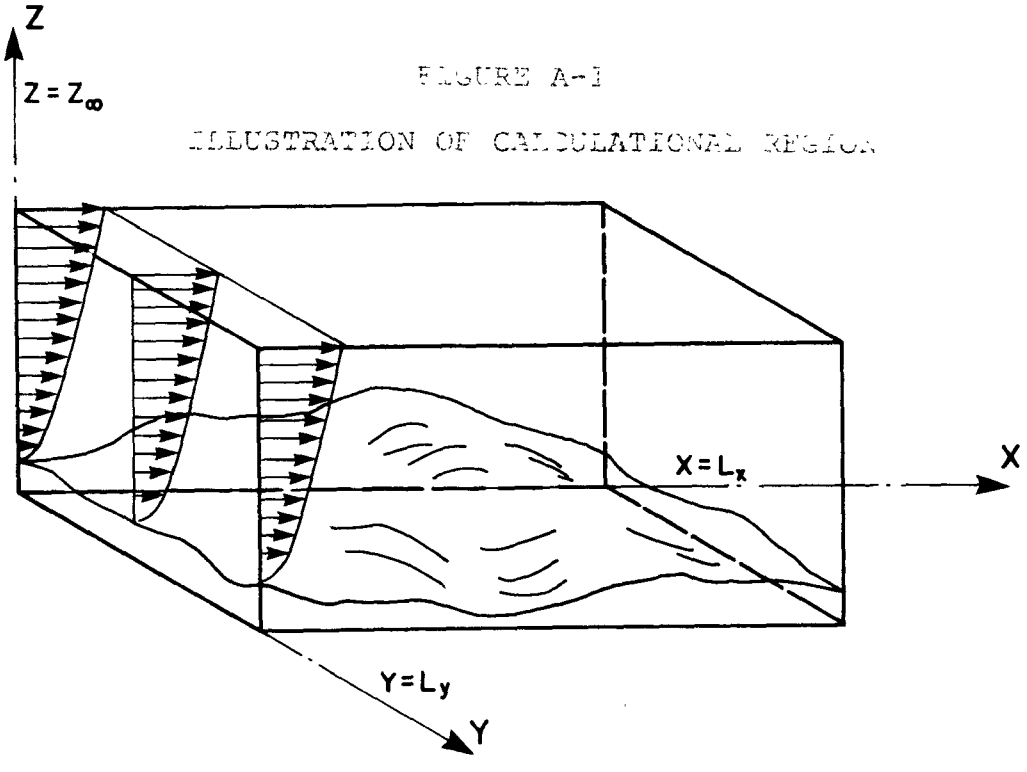

FIGURE A-1

ILLUSTRATION OF CALCULATIONAL REGION

it is bounded by ground surface of variable elevation and by a constant elevation z_∞, which is assumed to be the top of the turbulent boundary layer. It is assumed that the wind at x = 0 is in the direction of the x-axis and the velocity profile is known, i.e.,

$$u = U(y,z),\ v = w = 0 \text{ at } x = 0 \qquad \text{(A-5)}$$

The y boundaries and the boundary at z_∞ are assumed to be no-friction surfaces without flow across the boundary.

$$\frac{\partial u}{\partial y} = \frac{\partial w}{\partial y} = 0,\ v = 0 \text{ at } y = 0,\ L_y \qquad \text{(A-6)}$$

$$\frac{\partial u}{\partial z} = \frac{\partial v}{\partial z} = 0,\ w = 0 \text{ at } z = z_\infty \qquad \text{(A-7)}$$

At the groundlevel, friction is important. Therefore, the boundary conditions are:

$$u = v = w = 0 \text{ at the ground} \qquad \text{(A-8)}$$

Finally, at the outflow face, we specify a vertical pressure gradient that corresponds to one-dimensional flow over flat terrain (uniform pressure if gravity is neglected). Since the flow is incompressible with respect to pressure, pressure level is not important. Therefore, we can arbitrarily choose pressure at say z_∞ to obtain:

$$p = p(z),\ p(z_\infty) = P,\ \frac{dp}{dz} = -\rho g \text{ at } x = L_x \qquad \text{(A-9)}$$

Model of Turbulence

Consider one-dimensional flow over a flat plate at steady-state, for fully developed ($w \equiv 0$), incompressible flow, equations (A-4) reduce to

$$\frac{\partial p}{\partial x} = P' = \frac{\partial}{\partial z}\left(\mu_{xz}\frac{\partial u}{\partial z}\right) \qquad \text{(A-10)}$$

Define shear stress, τ, by

$$\tau = \tau(z) = \mu_{xz}(z)\frac{\partial u}{\partial z} \qquad \text{(A-11)}$$

Since at steady-state P' = const, we can integrate the equation

$$P' = \frac{\partial}{\partial z}\left(\tau(z)\right)$$

to obtain

$$\tau(z) = P'z + C_1 \qquad \text{(A-12)}$$

which shows that shear stress varies linearly with height. Let us now assume that the velocity over the flat surface is given by

$$u = U_\infty \left(\frac{z}{z_\infty}\right)^\alpha \qquad \text{(A-13)}$$

Differentiating and substitution into (A-11) and (A-12) gives

$$\mu_{xz} = \frac{z_\infty}{U_\infty \alpha}\left(\frac{z}{z_\infty}\right)^{1-\alpha}(P'z + C_1) \qquad \text{(A-14)}$$

The constant C_1 cannot be determined from the value of μ at $x = 0$, since $u(0) = 0$, but from the value $\mu_\infty = \mu_{xz}(z_\infty)$. Since $\partial u/\partial z(z_\infty) = U_\infty \alpha / z_\infty$, we have

$$\tau_\infty = \mu_\infty U_\infty / z_\infty, \quad \tau(z) = P'(z - z_\infty) + \tau_\infty, \text{ and}$$

$$\mu_{xz} = \frac{z_\infty}{U_\infty \alpha} \left(\frac{z}{z_\infty}\right)^{1-\alpha} [P'(z - z_\infty) + \tau_\infty] \qquad \text{(A-15)}$$

In order to obtain the pressure gradient, we must relate it to the magnitude of the eddy viscosity. It is convenient to choose the maximum viscosity, μ_M, which is equal to

$$\mu_M = \frac{z_\infty}{U_\infty} \frac{(1-\alpha)^{1-\alpha}}{(2-\alpha)^{2-\alpha}} \left(1 - \frac{\tau_\infty}{P' z_\infty}\right)^{1-\alpha} (\tau_\infty - P' z_\infty) \qquad \text{(A-16)}$$

at the height

$$z_M = z_\infty \left(\frac{1-\alpha}{2-\alpha}\right) \left(1 - \frac{\tau_\infty}{P' z_\infty}\right) \qquad \text{(A-17)}$$

If the height of the boundary layer z_∞ is chosen such that turbulence essentially disappears at z_∞, the viscosity μ_∞ will essentially be the molecular viscosity, μ_L, the shear stress, τ_∞, can be neglected in comparison to the maximum turbulent shear stress at the ground, thus $\tau_o = P' z_\infty$. The expressions (A-16) and (A-17) then simplify to

$$\mu_M = -\frac{z_\infty}{U_\infty \alpha} \frac{(1-\alpha)^{1-\alpha}}{(2-\alpha)^{2-\alpha}} P' = -\frac{z_\infty}{U_\infty \alpha} \frac{(1-\alpha)^{1-\alpha}}{(2-\alpha)^{2-\alpha}} \tau_o \qquad \text{(A-18)}$$

and

$$z_M = z_\infty \frac{(1-\alpha)}{(2-\alpha)} \qquad \text{(A-19)}$$

Therefore, equation (A-18) allows us to calculate μ_M from the measured values of τ_o. The final expression for μ_{xz} is then

$$\mu_{xz} = \left(\frac{z}{z_\infty}\right)^{1-\alpha} \left[\frac{(2-\alpha)^{2-\alpha}}{(1-\alpha)^{1-\alpha}} \mu_M \left(1 - \frac{z}{z_\infty}\right) + \mu_\infty\right] \qquad \text{(A-20)}$$

It is easy to see that the derivation of equation (A-19) can be interpreted as a derivation of the mixing length $\ell(z)$ in Prandtl's model of turbulence in order to satisfy the power law velocity profile. By Prandtl's hypothesis

$$\mu_{xz} = \rho \ell^2 \left|\frac{\partial u}{\partial z}\right| \qquad \text{(A-21)}$$

Since $\partial u/\partial z = (U_\infty \alpha / z_\infty)(z/z_\infty)^{\alpha-1}$, we obtain by comparison with (A-20) for $\mu_\infty = 0$.

$$\ell = \left(\frac{z}{z_\infty}\right)^{1-\alpha} \frac{z_\infty}{U_\infty \alpha} \left[\frac{\mu_M}{\rho} \frac{(2-\alpha)^{2-\alpha}}{(1-\alpha)^{1-\alpha}} \left(1 - \frac{z}{z_\infty}\right) + \frac{\mu_\infty}{\rho}\right] \qquad \text{(A-22)}$$

The equation (A-22) agrees very well with the measured mixing length in pipes, reported in reference 30, except for the region close to the centerline, which is to be expected. However, it is more important that the eddy viscosity itself agree with measurement rather than the mixing length, since ℓ is itself derived from observed values of μ.

Comparison of μ_{xz} by formula (A-20) with measurements by Nikuradse[30], Chapter XX is in Figure A-2. The agreement is excellent up to $z/z_\infty = 1/2$ and acceptable for larger z. It is clear that a function derived from a power law velocity profile cannot fit exactly experimental data in a tube or channel at the centerline because the boundary conditions are different at z_∞. However, the model can be used with the boundary conditions $\partial u/\partial z = 0$ at $z = z_\infty$ and will produce a solution that deviates from the power law as $z \to z_\infty$ (Figure 20) in agreement with experimental results[30].

The one-dimensional analysis presented thus far established only one component of the viscosity tensor. The other components can be obtained from the definitions of the turbulent stresses:

$$
\left.
\begin{aligned}
\tau_{xx}^{T} &= \mu_{xx}\frac{\partial u}{\partial x} = -\rho\,\overline{u'^2} \\
\tau_{xy}^{T} &= \mu_{xy}\frac{\partial u}{\partial y} = -\rho\,\overline{u'v'} \\
\tau_{xz}^{T} &= \mu_{xz}\frac{\partial u}{\partial z} = -\rho\,\overline{u'w'} \\
\tau_{yx}^{T} &= \mu_{yx}\frac{\partial v}{\partial x} = -\rho\,\overline{v'u'} \\
\tau_{yy}^{T} &= \mu_{yy}\frac{\partial v}{\partial y} = -\rho\,\overline{v'^2} \\
\tau_{yz}^{T} &= \mu_{yz}\frac{\partial v}{\partial z} = -\rho\,\overline{v'w'} \\
\tau_{zx}^{T} &= \mu_{zx}\frac{\partial w}{\partial x} = -\rho\,\overline{w'u'} \\
\tau_{zy}^{T} &= \mu_{zy}\frac{\partial w}{\partial y} = -\rho\,\overline{w'v'} \\
\tau_{zz}^{T} &= \mu_{zz}\frac{\partial w}{\partial z} = -\rho\,\overline{w'^2}
\end{aligned}
\right\} \qquad \text{(A-23)}
$$

The task of generating all nine stress components as functions of position and the current flow field is, in general, the subject of theoretical models of turbulence. Our approach is based on the model for μ_{xz} which gives correct results in one-dimensional shear flow. The work[26] concluded that in the planetary boundary layer this is indeed the most important component and, therefore, we can expect that the relations for other components may be considerably simplified without significant loss of accuracy.

The starting point is provided by experimental evidence, that the ratios of turbulent fluctuations $\overline{w'^2}/\overline{u'^2}$, $\overline{v'^2}/\overline{u'^2}$, $\overline{u'w'}/\overline{u'^2}$, etc. remain approximately constant[29,30]. These ratios perhaps should be a function of atmospheric stability as the mass diffusivities are. Furthermore, we can make a simplification that the burbulence is approximately homogeneous in the x-y (horizontal) plane, $\overline{v'^2} \sim \overline{u'^2}$, $\overline{v'w'} \sim \overline{u'w'}$. Then the structure of turbulence is determined by μ_M, a fluctuation ratio

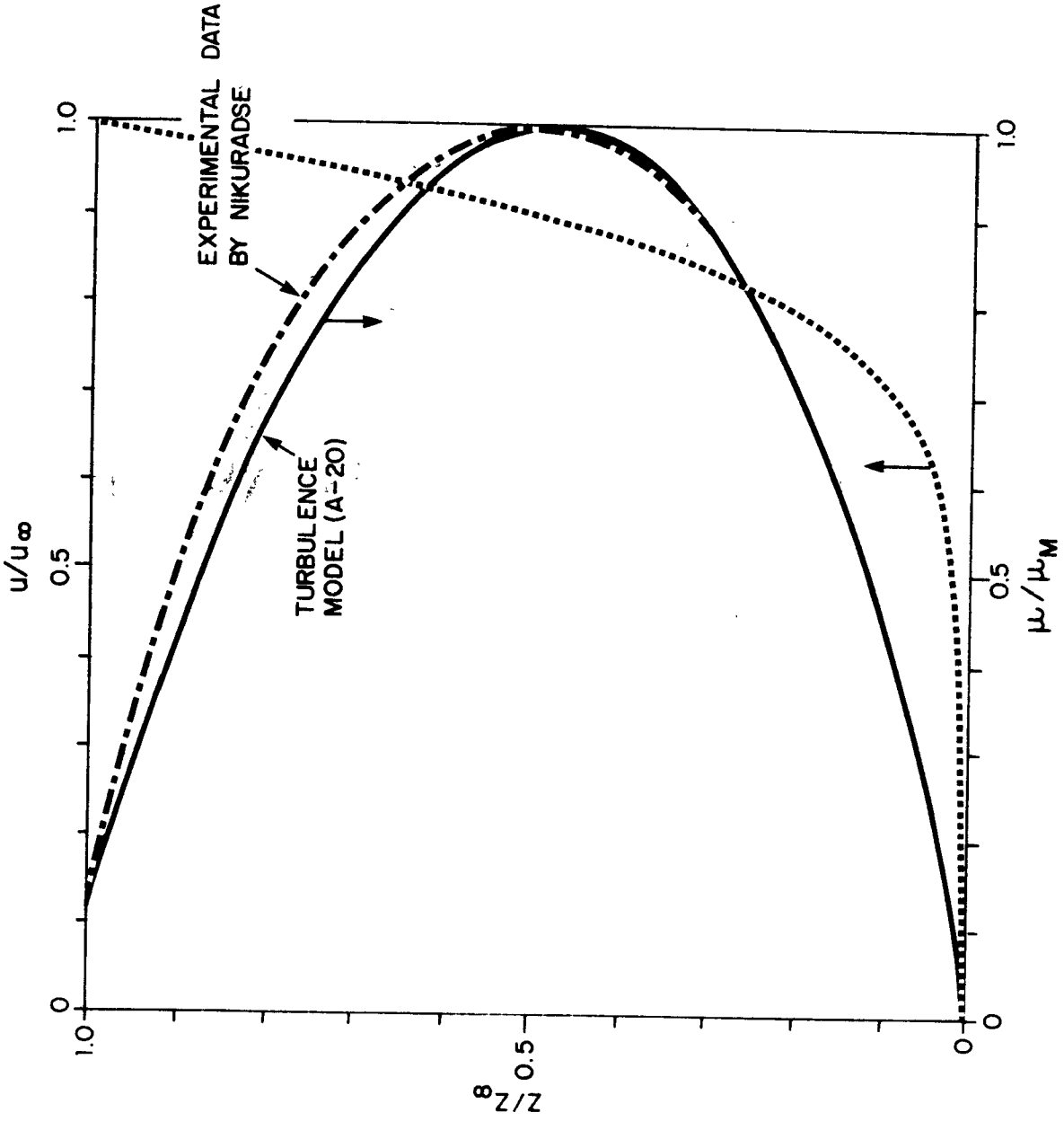
EXPERIMENTAL DATA
BY NIKURADSE
TURBULENCE
MODEL (A-20)
u/u∞
μ/μM
z/z8
0
0.5
1.0

FIGURE A-2

$$r = \frac{\sqrt{\overline{w'^2}}}{\sqrt{\overline{u'^2}}} \tag{A-24}$$

and two correlation coefficients

$$\psi_{xz} = \frac{\overline{u'w'}}{\sqrt{\overline{u'^2}} \cdot \sqrt{\overline{w'^2}}} \tag{A-25}$$

$$\psi_{xy} = \frac{\overline{u'v'}}{\sqrt{\overline{u'^2}} \cdot \sqrt{\overline{v'^2}}} = \frac{\overline{u'v'}}{\overline{u'^2}} \tag{A-26}$$

Using equations (A-24) through (A-26), we can express all viscosity components as a function of μ_{xz} and the three constants. We can write this in matrix form as

$$\underline{\mu} = \mu_{xz} \begin{bmatrix} \frac{1}{r\psi_{xz}} \frac{\partial u}{\partial z}\frac{\partial u}{\partial x} & \frac{\psi_{xy}}{r\psi_{xz}} \frac{\partial u}{\partial z}\frac{\partial u}{\partial y} & 1 \\ \frac{\psi_{xy}}{r\psi_{xz}} \frac{\partial u}{\partial z}\frac{\partial v}{\partial x} & \frac{1}{r\psi_{xz}} \frac{\partial u}{\partial z}\frac{\partial v}{\partial y} & \frac{\partial u}{\partial z}\frac{\partial v}{\partial z} \\ \frac{\partial u}{\partial z}\frac{\partial w}{\partial x} & \frac{\partial u}{\partial z}\frac{\partial w}{\partial y} & \frac{r}{\psi_{xz}} \frac{\partial u}{\partial z}\frac{\partial w}{\partial z} \end{bmatrix} = \mu_{xz} A_{\mu} \tag{A-2}$$

Matrix A depends on the current velocity field and will be, therefore different for each grid point and time step. The uncertainty in the data often justifies further simplification of the model (A-27), similar to the "order of magnitude" argument, common in boundary layer theory. The simplification consists of replacing the local values of derivatives by "mean value" estimates as follows:

$$\frac{\partial u}{\partial x} \sim \frac{V_\infty}{L_x} \quad , \quad \frac{\partial u}{\partial y} \sim \frac{V_\infty}{L_y} \quad , \quad \frac{\partial u}{\partial z} \sim \frac{V_\infty}{z}$$

$$\frac{\partial v}{\partial x} \sim \frac{V_{max}}{L_x} \quad , \quad \frac{\partial v}{\partial y} \sim \frac{V_{max}}{L_y} \quad , \quad \frac{\partial v}{\partial z} \sim \frac{V_{max}}{z_\infty}$$

$$\frac{\partial w}{\partial x} \sim \frac{W_{max}}{L_x} \quad , \quad \frac{\partial w}{\partial y} \sim \frac{W_{max}}{L_y} \quad , \quad \frac{\partial w}{\partial z} \sim \frac{W_{max}}{z_\infty}$$

If we now define ratios as

$$\frac{V_{max}}{U_\infty} = R_y \quad , \quad \frac{W_{max}}{U_\infty} = R_z \qquad \text{(A-28)}$$

we obtain a constant "average" matrix A:

$$A\mu = \begin{bmatrix} \frac{1}{r\psi_{xz}} & \frac{L_x}{z_\infty} & \frac{\psi_{xy}}{r\psi_{xz}} & \frac{L_y}{z_\infty} & 1 \\ \frac{\psi_{xy}}{r\psi_{xz}} & \frac{L_x}{z_\infty R_y} & \frac{1}{r\psi_{xz}} & \frac{L_y}{z_\infty R_y} & \frac{1}{R_y} \\ \frac{L_x}{z_\infty R_z} & & & \frac{L_y}{z_\infty R_z} & \frac{r}{\psi_{xz}} \quad \frac{1}{R_z} \end{bmatrix} \qquad \text{(A-29)}$$

The use of (A-29) is considerably simpler than the corresponding (A-27).

Computing Details

The program has the capability of solving both 2-D and 3-D problems. The solution method for the pressure equation is LSOR, with direct elimination as an option for 2-D problems. Handling of boundary conditions permits arbitrary specification of terrain as in the standard INTERCOMP air quality simulator. The program has a restart capability and an automatic time step control, based on the convective stability condition:

$$\Delta t < \min_{(i,j,k)} \left(\frac{\Delta x}{u} , \frac{\Delta y}{v} , \frac{\Delta z}{w}\right) \qquad \text{(A-30)}$$

The condition (III-5) alone is not sufficient for stability in all cases, but it is always necessary.

The optional modes in which the program can run include the laminar viscosity case, a constant density case, and different input velocity profiles.

APPENDIX B

COMPARISON OF MEASURED AND CALCULATED RESULTS

Results for Test 1 through 11 are summarized in the following tables. Tests 2 and 6 have been omitted because they were for easterly winds and contained only a few data points at the monitors north of the release point. Test 2, for example, contained only two groundlevel measured points.

A few comments concerning each test result are included in the appendix.

COMPARISON MEASURED AND CALCULATED VALUES

TEST NO. 1 - UP-CANYON

Location	Measured $\mu g/m^3$	Calculated, $\mu g/m^3$		
		INTERCOMP	EPA	GAUSSIAN
Deer Cr-Mtnghouse	-	2.0	1.6	1.8
White Ridge (1)	0.5	1.3		
(2)	0.3	1.0	1.2	1.3
(3)	0.1	0.7		
(4)	-	0.3		
Wild Draw (1)	0.6	0.7	0.9	1.0
(2)	-	0.5		
Wild Horse (1)	1.6	0.5		
(2)	1.3	0.2	0.9	1.0
(3)	0.8	0.1		
(4)	-	-		
Bear Creek (1)	-	-		
(2)	-	-	0.6	0.7
(3)	-	-		
(4)	-	-		
Red Face (1)	-		0.6	0.7
(2)	-			
Wet Man (1)	-			
(2)	-		0.5	0.6
(3)	-			
(4)	-			

Comments

Test No. 1 was a stack top release under Pasquill B stability. Each of the models gave calculated results which peaked closer to the stack than the measured results would indicate. As a consequence, the calculated results are decreasing while measured values are still increasing. This resulted in a negative correlation coefficient, R = -0.56.

Comparison of the calculated and measured results indicate the calculations would be in better agreement if the stability were more nearly class C.

COMPARISON MEASURED AND CALCULATED GROUNDLEVEL VALUES

TEST NO. 3 - UP-CANYON

Location	Measured $\mu g/m^3$	Calculated, $\mu g/m^3$		
		INTERCOMP	EPA	GAUSSIAN
Deer Cr-Mtnghouse	-	1.2	0.02	0.04
White Ridge (1)	1.7	0.7		
(2)	0.4	0.7	0.06	0.09
(3)	-	0.7		
Wild Draw (1)	3.4	1.8	0.15	0.26
(2)	0.3	1.4		
Wild Horse (1)	4.3	3.0		
(2)	2.4	2.8	0.17	0.34
(3)	2.2	2.5		
(4)	-	1.7		
Bear Creek (1)	2.6	2.5		
(2)	1.8	2.6	0.34	0.77
(3)	-	2.7		
(4)	-	2.3		
Red Face (1)	-	1.6	0.34	0.77
(2)	-	1.1		
Wet Man (1)	-	1.1	0.43	0.86
(2)	-	0.2		
(3)	-	0.0		

Comments

Test 3 calculations from the INTERCOMP model are in fair agreement with the measured results. A more northerly wind direction than the 135° would have improved the calculated result. Gaussian results have not reached the peak concentration within the monitored area. The correlation coefficient between INTERCOMP's calculation and the measurements was 0.67.

COMPARISON MEASURED AND CALCULATED GROUNDLEVEL VALUES

TEST NO. 4 - UP-CANYON

Location	Measured $\mu g/m^3$	Calculated, $\mu g/m^3$		
		INTERCOMP	EPA	GAUSSIAN
Deer Cr-Mtnghouse	-	0.1	0.0	0.0
White Ridge(1)	-	0.0	0.0	0.01
(2)	-	0.0		
Wild Draw(1)	0.2	0.1	0.01	0.02
(2)	0.2	0.1		
Wild Horse(1)	-	0.2	0.03	0.03
(2)	0.2	0.2		
(3)	-	0.2		
(4)	-	0.1		
Bear Creek(1)	0.2	0.2	0.03	0.06
(2)	0.2	0.2		
(3)	0.1	0.2		
(4)	-	0.2		
Red Face(1)	0.4	0.1	0.03	0.06
(2)	-	0.1		
Wet Man(1)	-	0.1	0.03	0.06
(2)	-	0.0		
(3)	-	0.0		

Comments

Test 4 calculated results from the INTERCOMP model were generally at the correct magnitude. There were few measured points available for comparison. This is a high wind neutral stability case, 10 m/sec. Because the measured concentrations are so uniform, the linear correlation coefficient came out negative, R = -0.54, even though the results appear reasonably good.

COMPARISON MEASURED AND CALCULATED GROUNDLEVEL VALUES

TEST NO. 5 - UP-CANYON

Location	Measured $\mu g/m^3$	Calculated, $\mu g/m^3$		
		INTERCOMP	EPA	GAUSSIAN
Deer Cr-Mtnghouse	0.2	0.5	0.01	0.02
White Ridge (1)	1.2	1.0		
(2)	1.0	1.0	0.03	0.04
(3)	-	0.5		
Wild Draw (1)	1.6	1.2		
(2)	0.8	1.5	0.07	0.11
Wild Horse (1)	1.0	1.0		
(2)	1.3	1.2		
(3)	1.2	1.2	0.08	0.15
(4)	1.0	1.0		
Bear Creek (1)	0.6	1.0		
(2)	0.7	1.0		
(3)	0.6	1.0	0.17	0.33
(4)	0.4	1.0		
Red Face (1)	0.3	0.5		
(2)	0.4	0.5	0.17	0.33
Wet Man (1)	0.1	0.7		
(2)	0.1	0.6		
(3)	0.2	0.5	0.18	0.37
(4)	-	0.1		

Comments

Test 5 has been discussed in some detail in the text. The results are generally good as evidenced by the 0.76 correlation coefficient.

COMPARISON MEASURED AND CALCULATED GROUNDLEVEL VALUES

TEST NO. 7 - DOWN-CANYON

Location	Measured $\mu g/m^3$	Calculated, $\mu g/m^3$		
		INTERCOMP	EPA	GAUSSIAN
0.6 km	-	0.0	135	770
1.2 km	-	0.0	43	240
Trail(1)	1.0	0.2		
(2)	0.9	0.3	17	86
(3)	1.1	0.5		
(4)	0.3	1.0		
Mill Fork(1)	1.6	1.5		
(2)	0.2	1.5	10	58
(3)	-	0.5		
Rilda(1)	-	0.8		
(2)	-	0.6	6	34
(3)	0.2	0.2		
(4)	0.0	0.1		
Bear Creek(1)	0.1	0.7		
(2)	0.1	0.8	5	24
(3)	0.1	1.0		
(4)	0.1	1.1		
Wet Man(1)	0.1	0.6		
(2)	-	0.5	5	24
(3)	-	0.5		
(4)	-	0.5		

Comments

Test 7 was the stable down-canyon release, but unlike the remaining stable cases was an elevated wall release. The measured results as the photographic evidence indicated in the Huntington report were considerably influenced by the flow up the shaded canyon wall. The correlation coefficient for this test was extremely low, only 0.06.

COMPARISON MEASURED AND CALCULATED GROUNDLEVEL VALUES

TEST NO. 8 - DOWN-CANYON

Location	Measured $\mu g/m^3$	Calculated, $\mu g/m^3$		
		INTERCOMP	EPA	GAUSSIAN
0.6 km	30	280	185	1070
1.3 km	25	120	60	325
Trail(1)	27	23		
(2)	4	20	25	120
(3)	-	0.5		
(4)	-	0.0		
Mill Fork(1)	9	5		
(2)	-	3	12	80
(3)	-	0.5		
Rilda(1)	5	8		
(2)	3	3	8	46
(3)	-	0.7		
(4)	-	0.0		
Bear Creek(1)	2	5		
(2)	1.3	3	5	33
(3)	0.8	2		
(4)	0.5	0.2		
Wet Man(1)	-	1.5		
(2)	-	0.3	5	33
(3)	-	0.0		
(4)	-	0.0		

Comments

Test 8 results were in good agreement with the measurements. The linear correlation coefficient for this test was 0.77. Most of the disagreement between calculated and measured results occurred at the closest two monitor points to the release point. The peak concentrations in the release must have flowed around these monitor stations because higher concentrations were often recorded downstream. The flow solution in the INTERCOMP model did not reflect this result.

COMPARISON MEASURED AND CALCULATED GROUNDLEVEL VALUES

TEST NO. 9 - DOWN-CANYON

Location	Measured $\mu g/m^3$	Calculated, $\mu g/m^3$		
		INTERCOMP	EPA	GAUSSIAN
0.6 km	6	90	37	210
1.3 km	12	50	12	48
Trail (1)	24	16		
(2)	16	2	5	16
(3)	-	0.0		
(4)	-	0.0		
Mill Fork (1)	8	3		
(2)	7	0.5	3	11
(3)	-	0.0		
Rilda (1)	6	2		
(2)	2	1	2	7
(3)	-	0.0		
(4)	-	0.0		
Bear Creek (1)	12	1.5		
(2)	6	1	1	4
(3)	2	0.3		
(4)	-	0.0		
Wet Man (1)	-	0.5		
(2)	-	0.0	1	4
(3)	-	0.0		
(4)	-	0.0		

Comments

Test No. 9 calculations did not agree well with the measured results. This was one of the tests mentioned as being more stable than class F. INTERCOMP calculations as well as the Gaussian results would have been in better agreement if the more stable atmospheric condition has been used. The correlation coefficient was equal to 0.05.

COMPARISON MEASURED AND CALCULATED GROUNDLEVEL VALUES

TEST NO. 10 - DOWN-CANYON

Location	Elevation Ft.	Measured $\mu g/m^3$	Calculated, $\mu g/m^3$		
			INTERCOMP	EPA	GAUSSIAN
0.6 km	7170	25	186	105	590
1.2 km	7120	35	80	32	180
Trail(1)	7120	9.5	15		
(2)	7250	19.0	14	13	60
(3)	7870	-	0.5		
(4)	8200	-	0.0		
Mill Fork(1)	7010	3.7	5.0		
(2)	7250	3.4	2.5	7	40
(3)	7700	-	0.0		
Rilda(1)	6940	6.1	5.5		
(2)	7240	2.1	2.50	4	25
(3)	7550	-	0.2		
(4)	7950	-	0.0		
Bear Creek(1)	6790	3.4	3.5		
(2)	6910	2.8	2.5	3	15
(3)	7090	2.0	1.5		
(4)	7170	-	0.2		
Wet Man(1)	7170	-	1.5		
(2)	7330	-	0.5	3	15
(3)	7400	-	0.0		
(4)	7650	-	0.0		

Comments

Test No. 10 results were in good agreement with the measurements. This test is discussed in detail in the text. The correlation coefficient was 0.74.

COMPARISON MEASURED AND CALCULATED GROUNDLEVEL VALUES

TEST NO. 11 - DOWN-CANYON

Location	Measured $\mu g/m^3$	Calculated, $\mu g/m^3$		
		INTERCOMP	EPA	GAUSSIAN
0.6 km	210	240	140	800
1.3 km	210	103	45	250
Trail (1)	200	19	18	90
(2)	60	18		
(3)	-	0.5		
(4)	-	0.0		
Mill Fork (1)	130	6.4	10	60
(2)	80	5.2		
(3)	-	0.2		
Rilda (1)	32	7.1	6	35
(2)	2.6	3.2		
(3)	-	0.3		
(4)	-	0.0		
Bear Creek (1)	3.0	4.5	5	25
(2)	2.0	3.2		
(3)	0.6	1.9		
(4)	-	0.3		
Wet Man (1)	-	2.0	5	25
(2)	-	0.5		
(3)	-	0.0		
(4)	-	0.0		

Comments

This test was again one of those mentioned as being more stable than class F. The INTERCOMP calculation again appears low and would have been in better agreement if a more stable class could have been used. The correlation coefficient was 0.68.

TECHNICAL REPORT DATA
(Please read Instructions on the reverse before completing)

1. REPORT NO.	2.	3. RECIPIENT'S ACCESSION NO.
EPA-450/3-75-059		

4. TITLE AND SUBTITLE	5. REPORT DATE
Evaluation of Selected Air Pollution Dispersion Models Applicable to Complex Terrain	Prepared September 18, 1974
	6. PERFORMING ORGANIZATION CODE
7. AUTHOR(S)	8. PERFORMING ORGANIZATION REPORT NO.
Ronald B. Lantz, Antonin Settari, and Gale F. Hoffnagle	
9. PERFORMING ORGANIZATION NAME AND ADDRESS	10. PROGRAM ELEMENT NO.
INTERCOMP Resource Development & Engineering, Inc. 2000 West Loop South, Suite 2200 Houston, Texas 77027	2AC 129
	11. CONTRACT/GRANT NO.
	68-02-1085
12. SPONSORING AGENCY NAME AND ADDRESS	13. TYPE OF REPORT AND PERIOD COVERED
Office of Air Quality Planning and Standards Environmental Protection Agency Research Triangle Park, N.C. 27711	FINAL July 19,1973-Sept., 197
	14. SPONSORING AGENCY CODE

15. SUPPLEMENTARY NOTES

16. ABSTRACT

A comparison has been made of three models which attempt to predict the dispersion of pollutants in situations with complex terrain. The three models are 1) a Gaussian calculation with terrain assumptions known as the NOAA model, 2) an EPA model, C4M3D also known as the "valley" model, which substitutes different terrain assumptions in the Gaussian calculations, and 3) the INTERCOMP combined wind flow and plume dispersion model which uses a numerical calculational method. Predictions made by each of these models are compared to measurements of ambient concentration data taken in Huntington Canyon, Utah and at El Paso, Texas. The results indicate that the INTERCOMP model has a predictive accuracy for terrain situations comparable to that normally expected for Gaussian predictions in flat terrain, i.e. a factor of two to three. For stable atmospheres, however, the Gaussian predictions of the NOAA model averaged a factor of fifteen higher than the measured results.

17. KEY WORDS AND DOCUMENT ANALYSIS

a. DESCRIPTORS	b. IDENTIFIERS/OPEN ENDED TERMS	c. COSATI Field/Group
Air Pollution Atmospheric Diffusion Mathematical Models Terrain Models	Complex terrain Rough terrain Model comparison NOAA model C4M3D valley model INTERCOMP air quality model	13/B 4

18. DISTRIBUTION STATEMENT	19. SECURITY CLASS *(This Report)*	21. NO. OF PAGES
Release unlimited	Unclassified	103
	20 SECURITY CLASS *(This page)*	22 PRICE
	Unclassified	

EPA Form 2220-1 (9-73)

ENVIRONMENTAL PROTECTION AGENCY
Technical Publications Branch
Office of Administration
Research Triangle Park, North Carolina 27711

OFFICIAL BUSINESS

AN EQUAL OPPORTUNITY EMPLOYER

POSTAGE AND FEES PAID
ENVIRONMENTAL PROTECTION AGENCY
EPA - 335

U.S.MAIL

Return this sheet if you do NOT wish to receive this material , or if change of address is needed ☐. (Indicate change, including ZIP code.)

PUBLICATION NO. EPA-450/3-75-059